DISSERTATION

STRUCTURAL COUPLING AND WIND-INDUCED RESPONSE OF TWIN TALL BUILDINGS WITH A SKYBRIDGE

Submitted by

Juntack Lim

Civil and Environmental Engineering Department

In partial fulfillment of the requirements

For the Degree of Doctor of Philosophy

Colorado State University

Fort Collins, Colorado

Fall 2008

COLORADO STATE UNIVERSITY

September 22, 2008

WE HEREBY RECOMMEND THAT THE DISSERTATION PREPARED UNDER OUR SUPERVISION BY JUNTACK LIM ENTITLED STRUCTURAL COUPLING AND WIND-INDUCED RESPONSE OF TWIN TALL BUILDINGS WITH A SKYBRIDGE BE ACCEPTED AS FULFILLING IN PART REQUIREMENTS FOR THE DEGREE OF DOCTOR OF PHILOSOPHY.

Committee on Gradate Work

Adviser

Department Head

ABSTRACT OF DISSERTATION

STRUCTURAL COUPLING AND WIND-INDUCED RESPONSE OF TWIN TALL BUILDINGS WITH A SKYBRIDGE

Twin tall buildings with a connecting skybridge involve two types of coupling: the structural coupling, developed by a skybridge and synchronizing the motions of vibration of the two building and the aerodynamic coupling resulting from high cross-correlations of the components of wind loading. The physical understanding of these couplings and their impacts on the wind-induced response of the buildings are not fully understood, when using a high-frequency force balance (HFFB) approach tailored for single tall buildings. Detailed laboratory mapping of the aerodynamic loading and coupling requires specialized experimental techniques. Predictions of the response of the structurally coupled buildings, due to correlated wind loading, involve utilization of advanced dynamic analysis.

This dissertation addresses the issues associated with correlated wind loading and structurally coupled response of twin buildings with a skybridge. Wind tunnel testing to acquire the correlated wind loading on twin buildings is described. The effects of the relative positions of the buildings on the loading correlations and coherences are discussed. These results are next used as an input to an analytical model developed to calculate the building wind-induced response. The building system, including the structural coupling, is represented by a six-degree-of-freedom model lumped at the skybridge level. In free vibration, the natural frequencies and modal shapes are obtained for various levels of the relative stiffness of the (inter-building) beam representing the skybridge. The model is subsequently used to investigate the effects of aerodynamic and structural couplings on the roof top accelerations of the buildings. Spectral integration and white-noise approximation approaches are employed in calculations of the building responses.

The presented results show significant effects of both the aerodynamic and structural couplings. Simplified empirical relations for application in preliminary design of structurally connected tall buildings are proposed. Recommendations for follow-up studies of coupled wind-induced response of tall twin buildings are discussed.

Juntack Lim
Civil and Environmental Engineering Department
Colorado State University
Fort Collins, CO 80523
Fall 2008

ACKNOWLEDGEMENTS

My first sincere gratitude is to my advisor, Dr. Bogusz Bienkiewicz. He gave me insights concerning my special topic and encouraged me to pursue my doctoral study with invaluable guidance whenever I struggled during my graduate study.

I am also deeply grateful to my graduate committee members, Dr. Robert Meroney, Dr. David Neff and Dr. Martin Gelfand. Dr. Meroney and Dr. Gelfand gave me constructive comments at an initial stage of my research. Dr. Neff helped me improve my knowledge about the wind tunnel test methodology related to my research.

I would like to acknowledge Mr. Menuhito Endo and Dr. Jaeyoung Chung. Mr. Endo provided frequent laboratory assistance. Dr. Chung introduced me to research opportunities from Samsung construction.

I am also indebted to Dr. Byunghae Lee and Dr. Sungwoo Shin at Hanyang University who initiated my interest in wind engineering and gave frequent advice.

Above all things, nothing of these achievements would have been possible without love and patience of my father, Changeun Lim, my mother, Sukjin Jung and my younger brother, Junho Lim. My family were always supportive, and I was dedicating this dissertation to them.

LIST OF CONTENTS

LIST OF FIGURES

CHAPTER 2

CHAPTER 3

CHAPTER 4

CHAPTER 5

LIST OF TABLES

CHAPTER 1

INTRODUCTION

1.1 Statement of problem

The architectural expression of modern skyscrapers is getting ever-increasingly dramatic, compared to a conventional design scheme of tall buildings of the past 50 years. This increases the complexity in the exterior and dynamic behaviors of buildings. In addition, contemporary designs of tall buildings involve surrounding structures in close proximity because of a limited availability of land. As a result, two or more tall buildings may be linked by inter-structures, e.g. a skybridge(s), a skygarden(s), or a common podium.

Such architectural and structural demands are challenging improvements in a currently popular technique, the high-frequency force balance (HFFB) method primarily tailored for laboratory investigations of single tall buildings. In fact, overall good progresses in research relevant to single tall buildings have to date been made, however, most of the studies involved single HFFB measurements (Tschanz and Davenport, 1983; Boggs and Peterka, 1989; Cheong et al., 1992; Yip and Flay, 1995; Zhou et al., 2003). Estimations of the dynamic wind response of structurally connected twin buildings have been mostly carried out in the same way as single tall buildings. However, structurally coupled twin buildings in close proximity involve two type of coupling:

- Structural coupling, introduced by inter-building structure, synchronizing the dynamic motions of the connected buildings and
- Aerodynamic coupling due to high level of the cross-correlations of the components of wind loading acting on each of the buildings.

These couplings can affect the dynamic wind response of the twin buildings. However, routine analysis using a single HFFB system cannot capture fully the structural and aerodynamic couplings inherent in the twin building configuration. As a result, an optimized wind-resistant design of such building complex may be limited.

To overcome the limitation of the HFFB technique, an enhanced HFFB approach, involving two or more force balances, has been advanced. Only a limited number of applications of these advancements have been reported in open literature (Xie and Irwin, 1998, 2001; Boggs and Hosoya, 2000). These efforts have provided insights into the enhanced HFFB system. Further studies are needed to improve understanding the aerodynamic performance of twin building configurations. The issues of primary interest are as follows:

- Modeling of structural linkages between the two buildings;
- The role of aerodynamic coupling due to correlated wind loading exerted on the two buildings;
- The accuracy of calculations of the building response using spectral modal analysis; and
- The combination of coupled modal responses.

1.2 Objective and topics

The primary objective of this study was to identify structural and aerodynamic couplings and their effects on the wind-induced response of twin tall buildings with a connecting skybridge. The secondary objective was to provide guidance for optimized wind-resistant designs of such building complexes. Specific goals to address the above objectives were:

- The development of a dual-force balance system for wind tunnel studies of twin buildings;
- The modeling of atmospheric boundary layer used for aerodynamic testing of twin buildings;
- The exploring and mapping of the correlations and coherences of the components of base wind loading exerted on twin tall buildings in close proximity;
- The analytical modeling of structural coupling for dynamic analysis of wind-induced response of coupled twin tall buildings;
- The formulation of a refined technique to calculate structurally and aerodynamically coupled response of twin tall buildings with a skybridge; and
- The evaluation of the effects of structural and aerodynamic couplings on the building response.

1.3 Organization and content

This dissertation is organized as follows. Chapter 2 describes a preliminary study of the effects of structural coupling on the wind-induced response of twin tall buildings connected by a skybridge. Development of a dual high-frequency force balance (DHFFB) used in wind tunnel investigation and background information on the methodology employed in the analysis are presented. A representative spacing between the buildings and one level of structural coupling are selected. Comparisons of the rooftop acceleration of structurally coupled and uncoupled twin buildings are provided and the influence of the selected structural coupling is assessed.

Chapter 3 describes a follow-up wind tunnel study of the base wind loading exerted on tall twin buildings in close proximity. The effects of the relative positions of the buildings on the correlations and coherences involving loading components on each building and on the two buildings are investigated. Mapping of the correlations and coherences, subsequently used in aerodynamic analysis of structurally coupled tall buildings in close proximity, is presented.

Chapter 4 describes analytical modeling of structural coupling for generic twin buildings with a skybridge. The structural coupling of the interconnected buildings is modeled by introducing a six-degree-of-freedom model lumped at the skybridge level. The equations of motion of the reduced system are derived. In free vibration analysis, the natural frequencies and modal shapes are obtained for various levels of the relative stiffness of the inter-building beam representing the skybridge. Dependence of the calculated natural frequencies and modes of vibration on the skybridge stiffness is investigated. Empirical formulas to approximate these quantities are proposed, for preliminary design of twin buildings with structural coupling.

Chapter 5 describes the effects of aerodynamic and structural couplings on the roof top acceleration of the twin buildings with a connecting skybridge. Refined treatments to deal with these couplings are formulated based on spectral integration and white-noise approximation methods. Comparisons of the two methods in estimation of the building acceleration are provided. Three cases of aerodynamic coupling are introduced: the full-coupling, no coupling and partial coupling. The impact of aerodynamic coupling is assessed. Five representative levels of structural coupling are chosen and their effects on the building acceleration are assessed for three wind speeds.

Chapter 6 provides a summary of the conclusions of this study and offers recommendations for further investigations. Representative references relevant to wind tunnel studies of tall buildings are collected in Appendix.

1.4 References

Boggs, D.W. and Hosoya, N. (2001), "Wind-tunnel techniques to address structures with multiple coupled interactions", In: Proceedings of Structures Congress 2001 – A Structural Engineering Odyssey, Washington, DC, USA, pp. 8.

Boggs, D.W. and Peterka, J.A. (1989), "Aerodynamic model tests of tall buildings", Journal of Engineering Mechanics, 115(3), 618-635.

Cheong, H.F., Balendra, Y., Chew, T., Lee, T.S. and Lee, S.L. (1992), "An experimental technique for distribution of dynamic wind loads on tall buildings", Journal of Wind Engineering and Industrial Aerodynamics, 40(3), 249-261.

Tschanz, T. and Davenport, A.G. (1983), "The base balance technique for the determination of dynamic wind loads", Journal of Wind Engineering and Industrial Aerodynamics, 13(1-3), 429-439.

Xie, J. and Irwin, P.A. (1998), "Application of the force balance technique to a building complex", Journal of Wind Engineering and Industrial Aerodynamics, 77-78, 579-590.

Xie, J. and Irwin, P.A. (2001), "Wind-induced response of a twin-tower structure", Wind and Structures, An International Journal, 4(6), 495-504.

Yip, D.Y.N. and Flay, R.G.J. (1995), "A new force balance data analysis method for wind response predictions of tall buildings", Journal of Wind Engineering and Industrial Aerodynamics, 54-55, 457-471.

Zhou, Y., Kijewski, T.L. and Kareem, A. (2003), "Aerodynamic loads on tall buildings: Interactive database", Journal of Structural Engineering, 129(3), 394-404.

CHAPTER 2

WIND-INDUCED RESPONSE OF STRUCTURALLY COUPLED TWIN TALL BUILDINGS

Chapter 2 has been previously published in Wind and Structures, An International Journal, 7(4), 383-398.

2.1 Introduction

The advent of innovative materials and construction technologies has led to design and construction of slender modern tall buildings, of reduced mass and damping. This trend has resulted in an increased susceptibility of such buildings to wind-induced excitation. To date, the aerodynamic performance of tall buildings has not been fully understood and no comprehensive analytical nor codified models have been developed to adequately address this topic. Accordingly, wind tunnel testing remains the only reliable tool used in fundamental and applied studies of wind effects on tall buildings.

Most of basic wind tunnel investigations of tall buildings have been focused on isolated buildings of generic shapes. However, many contemporary architectural designs involve two or more tall buildings of complex geometries, located in close proximity. In many cases, individual buildings are connected by one or more skybridges or skygardens located at various elevations and/or by ground-level podiums. In addition to the aerodynamic interference effects, caused primarily by close proximity of buildings, the aerodynamic performance of the buildings may be significantly affected by structural coupling due to inter-building connections. These effects increase complexity of wind-resistant design of such buildings. This in turn leads to challenges imposed on wind tunnel techniques needed to adequately model wind loading and, at times, to simulate the wind-induced building response.

A number of conventional wind tunnel techniques, e.g., the high-frequency force balance (HFFB) approach employing a single high-frequency force balance, have been used in wind engineering studies of tall buildings. However, typical applications of such tools do not allow for direct inclusion of the structural and aerodynamic coupling effects in predictions of the wind-induced response of connected buildings. As a result, the impact of structural linkages (coupling) on the aerodynamic performance of twin and multiple interconnected buildings has been frequently neglected or only approximately (indirectly) accounted for.

Advances in instrumentation render synchronous acquisition of data from multiple devices feasible. This feature can be utilized in nearly simultaneous acquisition of time series of wind loading from two or more high-frequency force balances. The obtained data can be used in investigations of complex dynamic responses of structurally connected twin buildings. A limited number of such studies have been reported in open literature, e.g. Xie and Irwin (1998, 2001) and Boggs and Hosoya (2001). In these efforts, the base aerodynamic loading was measured simultaneously for all major buildings of a multi-building complex involving structural coupling. Xie and Irwin (1998, 2001) employed such approach in a study of structurally connected twin buildings and have shown that the structural coupling effects led to equalized dynamic responses of the buildings. Boggs and Hosoya (2001) reported a study of a two-tower structure with a common podium, susceptible to coupled wind-induced motions. They measured the aerodynamic forces using two force balances mounted inside two isolated models of tall buildings and acquired a simultaneously sampled wind pressures acquired at a large number of pressure taps distributed on the located on the building surfaces. The obtained synchronized data were subsequently employed to calculate the wind-induced building response incorporating structural coupling. These techniques can be extended to building configurations comprising of a larger number of interconnected tall buildings. Overall, they represent a significant improvement in treatment of aerodynamic loading and structural coupling effects, for twin and multiple buildings.

Based on the experiences reported above and in other references, a dual-force-balance technique has been recently developed and applied in tall building investigations carried out at the Wind Engineering and Fluids Laboratory (WEFL), Colorado State University. This chapter describes one of the studies – an investigation of the aerodynamic interference and structural coupling effects on generic tall buildings located in close proximity and connected by a skybridge. This chapter is organized as follows. First, background information is presented. Next, the experimental configuration and instrumentation are described. The details of data acquisition and processing are provided. Finally, representative results illustrating the aerodynamic interference and structural coupling effects are presented. The findings of this study are summarized in a concluding section of this chapter.

2.2 Background

The essence of the HFFB technique applied for linear structural systems is an experimental determination of base wind loading and calculation of the wind-induced structural responses. The analytical process involves the use of the modal superposition technique, which for an isolated tall building can be expressed as follows

$$u_s(z,t) = \sum_j q_j(t)\Phi_{js}(z) \tag{2.1}$$

where $u_s(z,t)$ is the s-component of the linear ($s = x, y$) or rotational about the z-axis ($s = \theta$) displacement of a building at the elevation z and time t, and $\Phi_{js}(z)$ is the s-component of the j-th modal shape. The principal coordinate $q_j(t)$ is determined from

$$m_j^*\ddot{q}_j(t) + c_j^*\dot{q}_j(t) + k_j^*q_j(t) = P_j^*(t) \tag{2.2}$$

where m_j^*, c_j^*, k_j^*, and $P_j^*(t)$ are, respectively, the generalized mass, damping, stiffness, and loading in the j-th mode. The generalized mass is $m_j^* = \sum_{s=x,y,\theta} \int_0^H \mu_s(z)\Phi_{js}^2(z)dz$, where $\mu_s(z)$ is the mass or mass moment of inertia per unit height for respectively, the sway ($s = x, y$) or torsional ($s = \theta$) modal components, while z is the vertical ordinate and H is the building height. When the modes are assumed linear and uncoupled, the generalized loading $P_j^*(t)$ can be expressed in terms of the base aerodynamic overturning (sway) moment, Eq. (2.3a), or torque, Eq. (2.3b), which can be experimentally determined from the HFFB measurements.

$$P_j^*(t) = \int_0^H \Phi_j(z) p_j(z,t) dz = \int_0^H \left(\frac{z}{H}\right) p_j(z,t) dz = \frac{M_j(t)}{H} \tag{2.3a}$$

$$P_j^*(t) = \lambda M_j(t) \tag{2.3b}$$

where $p_j(z,t)$ is the externally applied loading (per unit height); $M_j(t)$ is the external base aerodynamic moment or torque; λ is the empirical mode correction factor for generalized torsional loading, typically in the range of 0.5 to 0.7. A representative value of $\lambda = 0.6$ is assumed.

The modal superposition technique, applied in analysis of the wind-induced response of structurally coupled twin tall buildings, requires more than three modes of vibration. Investigations limited to only three modes are incapable of capturing the modal coupling effects, Xie and Irwin (2001), and Boggs and Hosoya (2001), and they may lead to an overestimation or underestimation of the wind-induced building responses. For a case of structurally connected two identical tall buildings of square plan – a twin building configuration – a set of six generic modes capable of capturing the coupling effects is depicted in Fig. 2.1.

The building motion, for such configuration, can be described by expanding Eq. (2.2), as follows

$$m_{cj}^{*}\ddot{q}_{cj}(t)+c_{cj}^{*}\dot{q}_{cj}(t)+k_{cj}^{*}q_{cj}(t)=P_{cj}^{*}(t) \tag{2.4}$$

where m_{cj}^{*}, c_{cj}^{*}, k_{cj}^{*} , $q_{cj}(t)$ and $P_{cj}^{*}(t)$ are, respectively, the coupled generalized mass, damping, stiffness, principal coordinate, and loading in the j-th mode; subscript c denotes a structurally coupled case. The coupled properties can be obtained via a superposition accounting for contributions from the two buildings. For example, the coupled generalized mass can be written as follows

$$m_{cj}^{*}=\sum_{n=1}^{2}\sum_{s=x,y,\theta}m_{jsn}^{*} \tag{2.5}$$

where m_{jsn}^{*} is the generalized mass in the j-th mode and s-direction (s = x, y, θ), for building n (n = 1, 2).

The coupled generalized (modal) loading $P_{cj}^{*}(t)$, in Eq. (2.4), can be expressed in terms of the modal loading $P_{sn}^{*}(t)$ along axis s on building n, simultaneously acquired using the dual high-frequency force balance system, and the directional mode correction coefficients η_{jsn}.

$$P_{cj}^{*}(t)=\sum_{n=1}^{2}\sum_{s=x,y,\theta}\eta_{jsn}P_{sn}^{*}(t) \tag{2.6}$$

where

$$P^*_{sn}(t) = \sum_{i=1}^{N} p_{isn}(t)\,\Phi_{ijsn} \tag{2.7}$$

where $p_{isn}(t)$ is the externally applied loading at the i-th floor, along s-axis, for building n; Φ_{ijsn} is the modal shape at the i-th floor, in the j-th mode and s-direction, for building n; and N is the number of floors, assumed to be the same for the two buildings.

Eq. (2.6) can be expanded as follows

$$\begin{Bmatrix} P^*_{c1}(t) \\ P^*_{c2}(t) \\ P^*_{c3}(t) \\ P^*_{c4}(t) \\ P^*_{c5}(t) \\ P^*_{c6}(t) \end{Bmatrix} = \begin{bmatrix} \eta_{1x1} & \eta_{1y1} & \eta_{1\theta 1} & \eta_{1x2} & \eta_{1y2} & \eta_{1\theta 2} \\ \eta_{2x1} & \eta_{2y1} & \eta_{2\theta 1} & \eta_{2x2} & \eta_{2y2} & \eta_{2\theta 2} \\ \eta_{3x1} & \eta_{3y1} & \eta_{3\theta 1} & \eta_{3x2} & \eta_{3y2} & \eta_{3\theta 2} \\ \eta_{4x1} & \eta_{4y1} & \eta_{4\theta 1} & \eta_{4x2} & \eta_{4y2} & \eta_{4\theta 2} \\ \eta_{5x1} & \eta_{5y1} & \eta_{5\theta 1} & \eta_{5x2} & \eta_{5y2} & \eta_{5\theta 2} \\ \eta_{6x1} & \eta_{6y1} & \eta_{6\theta 1} & \eta_{6x2} & \eta_{6y2} & \eta_{6\theta 2} \end{bmatrix} \begin{Bmatrix} P^*_{x1}(t) \\ P^*_{y1}(t) \\ P^*_{\theta 1}(t) \\ P^*_{x2}(t) \\ P^*_{y2}(t) \\ P^*_{\theta 2}(t) \end{Bmatrix} \tag{2.8}$$

For an idealized case of twin square buildings and six modal shapes shown in Fig. 2.1, Eq. (2.8) can be significantly simplified if the modes are assumed to be linearly dependent on the vertical ordinate z. After incorporating Eq. (2.3) in Eq. (2.8) the time series of the coupled modal loading $P^*_{cj}(t)$ can be expressed in terms of the time series of the measured sway and torsional base moments M_{sn}.

$$\begin{Bmatrix} P_{c1}^*(t) \\ P_{c2}^*(t) \\ P_{c3}^*(t) \\ P_{c4}^*(t) \\ P_{c5}^*(t) \\ P_{c6}^*(t) \end{Bmatrix} = \begin{bmatrix} 1 & 0 & 0 & 1 & 0 & 0 \\ 0 & 1 & 0 & 0 & 1 & 0 \\ 0 & 1 & 0 & 0 & -1 & 0 \\ 1 & 0 & 0 & -1 & 0 & 0 \\ 0 & 0 & \lambda & 0 & 0 & \lambda \\ 0 & 0 & \lambda & 0 & 0 & -\lambda \end{bmatrix} \begin{Bmatrix} M_{y1}(t)/H \\ M_{x1}(t)/H \\ M_{\theta 1}(t) \\ M_{y2}(t)/H \\ M_{x2}(t)/H \\ M_{\theta 2}(t) \end{Bmatrix} \tag{2.9}$$

Subsequently, the wind-induced modal accelerations of structurally coupled twin buildings can be computed, in a manner similar to that for an isolated building. Using white noise approximation, the standard deviation of the resonant modal acceleration is given by

$$\sigma_{\ddot{q}_{cjr}} = \frac{1}{m_{cj}^*}\sqrt{\frac{\pi f_{cj} S_{P_{cj}^*}(f_{cj})}{4\zeta_j}} \tag{2.10}$$

where f_{cj} is the coupled modal frequency in the j-th mode; $S_{P_{cj}^*}(f_{cj})$ is the power spectral density of the coupled modal loading; and ζ_j is the structural damping ratio.

The modal contribution, in the j-th mode and s-direction, to the peak rooftop acceleration of the n-th building is given by

$$\hat{a}_{jsn} = g_j \sigma_{\ddot{q}_{cjr}} \Phi_{jsn} \tag{2.11}$$

where g_j is the peak factor in the j-th mode.

To determine the coupled wind-induced acceleration for primary structural directions, $\hat{a}_{cs}$, from the calculated modal peak wind responses, the modal combination including cross-modal coupling is employed. In the present study, the CQC (complete quadratic combination), Wilson et al. (1981), is applied and the directional peak accelerations are computed as follows

$$\hat{a}_{cs} = \sqrt{\sum_{j=1}^{6}\sum_{m=1}^{6} \hat{a}_{jsn}\hat{a}_{msn}\rho_{jm}} \tag{2.12}$$

where a_{jsn} and a_{msn} are, respectively, the modal peak accelerations of the n-th building, associated with the s-direction of the j-th and m-th modes. The cross-modal coefficient ρ_{jm} between the j-th and m-th modes is expressed as

$$\rho_{jm} = \frac{8\zeta^2(1+r_{jm})r_{jm}^{1.5}}{(1-r_{jm}^2)^2 + 4\zeta^2 r_{jm}(1+r_{jm})^2} \tag{2.13}$$

where ζ is the structural damping ratio and r_{jm} denotes the frequency ratio, f_{cj}/f_{cm}.

Finally, total peak acceleration at the roof-top corner of the building is determined

$$\hat{a}_{total} = \sqrt{\hat{a}_{cx}^2 + \hat{a}_{cy}^2 + \hat{a}_{c\theta}^2 - \sqrt{2}\hat{a}_{cx}\hat{a}_{cz} + \sqrt{2}\hat{a}_{cy}\hat{a}_{c\theta}} \tag{2.14}$$

2.3 Experimental details and data processing

2.3.1 Dual force balance system and models

The dual force balance system employed in the present study consisted of two high-frequency six-component force balances and two data acquisition boards coupled by a synchronizing cable installed in a personal computer. This arrangement allowed for synchronized acquisition of the data from the two balances, needed for evaluation of the structural coupling effects on the wind induced response of tall twin buildings. Light-weight models of tall buildings arranged in various twin-building configurations were attached to the balances. A modular support of the models and the force balances was developed to sustain high resonant frequency of the system and to facilitate versatile adjustment in the relative position of and spacing between the models. A close-up view of the balances and the support system, as well as overall views of the model of the tested twin-building configuration with a skybridge are shown in Fig. 2.2.

Twin buildings of fixed square plan and five aspect ratios (height-to-planar dimension), ranging from 4 through 8, were considered. The geometrical scale was 1:500. The models were 7.6 cm x 7.6 cm in cross section and they were made of thin sheets of balsa wood. The spacing between the adjacent (parallel) facades of the models was kept constant, 5 cm. A skybridge located at the building mid-height was modeled using two pieces of solid balsa wood. Each piece was attached to one of the (two) model buildings and a small gap between these pieces was maintained to ensure acquisition of unbiased wind loading exerted on each model. An overall view of a representative twin-building model, mounted on the dual-force balance system and installed in the Meteorological Wind Tunnel (MWT) at WEFL, Colorado State University, is included in Fig. 2.2.

For reference (in discussion of the results), one of the buildings was denoted the primary building and was labeled as B1, while the remaining building was labeled B2. This notation and the definitions of the coordinate systems and the wind direction are displayed in Fig. 2.3. The geometrical parameters of the considered prototype tall buildings are listed in Table 2.1.

2.3.2 Approach flow

Wind tunnel testing was carried out in the MWT, in the ABL (atmospheric boundary layer) flow representative for suburban wind exposure (with power exponent $\alpha = 0.21$), modeled at a 1:500 geometrical scale. Passive devices (spires and barriers) similar to those used in past studies of tall buildings, carried out at WEFL, were used in combination with a long upstream fetch of floor roughness.

Fig. 2.4 shows the mean velocity and the along-wind turbulence intensity profiles, and the along-wind velocity spectrum at the prototype height of 50 m, acquired immediately upstream of the model, with the model removed from the turn-table. The measured spectrum is compared with the empirical velocity spectra proposed by Kaimal and Tieleman.

2.3.3 *Data acquisition and analysis*

The wind-induced base loadings – the overturning (sway) and torsional moments and shear forces – were acquired for the two buildings at 19 wind directions with a 10^{o}-interval in the wind azimuth. The resonant frequency of the force balance with an attached building model varied depending on the model height. Its lowest value (corresponding to the tallest model) was 86 Hz. A typical record of the acquired data comprised 16384 data points per segment, sampled at 2000 samples per second. The corresponding full-scale record length of the data was 10 minutes. Thirty six segments of the data were acquired for each wind direction. Segment and two-point frequency averaging was carried out during calculation of the wind loading power spectra. As a result, the normalized spectral error, Bendat and Piersol (2000), was approximately equal to 12%.

The data analysis discussed in Section 2.2 was employed to process the measured aerodynamic loading and to determine the coupled dynamic responses of the considered twin buildings. Wind-induced rooftop corner accelerations associated with the assumed building damping ratio of 1.5%, gross mass density of 200 kg/m^3, and 1-year return period were determined.

For comparison, an uncoupled case was also considered. For this case, three uncoupled modes, linearly dependent on the vertical ordinate z were assumed. Two modes were translational (in the x- and y-directions) and the third mode was torsional (about z-axis). It should be noted that a set of six idealized (linear) modes of vibration, shown in Fig. 2.1, was employed in the coupled case.

For the uncoupled cases, the fundamental natural frequencies listed in Table 2.2 were determined using empirical formulae proposed by Lagomarsino (1993). Based on feedback received from structural engineering consultants, these frequencies were adjusted to account for structural coupling, see Table 2.3, and the adjusted values were used in the response calculations carried out for the coupled case.

2.4 Results and discussion

2.4.1 Comparison of modal wind loading spectra

Representative normalized power spectra of the modal aerodynamic loading, for a twin-building configuration comprising of buildings of the 8:1 aspect ratio (denoted TBS8 in Table 2.1), are shown in Fig. 2.5, wind direction of 0^{o} (see Fig. 2.3). The results for the uncoupled, Fig. 2.5(a), and coupled, Fig. 2.5(b), cases are presented. Of principal interest in this comparison were the loading spectra in the frequency range of importance in serviceability analyses, shown shaded in Fig. 2.5.

In this range, the uncoupled spectra for the along-wind (x) and torsional (θ) loading components of the downwind building B1 are higher than those for the upwind building B2. This difference is attributed to unsteadiness in the wake generated by the upstream building B2. In the cross-wind (y) direction, the spectra on the two buildings are approximately the same.

A similar comparison carried out for the coupled case reveals that the coupled spectra in the along-wind (x) and torsional (θ) directions are approximately the same spectral levels for the two contributing modes – 1 and 4 for the x-direction, and 5 and 6 for the θ-direction. In the cross-wind (y) direction, the spectrum is higher for mode 2, associated with the in-phase motion, than that for the "out-of-phase" mode 3.

2.4.2 Uncoupled response

Four critical wind directions that were identified in analysis of the wind-induced top-floor accelerations of the considered twin-building configurations are indicated in Fig. 2.6, cases (a) through (d). The peak accelerations of uncoupled buildings B1 and B2 are presented in Figs. 2.7 and 2.8, respectively. In case (a) – wind aligned with the twin buildings – no shielding effects are exhibited and the accelerations of the downwind building B1 are higher than those of the upwind building B2. For cornering winds – cases (b) and (d) – the accelerations of the upwind building are higher than those of the downwind building – by up to 50% in the x- and θ-directions. For the normal wind direction – case (c) – the peak accelerations of the two buildings are very similar. These results are in agreement with the aerodynamic interference effects reported by Bailey and Kwok (1985), Huang and Gu (2005), and others.

The above findings indicate that in absence of structural coupling the wind-induced responses of the two buildings are different and this disparity depends on the wind direction and on the aspect ratio.

2.4.3 Coupled response

Fig. 2.9 shows modal contributions to the peak acceleration of the building roof corner. It can be seen that, depending on the wind direction, either the modal peak responses generated by in-phase building motions (the first, second, and fifth modes) or those associated with out-of-phase motions (the third, fourth, and sixth modes) are dominant. For wind aligned with the twin buildings (wind direction of 0 and 180 degrees), the dominant contribution of the second mode (in cross-wind direction) is clearly displayed in Fig. 2.9. It can be seen that this modal participation significantly increases with a rise in the building aspect ratio.

The modal peak accelerations in Fig. 2.9 were subsequently used to calculate the directional top-floor peak accelerations (as discussed in Section 2.2), see Fig. 2.10. As expected, the accelerations increase with the building aspect ratio and they are dependent on the wind direction. All the acceleration components exhibit large values in vicinity of wind directions of 0° and 180°. This is in contrast with small magnitudes occurring in vicinity of wind directions of 30° and 150°. For the remaining wind directions, the acceleration magnitudes of the x- and θ-components are moderate to large and they exhibit strong dependence on the aspect ratio. In the y-direction, they are smaller and less dependent on the aspect ratio.

2.4.4 Comparison of coupled and uncoupled responses

A comparison of the results obtained for the coupled and uncoupled cases is presented in Figs. 2.11 through 2.13. The coupled-to-uncoupled response ratios are shown in Figs. 2.11 and 2.12, respectively for buildings B1 and B2. It can be seen that for wind directions associated with significant aerodynamic interference effects – cases (a), (b) and (d) in Fig. 2.6 – the peak accelerations are reduced (in one or more components) by up to 30%, in presence of structural coupling. For the wind direction of 90°, case (c), the coupled and uncoupled peak accelerations are similar, in all the components.

The overall effects of structural coupling on the total peak accelerations of the top-floor roof corner can be inferred from Fig. 2.13. It is shown that the largest wind-induced response – building B1 at the wind direction of 0° and building B2 at 180° – can be reduced by up 30%. This reduction is accompanied by an increase in the response of the companion building. As a result, the response equalization is achieved and the largest response is significantly reduced when structural coupling is included. These findings are in agreement with the results for tall twin buildings with a skybridge, reported by Xie and Irwin (1998, 2001).

2.5 Concluding remarks

The findings of this investigation can be summarized as follows:

(1) The aerodynamic response – peak acceleration of top floor corner – of twin buildings was significantly affected by aerodynamic interference and structural

coupling. These effects were dependent on the wind direction and building aspect ratio.

(2) In the absence of structural coupling, the top floor accelerations were the largest for the downwind building and wind aligned with the twin buildings. For cornering winds, the upwind building exhibited a moderately bigger response than the downstream building. Small differences in the responses were observed for wind normal to the twin buildings.

(3) Structural coupling of buildings in twin arrangement (with skybridge) led to equalization of the response of the buildings. Effectively, the largest response of the buildings was reduced by approximately 30%. These observations are in agreement with findings reported by Xie and Irwin (1998, 2001).

(4) In view of significant potential benefits, structural coupling should be taken into account in wind-resistant design of twin tall buildings.

(5) In practice, inclusion of structural coupling increases complexity of design. Systematic fundamental and applied studies are needed to improve the understanding of this subject and to aid development of optimized framework for wind-resistant design of twin tall buildings and other building complexes involving structural coupling.

2.6 References

Bailey, P.A. and Kwok, K.C.S. (1985), "Interference excitation of twin tall buildings", Journal of Wind Engineering and Industrial Aerodynamics, 21(3), 323-338.

Bendat, J.S. and Piersol, A.G. (2000), Random Data: Analysis & Measurement Procedures, 3rd Edition, Wiley-Interscience, NY, USA.

Boggs, D.W. and Hosoya, N. (2001), "Wind-tunnel techniques to address structures with multiple coupled interactions", In: Proceedings of Structures Congress 2001 – A Structural Engineering Odyssey, Washington, D.C., USA, pp. 8.

Huang, P. and Gu, M. (2005),"Experimental study on wind-induced dynamic interference effects between two tall buildings", Wind Structure, An International Journal, 8(3), 147-161.

Lagomarsino, S. (1993), "Forecast models for damping and vibration periods of buildings", Journal of Wind Engineering and Industrial Aerodynamics, 48(2-3), 221-239.

Wilson, E.L., Kiureghian, A. Der, and Bayo, E.P. (1981), "A replacement for the SRSS method in seismic analysis", Earthquake Engineering and Structural Dynamics, 9, 187-192.

Xie, J. and Irwin, P.A. (1998), "Application of the force balance technique to a building complex", Journal of Wind Engineering and Industrial Aerodynamics, 77-78, 579-590.

Xie, J. and Irwin, P.A. (2001), "Wind-induced response of a twin-tower structure", Wind Structure, An International Journal, 4(6), 495-504.

2.7 Figures

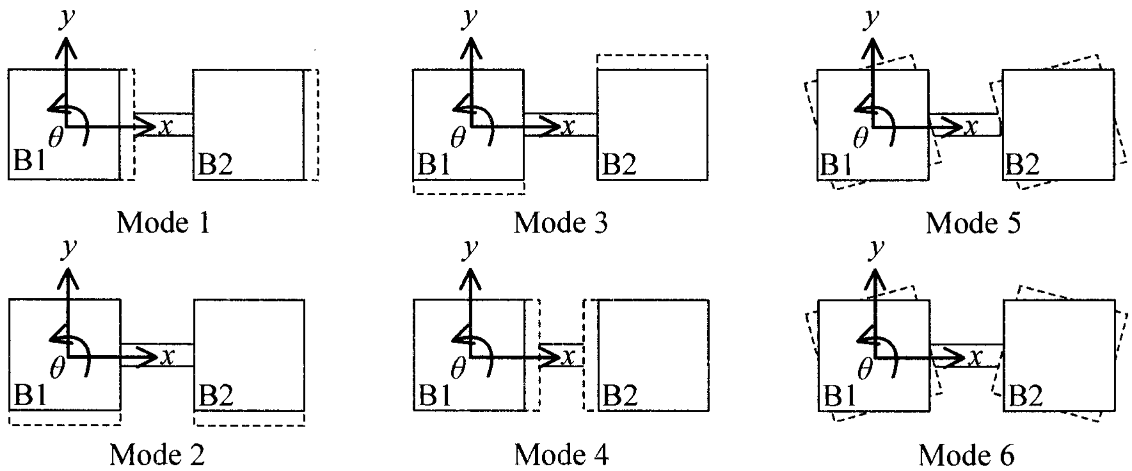

Fig. 2.1 Dominant natural modes of vibration, coupled twin buildings

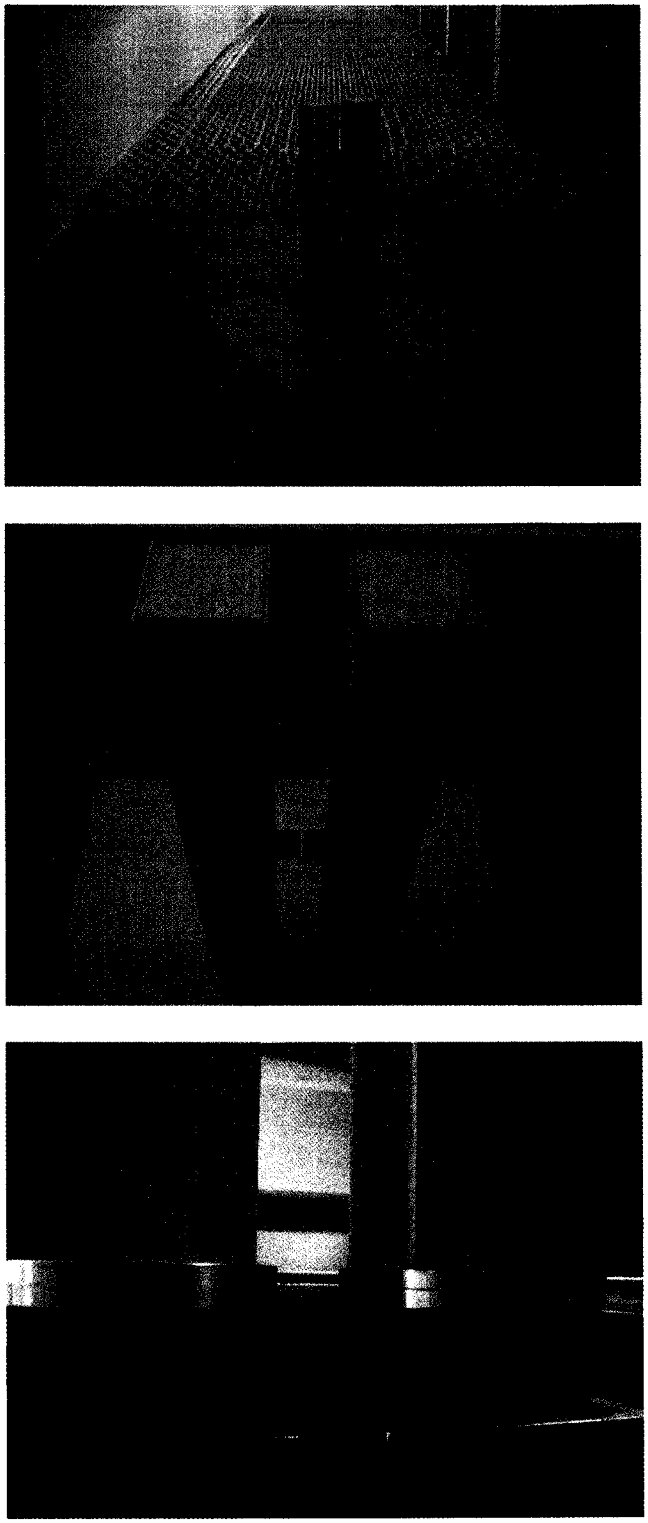

Fig. 2.2 Representative twin-building model and force balance system

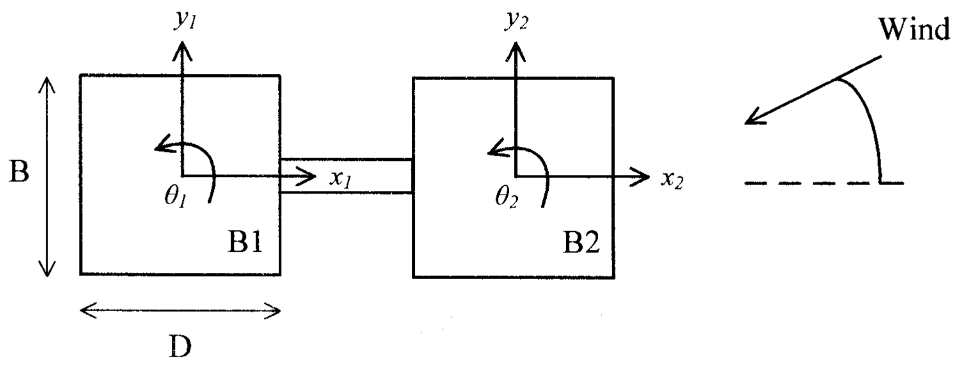

Fig. 2.3 Coordinate systems and wind direction

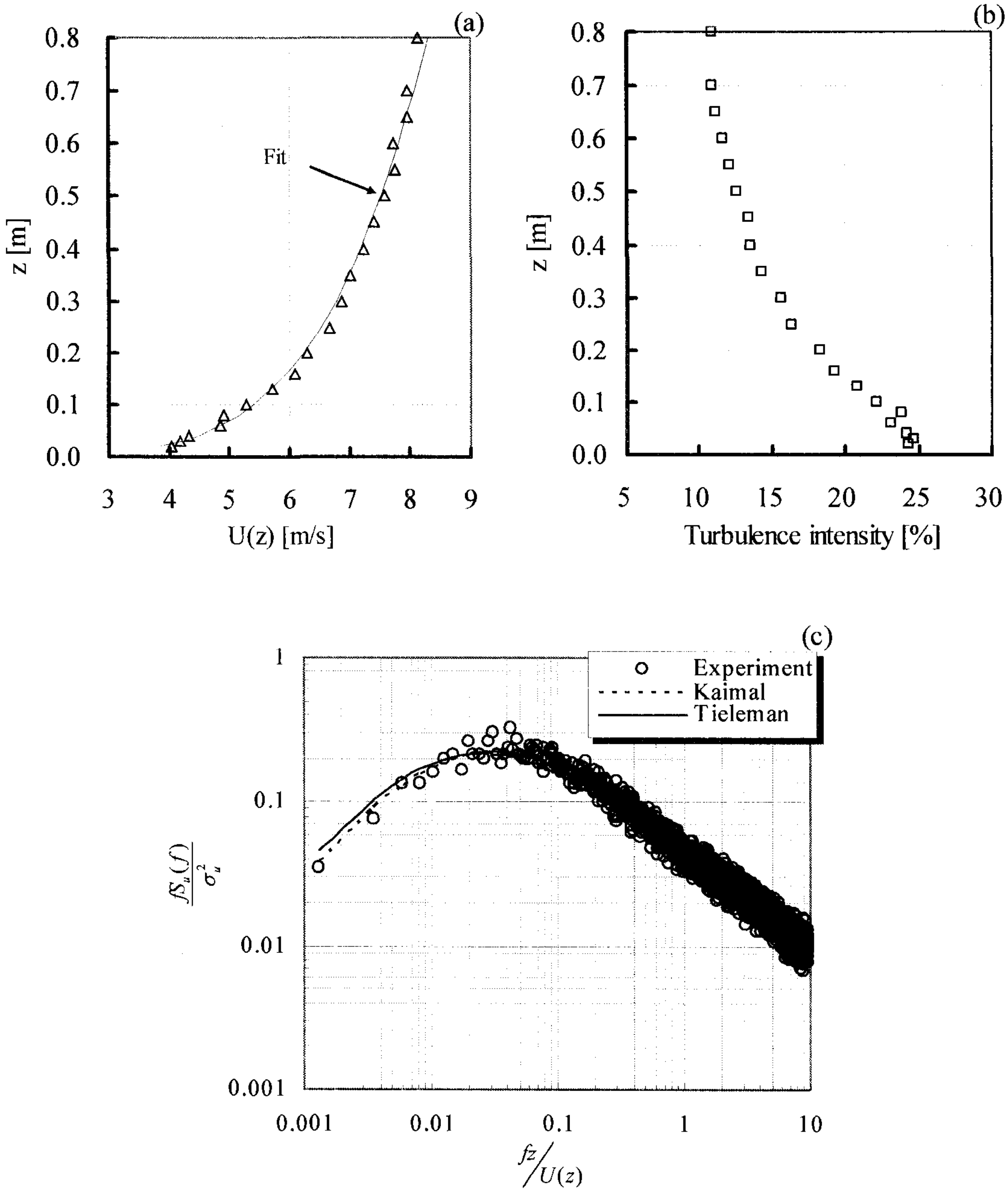

Fig. 2.4 Simulated approach flow: (a) mean wind velocity, (b) along-wind turbulence intensity and (c) along-wind velocity spectrum at prototype elevation $z = 50$ m

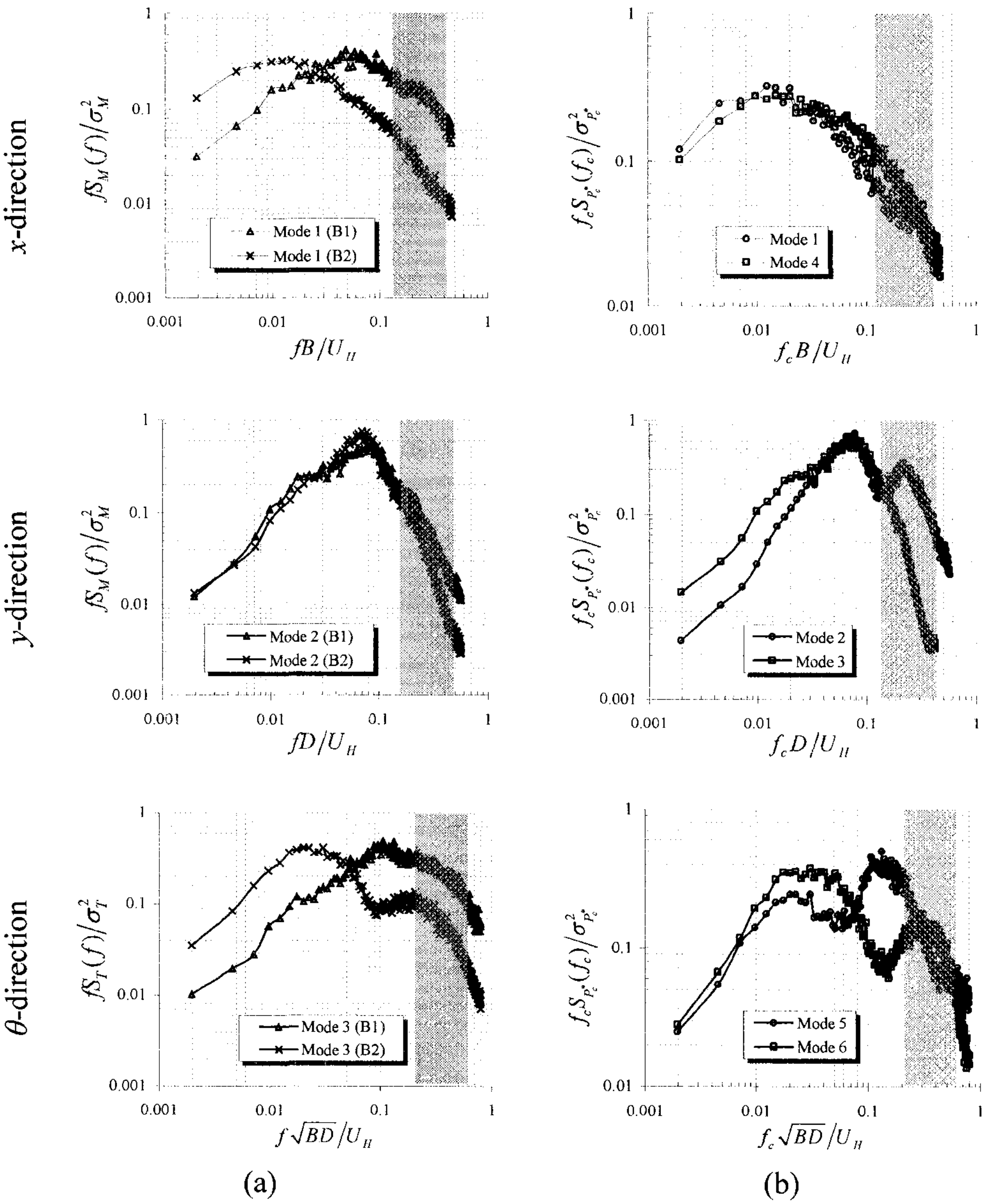

Fig. 2.5 Modal normalized power spectra of wind loading for TBS8, wind direction 0°: (a) uncoupled and (b) coupled cases

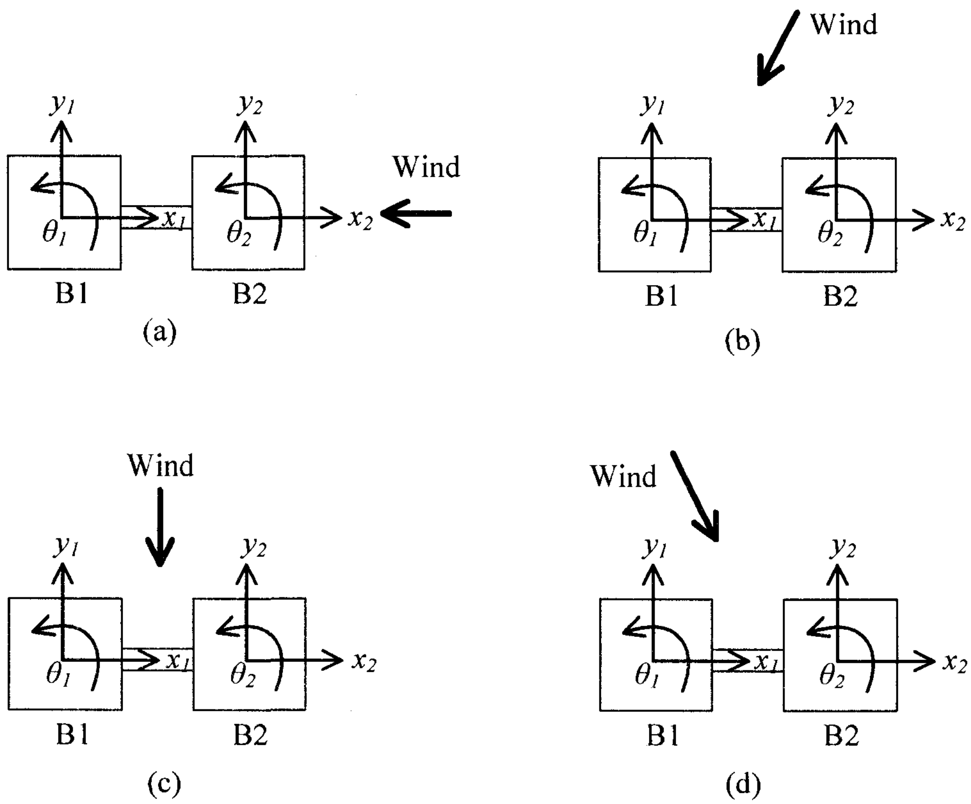

Fig. 2.6 Critical wind directions: (a) 0°, (b) 60° ~ 80°, (c) 90° and (d) 100° ~ 120°

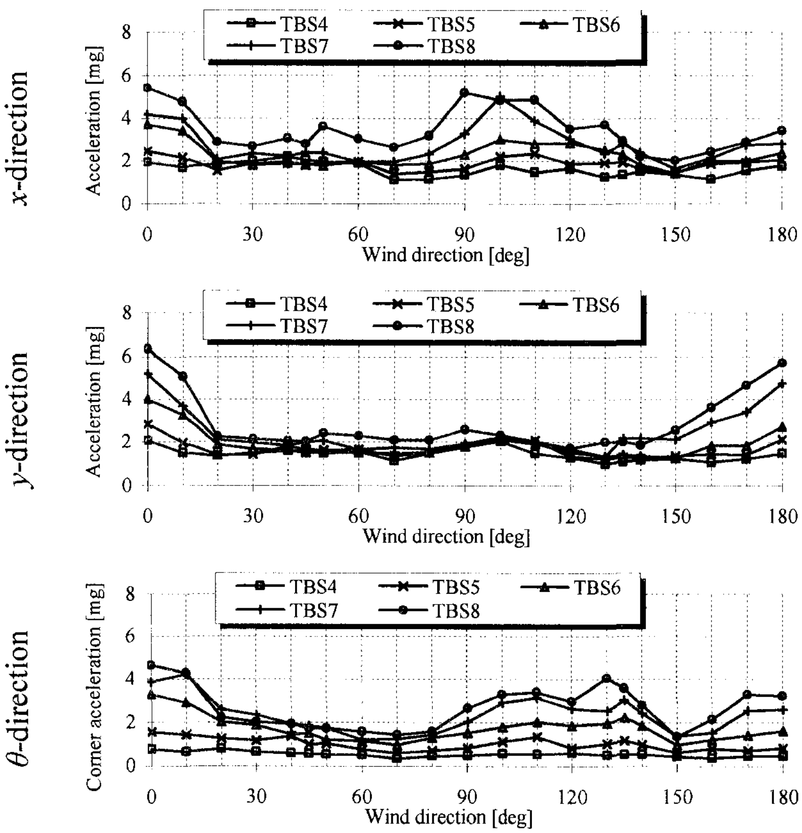

Fig. 2.7 Peak accelerations of B1, uncoupled case

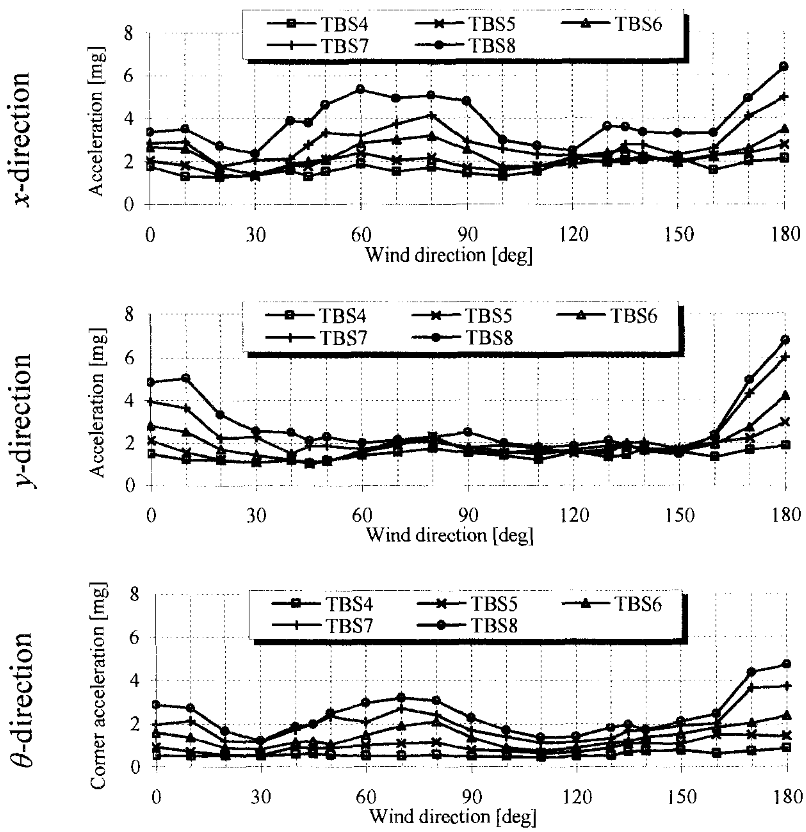

Fig. 2.8 Peak accelerations of B2, uncoupled case

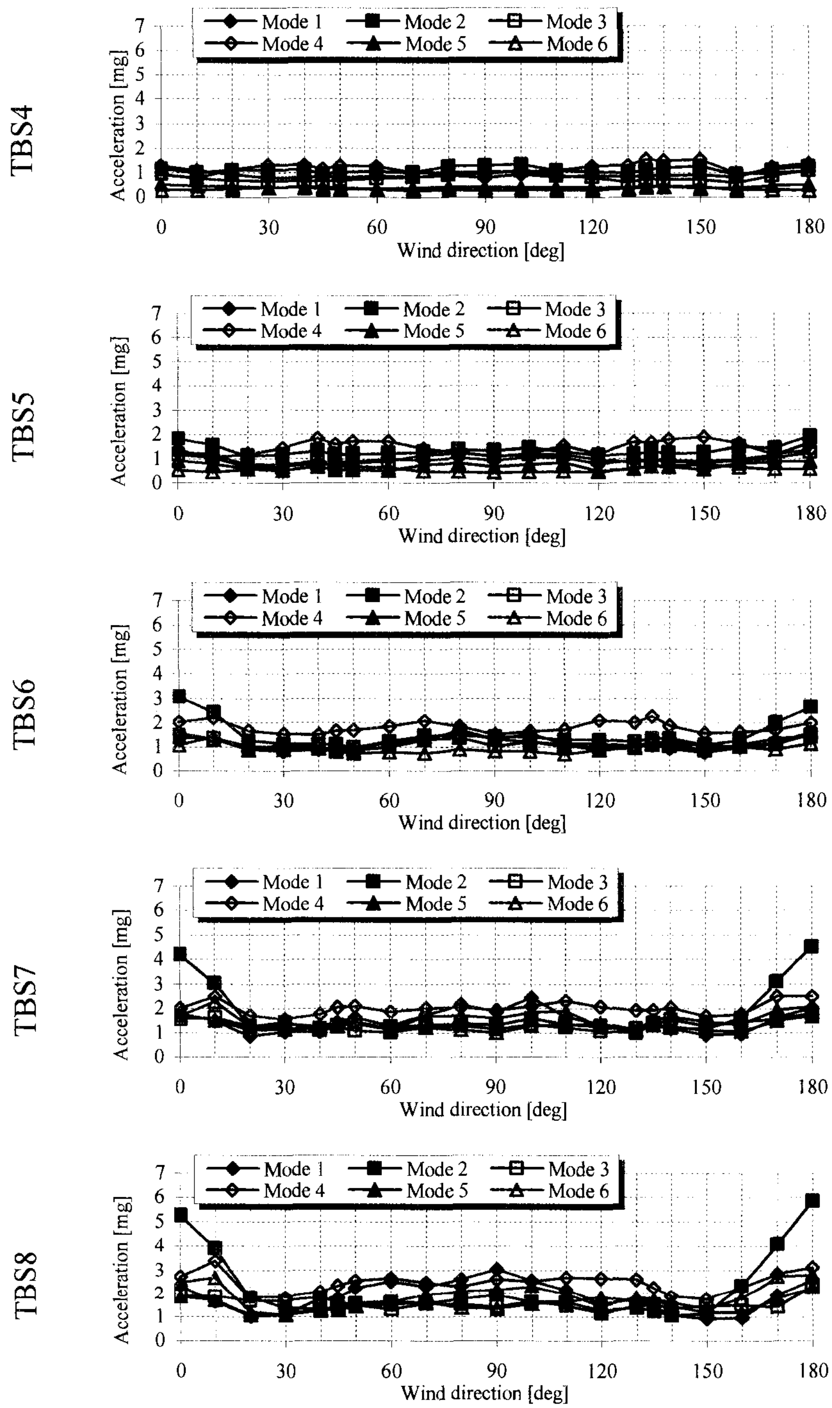

Fig. 2.9 Modal contributions to peak acceleration, coupled case

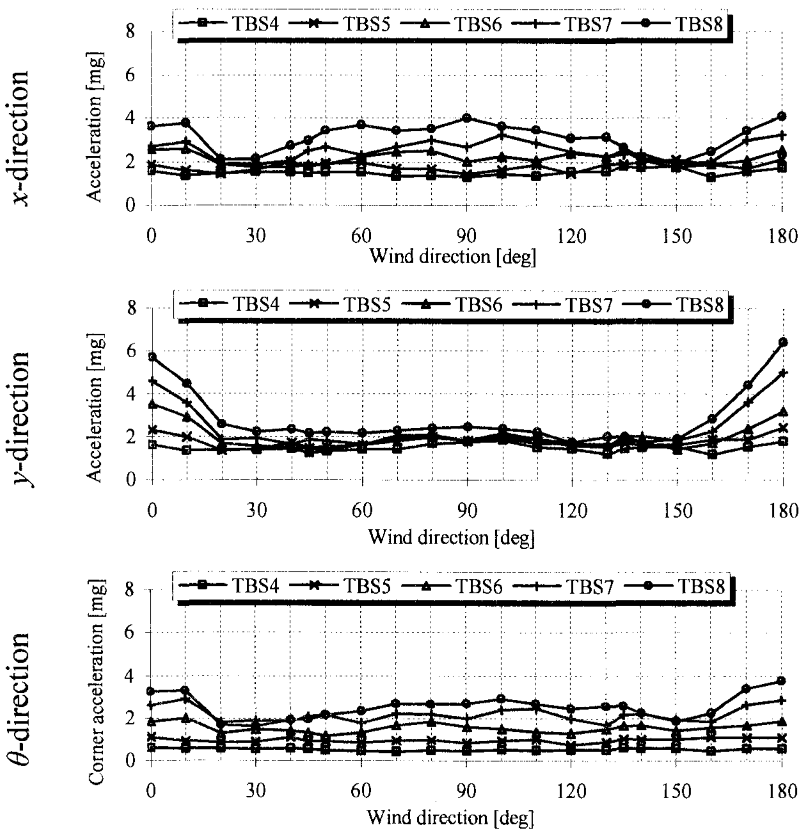

Fig. 2.10 Peak accelerations, coupled case

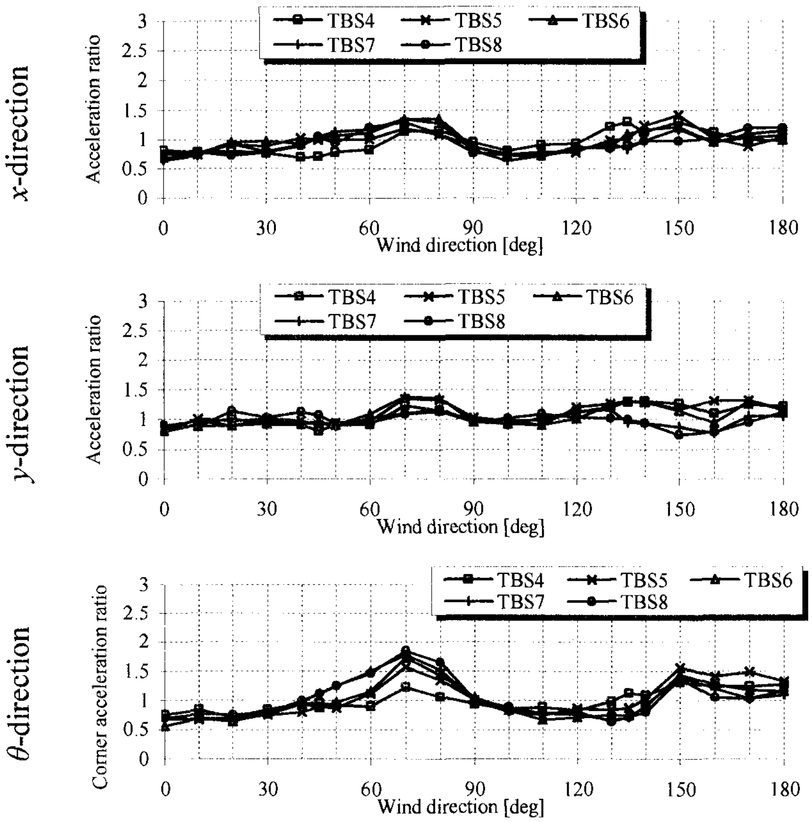

Fig. 2.11 Coupled-to-uncoupled acceleration ratios, building B1

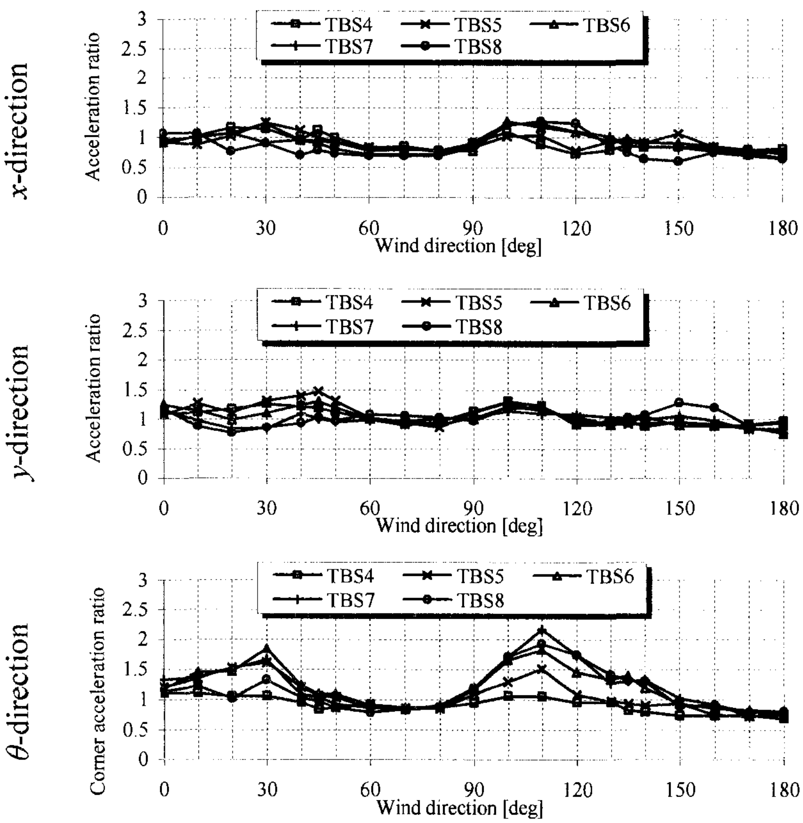

Fig. 2.12 Coupled-to-uncoupled acceleration ratios, building B2

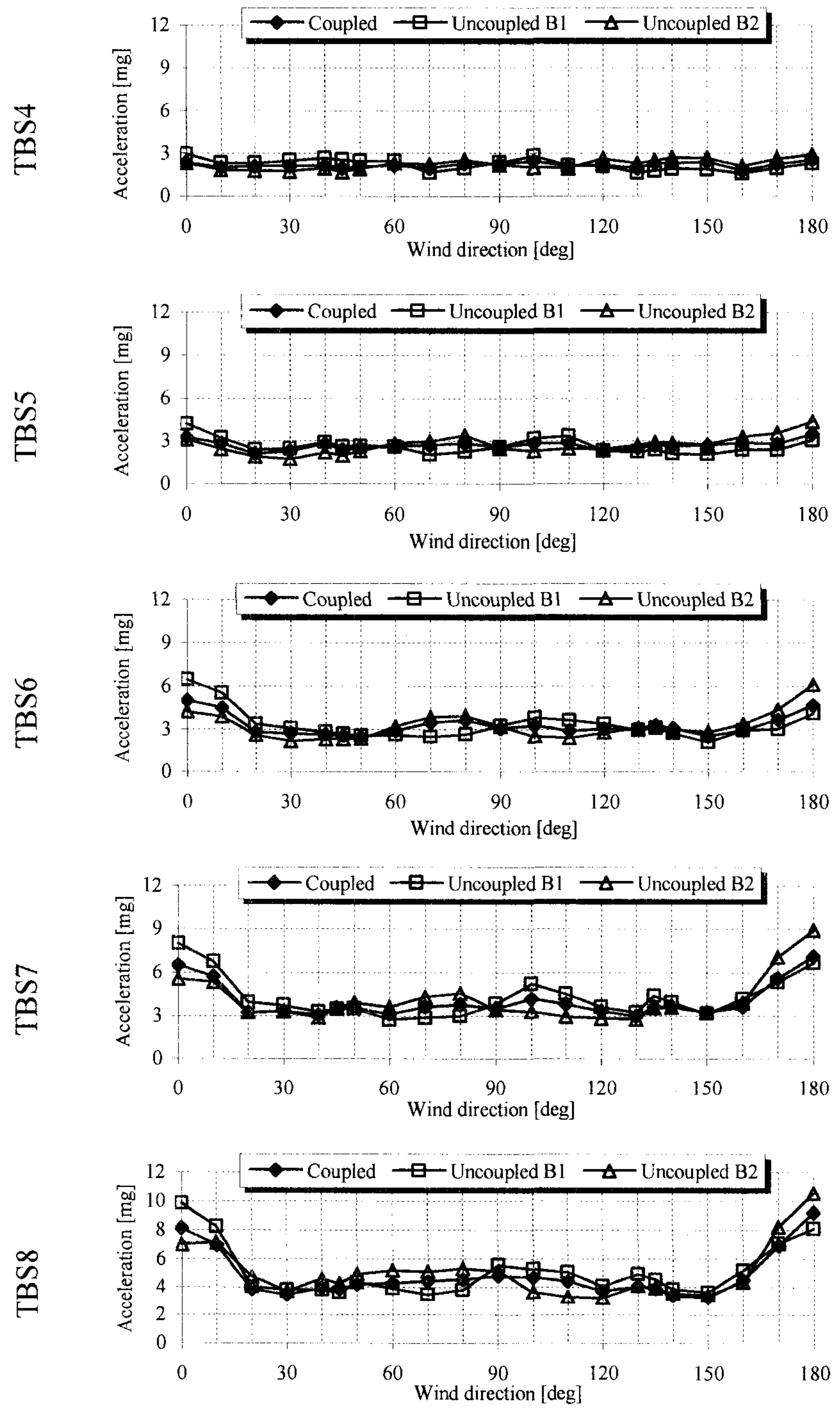

Fig. 2.13 Comparisons of total peak accelerations, top-floor corner

2.8 Tables

Table 2.1 Geometrical properties of prototype buildings

Building model	Planar dimension (m)	Height (m)	Side ratio	Aspect ratio
TBS4	38	152	1	4
TBS5	38	191	1	5
TBS6	38	229	1	6
TBS7	38	267	1	7
TBS8	38	305	1	8

Table 2.2 Natural frequencies of uncoupled vibration of prototype buildings (Hz)

Building model	f_x	f_y	f_θ
TBS4	0.3	0.3	0.45
TBS5	0.25	0.25	0.37
TBS6	0.21	0.21	0.31
TBS7	0.18	0.18	0.27
TBS8	0.16	0.16	0.24

Table 2.3 Natural frequencies of the lowest six modes of coupled prototype tall buildings (Hz)

Model	Mode 1	Mode 2	Mode 3	Mode 4	Mode 5	Mode 6
TBS4	0.3	0.31	0.33	0.38	0.45	0.5
TBS5	0.25	0.26	0.28	0.33	0.37	0.4
TBS6	0.21	0.22	0.24	0.27	0.31	0.34
TBS7	0.18	0.19	0.21	0.24	0.27	0.29
TBS8	0.16	0.17	0.19	0.22	0.24	0.26

CHAPTER 3

CORRELATION AND COHERENCE OF WIND LOADING ON TALL TWIN BUILDINGS IN CLOSE PROXIMITY

Chapter 3 has been presented during the 4th International Conference on Advances in Wind and Structures and submitted for publication to Wind and Structures, International Journal.

3.1 Introduction

Design of modern tall buildings involves evaluation of the effects of surrounding tall structures on the aerodynamic response of the building under consideration. For the past three decades, a host of generic studies addressing such interference effects have been reported in open literature. Saunders and Melbourne (1979), To and Lam (2003), and Huang and Gu (2005) have evaluated these influences by examining aerodynamic loading on or wind-induced response of a primary (instrumented) building in the presence of interfering (dummy) building or buildings. Thoroddsen et al. (1988) and Ni et al.

(2001) have addressed the significance of correlation between the components of wind loading on tall buildings.

The above efforts have significantly improved understanding of wind loading on and aerodynamic response of tall buildings surrounded by other buildings or structures of comparable height. Most of the reported studies have been based on wind tunnel data obtained using a single high-frequency force balance (HFFB). Application of such data for cases involving tall twin buildings in close proximity is limited since buildings in such configurations may be structurally linked. This limitation is overcome when a dual-HFFB (DHFFB) is used to measure the aerodynamic loading (Boggs and Hosoya 2001, Xie and Irwin 2001, and Lim and Bienkiewicz 2007).

In the presence of structural coupling, a precise mapping of the inter-building wind loading correlations and coherences is needed for accurate prediction of the building aerodynamic response. Current understanding of these parameters and their effects on the building response is incomplete due to the complexity of the problem and limited number of related investigations and data published in open literature.

In this chapter, an experimental study of the correlations and coherences of wind loading components on twin tall buildings is presented. First, the experimental set-up, building models and instrumentation are described. Then, the representative results, the correlation and coherence of various wind loading components, are discussed. These properties were computed for the wind loading components exerted on the same building (they are denoted hereafter as building correlations and coherences) and for the loading components on the two buildings (denoted hereafter as inter-building correlations and coherences). The results obtained for each building of the twin building configuration are compared with those for an isolated tall building case. The findings of this study are summarized in the concluding section of this chapter.

3.2 Experimental set-up

3.2.1 Dual-HFFB system

A dual-HFFB (DHFFB) system developed at the Wind Engineering and Fluids Laboratory (WEFL) at Colorado State University (CSU) was used in measurements of base wind-induced loading on models of two buildings in close proximity. It consisted of two high-frequency force balances (ATI Inc., Model: Gamma US-15-50) and a mechanical support system. The balances were electronically synchronized to allow for simultaneous acquisition of the measurements from ten data channels – five components of the base wind loading – sampled from the two balances. The DHFFB was fastened to a rigid support system that was designed to accommodate precise and versatile modifications of the tested twin building configurations.

3.2.2 Flow simulation

The wind tunnel testing was carried out in a boundary-layer wind tunnel (the Meteorological Wind Tunnel) at WEFL. The ABL (atmospheric boundary layer) flow was modeled at a 1:500 geometrical scale. The approach flow represented a wind exposure with a power law exponent of 0.21. The turbulence intensity at the building rooftop level was 12%. Further details on the technique employed in modeling of this flow and on the flow properties were presented by Lim and Bienkiewicz (2007).

3.2.3 Twin building configurations

The considered twin building (TB) configuration comprised of two identical buildings, 38 m x 38 m in plan and 305 m in height. Fig. 3.1 shows the coordinate system and the grid used to define the relative positions of the buildings. During the wind tunnel testing, the position of the interfering building B1 was varied, while the location of the primary building B2 was kept unchanged. As indicated in Fig. 3.1, the minimum and maximum normalized x- and y-distances between the centers of the buildings were respectively 1.66 and 3. The wind tunnel testing described in this study was carried out for the wind direction aligned with the x-axis, as depicted in Fig. 3.1.

3.2.4 Data acquisition

The wind-induced base moments and torques exerted on the two building models were simultaneously acquired at a sampling rate of 2000 data samples per second. Thirty six segments of the data, each comprising of 16384 data points, were acquired for the considered (relative) spacing of the buildings. The collected data were subsequently used to calculate the building and inter-building correlations and coherences of the components of the base wind loading.

3.3 Loading correlation matrix

The wind loading correlations and coherences discussed in this study are schematically indicated using a 6 x 6 symmetric matrix shown in Fig. 3.2. In presence of the structural coupling between the buildings, the off-diagonal elements of the loading correlation matrix could be pivotal in predictions of the building response and they should be retained in calculations. Herein they are divided into the following three groups: (a) the correlations between loading components on each building, (b) the correlations between the same loading components on the two buildings and (c) the correlations between different loading components on the two buildings. These groups are schematically depicted in Fig. 3.2. The first group is denoted as the "building coupling" of wind loading components, while the second and the third are labeled as the "inter-building coupling". Overall, these correlations are the result of the flow-structure interaction commonly termed as the aerodynamic coupling (Lim and Bienkiewicz, 2008).

3.4 Results and discussion

3.4.1 Building correlations

Fig. 3.3 presents the correlation coefficients (ρ) of the crosswind (*Mx*), alongwind (*My*) and torsional (*Mz*) loading components on the buildings B1 and B2. The relative orientation of the buildings and the wind loading components involved in the correlations (marked in boldface) are schematically indicated in inserts in Fig. 3.3, see also Fig. 3.1.

Vector notation is used to denote the sway moments *Mx* and *My*. The crosswind moment (*Mx*) denotes the overturning moment about *x*-axis, while alongwind moment (*My*) indicates the overturning moment about *y*-axis. The borders of zones (of locations of building B1) exhibiting high correlations are marked using dashed lines.

As can be observed in Figs. 3.3(a) and 3.3(b), the magnitude of the crosswind-alongwind building correlation coefficients (ρ_{Mx1y1} and ρ_{Mx2y2}) was large, up to 0.45, at some locations of the interfering building B1, e.g. (X/D, Y/D) = (1, 1.66) for loading on building B1 (ρ_{Mx1y1}) and (X/D, Y/D) = (0.33, 1.66) for loading on building B2 (ρ_{Mx2y2}). However for most of the configurations these coefficients were lower than 0.2. The crosswind-torsional correlations (ρ_{Mx1z1} and ρ_{Mx2z2}), Figs. 3.3(c) and 3.3(d), were at most locations lower than the crosswind-torsional correlation for the single building (SB) case, discussed below. For building B1, the highest magnitude of correlation (0.54) was observed for Y/D = 0, see Fig. 3.3(c), while for building B2 the highest value of ρ_{Mx2z2} was 0.62 and it occurred when building B1 was located at (X/D, Y/D) = (1.66, 0), Fig. 3.3(d). At some locations the correlation magnitude was small. It was found that the alongwind and torsional loadings (*My* and *Mz*) on both the buildings were highly correlated (ρ_{My1z1} and ρ_{My2z2}). The highest magnitude of ρ_{My1z1} (0.54) was observed for building B1 located at (X/D, Y/D) = (0.66, 2), Fig. 3.3(e). The largest observed value of ρ_{My2z2} was 0.66 and it occurred when building B1 was upstream of B2 and Y/D = 0.66, see Fig. 3.3(f). These results indicate that, depending on relative positions of the buildings, all the wind loading components on each building can be strongly correlated (aerodynamically coupled).

The above findings are contrast to an isolated (single) building (SB) case, where for buildings of generic (prismatic) geometry only the crosswind-torsional correlation (ρ_{Mxz}) is significant. For such a case, representative values of the correlation coefficients, used herein as the reference values, were determined by the authors, Lim et al. (2006), during a related wind tunnel study carried out at WEFL. Their magnitudes were 0.02, 0.53 and 0.13, respectively, for the alongwind-crosswind (ρ_{Myx}), crosswind-torsional (ρ_{Mxz}) and alongwind-torsional (ρ_{Myz}) components. Similar values were reported by Tallin and Ellingwood (1985) and Makino and Mataki (1993).

3.4.2 Inter-building correlations

As defined in Section 3.1, the correlations of wind loading components on the two buildings are labeled as inter-building correlations. For the same components, these correlations are presented in Fig. 3.4. As can be seen, for the crosswind components (*Mx1* and *Mx2*), very high correlation ρ_{Mx1x2} (the magnitude of 0.68) was obtained when the two buildings were aligned with wind (X/D > 1.66, Y/D < 0.33), a dashed region in Fig. 3.4(a). In the remaining region, the correlation was significantly lower. An opposite trend was observed for the alongwind correlation (ρ_{My1y2}), Fig. 3.4(b). The high correlation occurred for Y/D > 1.33, with the largest value of approximately 0.83. In the case of the torsional components (*Mz1* and *Mz2*), Fig. 3.4(c), the largest correlation ρ_{Mz1z2} = 0.54 was found when the building B1 was located upstream of B2 (X/D = 2, Y/D = 0.66). These results suggest that the same loading components induced on the two buildings in close proximity may be strongly coupled.

Fig. 3.5 shows the inter-building correlations of different loading components. As can be seen in Fig. 3.5(a), the crosswind component on building B1 was highly correlated with the alongwind component on building B2, and the magnitude of ρ_{Mx1y2} reached up to 0.55. On the other hand, the alongwind-crosswind correlation (ρ_{My1x2}), Fig. 3.5(b), was very low, except for (X/D, Y/D) = (0, 1.66).

In the case of the alongwind-torsional correlations ρ_{My1z2}, Fig. 3.5(c), and ρ_{Mz1y2}, Fig. 3.5(d), the highest magnitude of the coefficient was 0.63 and it occurred when building B1 was placed upstream of B2 (X/D, Y/D) = (2.33, 1). For Y/D < 0.33 the correlations were negligible (< 0.2). The largest magnitude of the crosswind-torsional correlations (ρ_{Mz1x2} and ρ_{Mx1z2}, Figs. 3.5(e) and 3.5(f)) was 0.61 and it occurred when the building B1 was located upstream of B2 (X/D < 2.33, Y/D < 0.33) for ρ_{Mz1x2}, Fig. 3.5(e), and (X/D < 2.33, 0.5 < Y/D < 1) for ρ_{Mx1z2}, Fig. 3.5(f). In addition, high correlation, ρ_{Mx1z2}, was observed at (X/D, Y/D) = (0.33, 2), Fig. 3.5(f).

The above results indicate high inter-building coupling between the same as well as different components of wind loading, on tall buildings in close proximity. Use of the DHFFB allows for accurate quantification of this coupling.

3.4.3 Critical building spacings

Fig. 3.6 schematically shows the locations of building B1 associated with the highest magnitude of the building and inter-building correlations. It can be seen that significant correlations, the magnitude of the correlation coefficient ranging from 0.37 through 0.83, are exhibited when building B1 is placed in the following (X/D, Y/D) regions: (1.66-2, 0), (1.66-2.33, 0.66), (0-1.33, 1.66) and (0.66, 2). These locations are within the range of interest in design of twin buildings and further analysis of wind loading was carried out for such cases. The coherences of the loading components are discussed next.

3.4.4 Wind loading coherences

The coherence is defined as

$$Coh_{Mxy}(f) = \frac{\left|S_{Mxy}(f)\right|}{\sqrt{S_{Mxx}(f)S_{Myy}(f)}} \tag{3.1}$$

where $S_{Mxx}(f)$ and $S_{Myy}(f)$ are, respectively, the power spectra of *Mx* and *My* components; and $\left|S_{Mxy}(f)\right|$ is the magnitude of the cross-power spectrum of *Mx* and *My*. Fig. 3.7 presents the crosswind-alongwind, Fig. 3.7(a), crosswind-torsional, Fig. 3.7(b) and alongwind-torsional, Fig. 3.7(c), coherences involving wind loading components on the same building. These coherences are denoted herein as the building coherences. The selected relative spacing of the buildings, indicated in parentheses, is associated with the highest magnitude of the correlation coefficient of a particular combination of the loading components. For comparison, the coherences obtained for a single building (SB) case are included. The shading in Fig. 3.7 (and Fig. 3.8) indicates the range of the reduced frequency, 0.12 through 0.5, of interest in design of typical twin tall buildings.

It can be seen in Fig. 3.7 that the alongwind-crosswind and alongwind-torsional coherences were overall higher than those for the SB case. For the moderate to high reduced frequencies, the crosswind-torsional coherences were similar to the coherence for the SB case, see Fig. 3.7(b). At low frequencies, a close agreement between the crosswind-torsional coherences on the upstream building B1 (*Mx1z1*) and the SB case is noteworthy. In passing, it should be pointed out that coherences for the SB case, displayed in Fig. 3.7 are in agreement with those reported by other researchers (Tallin and Ellingwood, 1985; Thoroddsen et al., 1988; Ni et al., 2001).

These results show that in addition to high crosswind-torsional coherence, each of the two buildings (in close proximity) experiences enhanced alongwind-crosswind and alongwind-torsional loading coherences. These coherences are negligible for the SB case.

3.4.5 Inter-building coherences

Fig. 3.8 shows the inter-building coherences – coherences involving the components of wind loading exerted on the two buildings. The selected locations correspond to the largest magnitudes of the appropriate correlation coefficients. It can be seen in Fig. 3.8(a) that the highest coherence of the same components exerted on the two buildings was obtained for the crosswind direction, while for the remaining directions (alongwind and torsional) the coherences were low.

The inter-building coherences involving pairs of wind components in differing directions are shown in Figs. 3.8(b) through 3.8(d). The alongwind-crosswind coherence, see Fig. 3.8(b), was significantly higher than that for the remaining wind loading combinations in Fig. 3.8. It is noteworthy that the frequency dependence of crosswind-torsional inter-building coherences in Fig. 3.8(d) was similar to that exhibited by the building coherence of the upwind building B1 (*Mx1z1*) and the SB case in Fig. 3.7(b).

The obtained correlation and coherence results are summarized in Table 3.1. The building and inter-building correlation coefficients and the average coherences are displayed, for locations of building B1 associated with the largest magnitude of the correlation coefficient, indicated in Fig. 3.6. The coherence averaging was carried out over the frequency range shown shaded Figs. 3.7 and 3.8. It can be seen that the crosswind-torsional average coherences on each building (building coupling) were close to a conservative value of 0.7 assumed by Tallin and Ellingwood (1985) and Chen and Kareem (2005). For some building spacings, the inter-building average coherence was significant. The inter-building average coherences of similar components were moderate for the alongwind (0.28) and torsional (0.22) directions. A high value (0.71) was observed for the crosswind direction. The maxima of the inter-building average coherences involving different loading components were: 0.61 for the along-crosswind, 0.33 for the along-torsional and 0.51 for the crosswind-torsional directions.

Based on the results presented in Table 3.1, two representative configurations of the overall highest average coherence were identified, see Fig. 3.9: (X/D, Y/D) = (1.66, 0.0) – two buildings aligned with the wind, and (X/D, Y/D) = (1.66, 0.66) – upwind building (B1) with an offset in the crosswind direction. The average coherences associated with these configurations are included in Fig. 3.9. The high level of the coherence (approximately equal or exceeding 0.45) is indicated using the boldface. As shown in Fig. 3.9(a), for the buildings aligned with the wind, the building and inter-building crosswind-torsional coherences were high (equal or exceeding 0.5). A similar (high) level was exhibited by the inter-building coherences of the loading components in the same direction. The remaining coherences were low, not exceeding 0.17. The average coherences of the remaining critical configuration, listed in Fig. 3.9(b), indicated a similar level of coupling of wind loading for the upstream building (B1) and a stronger coupling for the downstream building (B2). The inter-building loading coupling was weaker than that for the wind-aligned configuration, see Fig. 3.9(a).

The above results indicate that significant building and inter-building coherence of wind loading exists within the frequency range of interest. The implied aerodynamic coupling depends on the relative position of the buildings. This coupling should be carefully examined during evaluation of wind effects on tall buildings in close proximity.

3.5 Concluding remarks

The major findings of this study are summarized as follows:

(1) The alongwind loading was strongly coupled with the crosswind and torsional loadings induced on the same building of the twin building (TB) configuration. The observed correlation coefficients and the average coherences reached up to 0.66 and 0.59, respectively. These high values are in contrast with a case of an isolated building (SB), where the above couplings are significantly weaker.

(2) The crosswind-torsional correlation and coherence of loading on each building were approximately similar to those for the SB case. The maximum values of the correlation coefficient and the average coherence were 0.62 and 0.69, respectively.

(3) For some building spacings, the inter-building correlation (correlation involving wind loading components on the two buildings) was significant. The maxima of the inter-building correlation coefficient and the average coherence of similar components reached up to 0.83 and 0.71, respectively. For different loading components they were equal to 0.63 and 0.61, respectively.

(4) Ten configurations of high correlation coefficients of the wind loading components were identified. Examination of the average coherences associated with these configurations led to identification of two configurations of the strongest aerodynamic coupling: (a) two buildings aligned with the wind and (b) wind-aligned buildings with a crosswind offset of the upstream building.

(5) In view of the high correlations and coherences of the wind loading, the use of DHFFB is recommended in studies of wind effects of tall twin buildings with structural coupling.

(6) Systematic studies are needed to investigate the impact of the correlations and coherences of specific wind loading components on the aerodynamic response of tall buildings in close proximity.

3.6 References

Boggs, D.W. and Hosoya, N. (2001), "Wind-induced techniques to address structures with multiple coupled interactions", In: Proceedings of Structures Congress 2001 – A Structural Engineering Odyssey, Washington, D.C., USA, pp. 8.

Chen, X. and Kareem, A. (2005), "Coupled dynamic analysis and equivalent static wind loads on buildings with three-dimensional modes", Journal of Structural engineering, 131(7), 1071-1082.

Huang, P. and Gu, M. (2005),"Experimental study on wind-induced dynamic interference effects between two tall buildings", Wind Structure, An International Journal, 8(3), 147-161.

Lim, J. and Bienkiewicz, B. (2007), "Wind-induced response of structurally coupled twin tall buildings", Wind Structure, An International Journal, 10(4), 383-398.

Lim, J. and Bienkiewicz, B. (2008), "Cross-correlation of wind loading on tall twin buildings in close proximity", In: Proceedings of the 4th International Conference on Advances in Wind and Structures, Seogwipo, Jeju, Korea, 503-512.

Lim, J., Bienkiewicz, B. and Endo, M. (2006), "Investigation of interference and coupling wind effects on tall buildings", Technical Report Submitted to Samsung Corporation, Wind Engineering and Fluids Laboratory, Colorado State University, pp. 302.

Makino A. and Mataki Y. (1993), "Combination method maximum response in consideration of statistical correlation of wind forces acting on high-rise building:

study on rectangular section models", In: Proceedings of the 1st IAWE European and African Regional Conference, Guernsey, UK, 257-266.

Ni, Z.H., He, C.K., Xie, Z.N., Shi, B.Q. and Chen, D.J. (2001), "Experimental test on bridge jointed twin-towered buildings to stochastic wind loads", Wind Structure, An International Journal, 4(1), 63-72.

Saunders, J.W. and Melbourne, W.H. (1979), "Buffeting effects of upstream buildings", Proceedings of the 5th International Conference on Wind Engineering, Fort Collins, CO, USA, 593-606.

Tallin, A. and Ellingwood, B. (1985), "Wind induced lateral-torsional motion of buildings", Journal of Structural Engineering, 111(10), 2197-2213.

To, A.P. and Lam, K.M. (2003), "Wind-induced interference effects on a group of buildings", In: Proceedings of the 11th International Conference on Wind Engineering, Lubbock, TX, USA.

Thoroddsen, S.T., Peterka, J.A. and Cermak, J.E. (1988), "Correlation of the components of wind-loading on tall buildings", Journal of Wind Engineering and Industrial Aerodynamics, 28(1-3), 351-360.

Xie, J. and Irwin, P.A. (2001), "Wind-induced response of a twin-tower structure", Wind Structure, An International Journal, 4(6), 495-504.

3.7 Figures

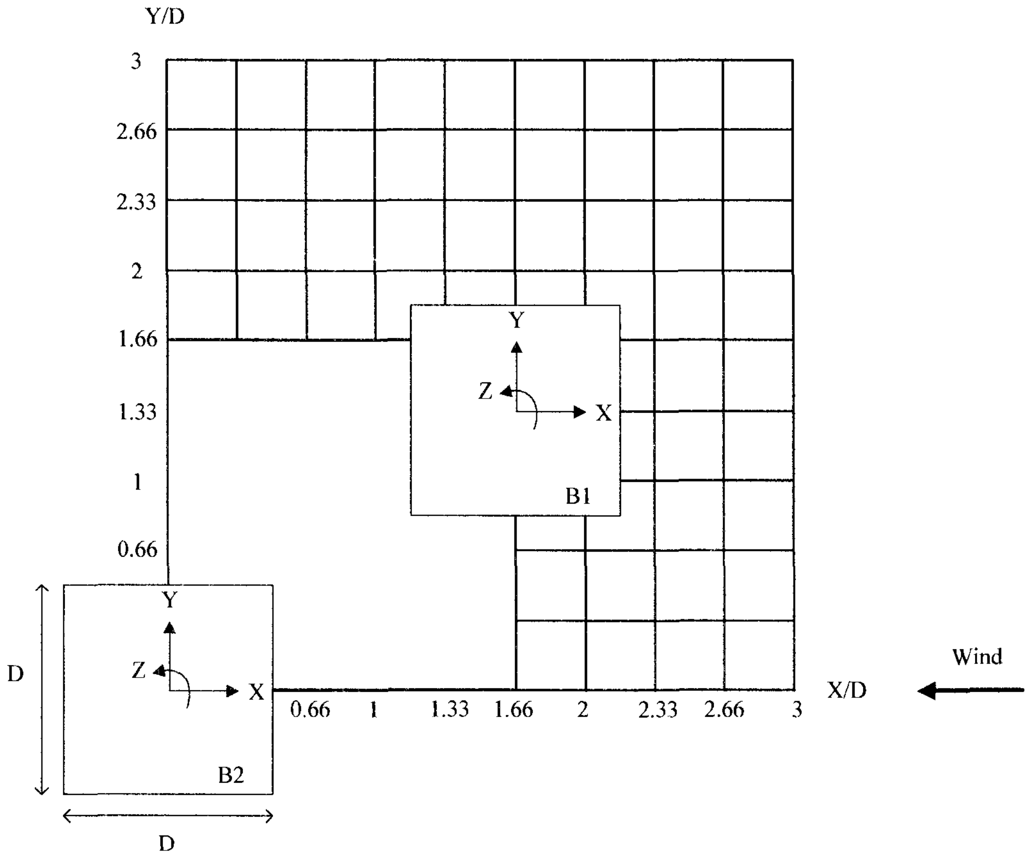

Fig. 3.1 Twin building configuration and reference coordinate systems

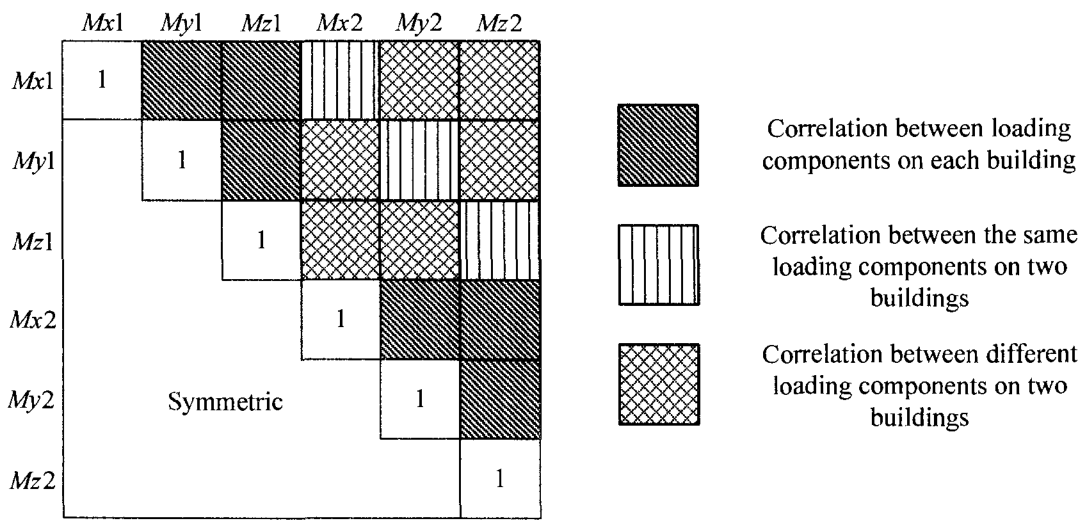

Fig. 3.2 Schematic representation of wind loading correlation matrix

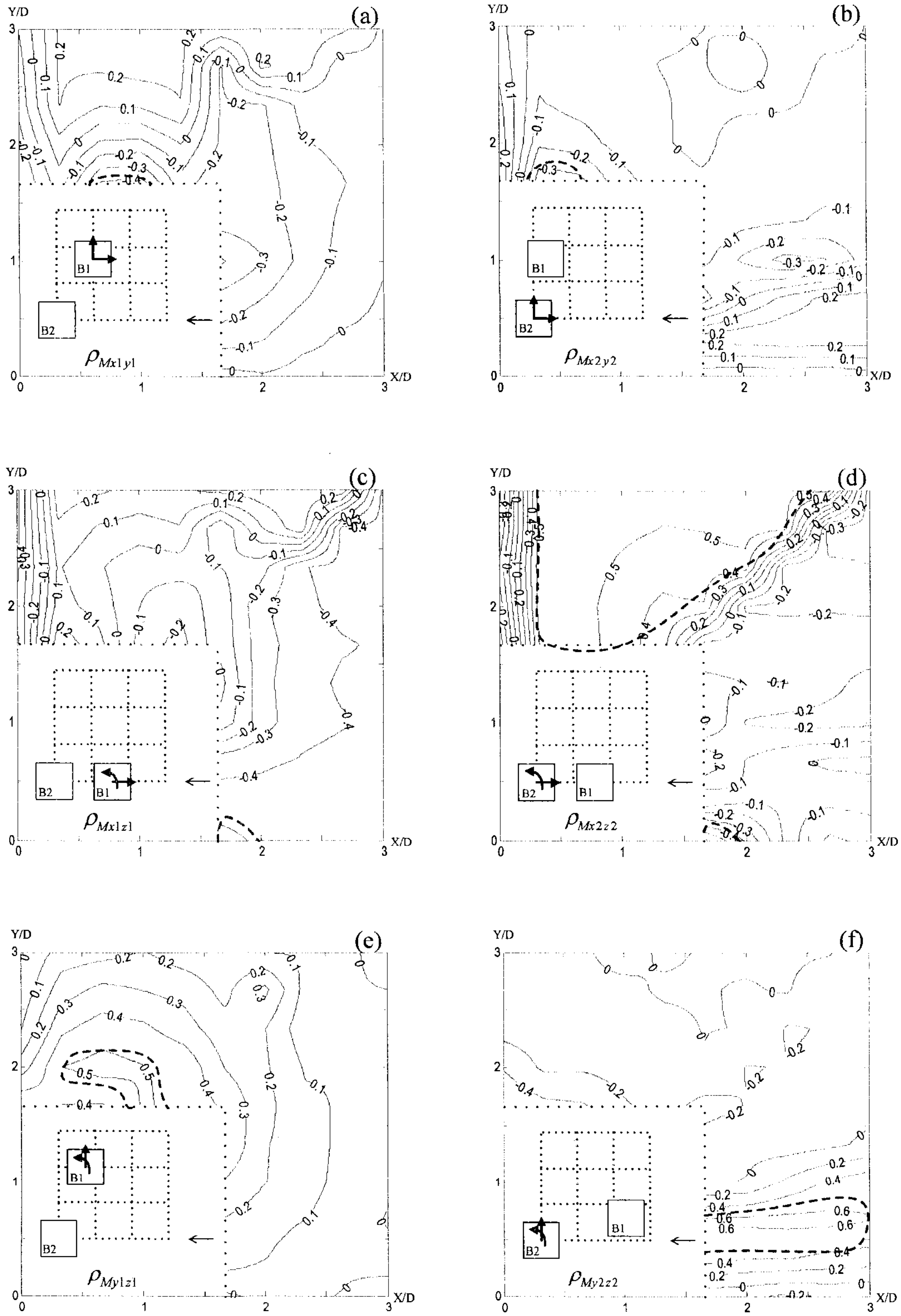

Fig. 3.3 Building correlations of wind loading components

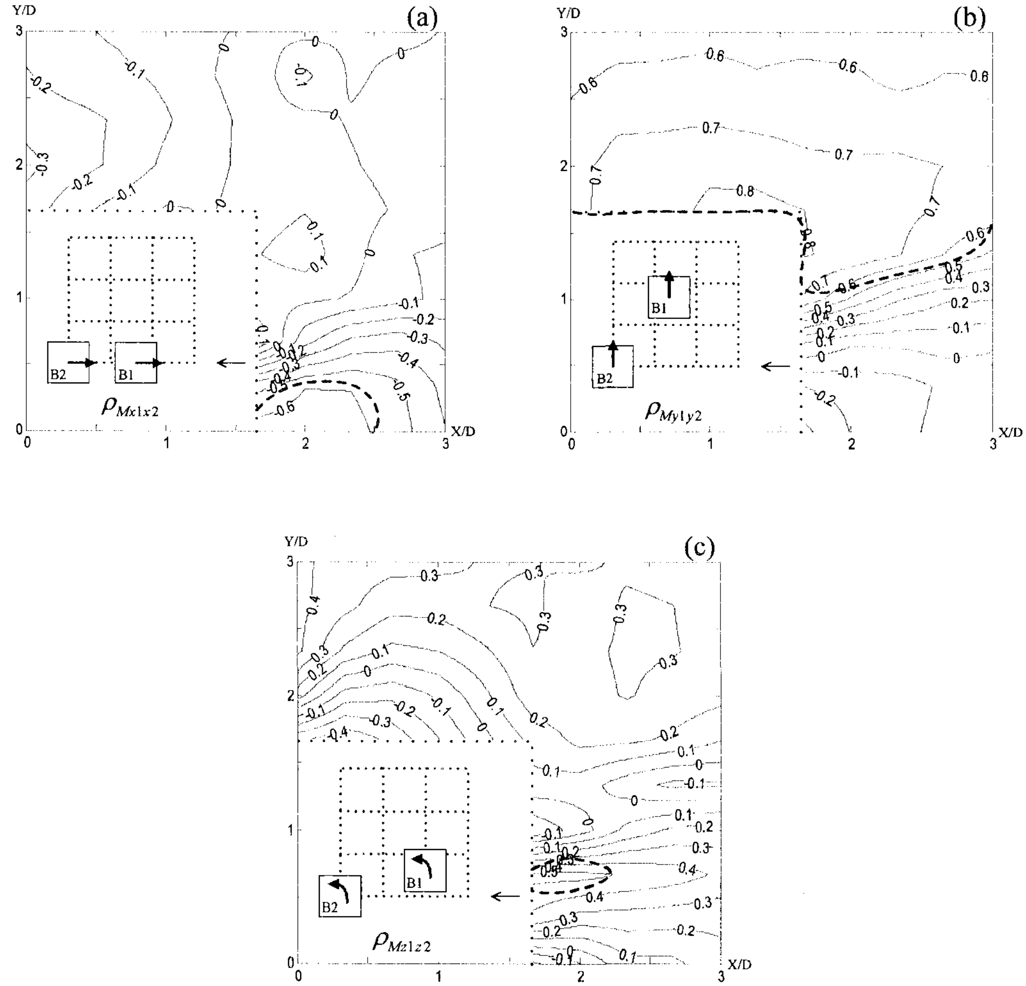

Fig. 3.4 Inter-building correlations of the same loading components

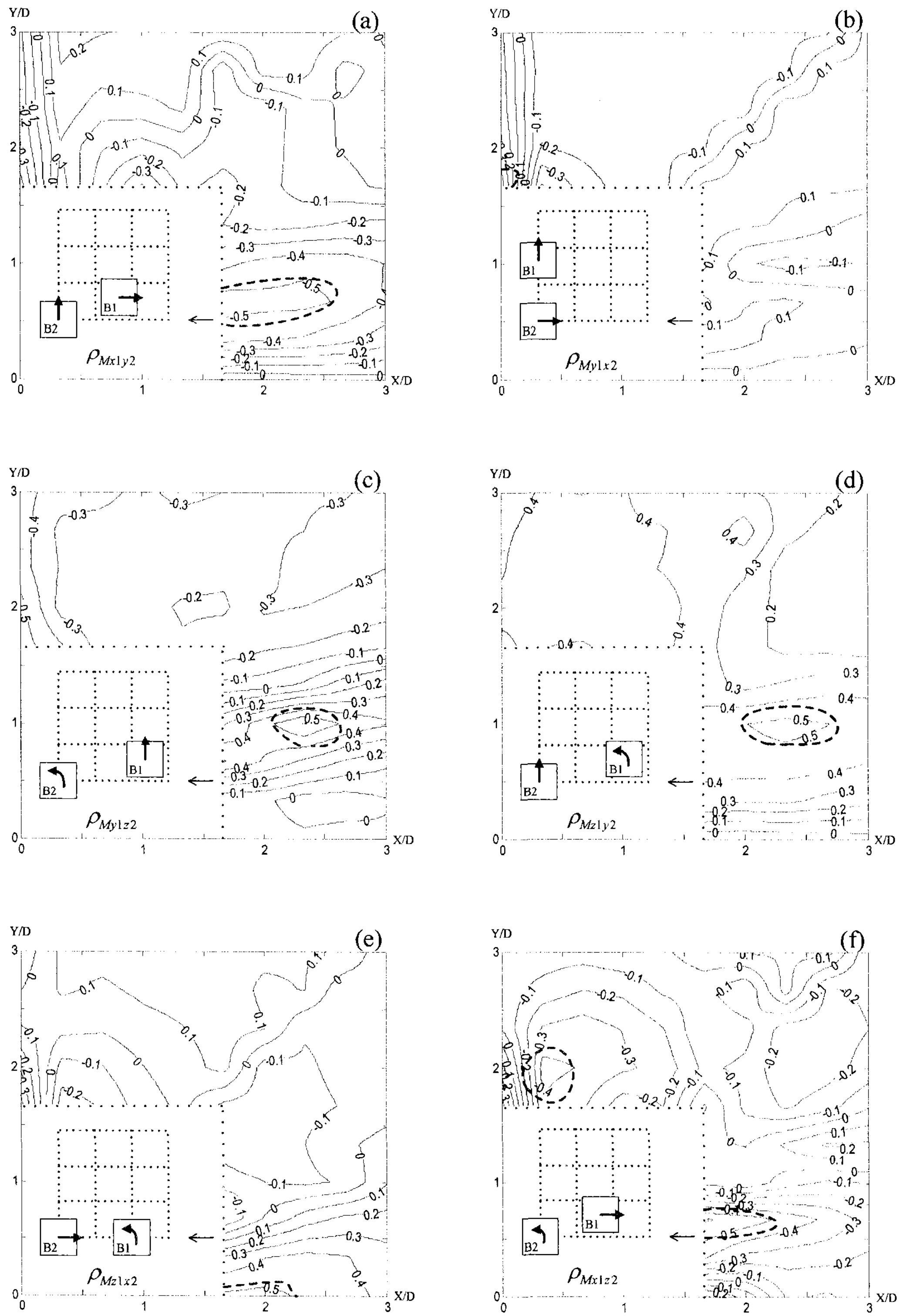

Fig. 3.5 Inter-building correlations of different loading components

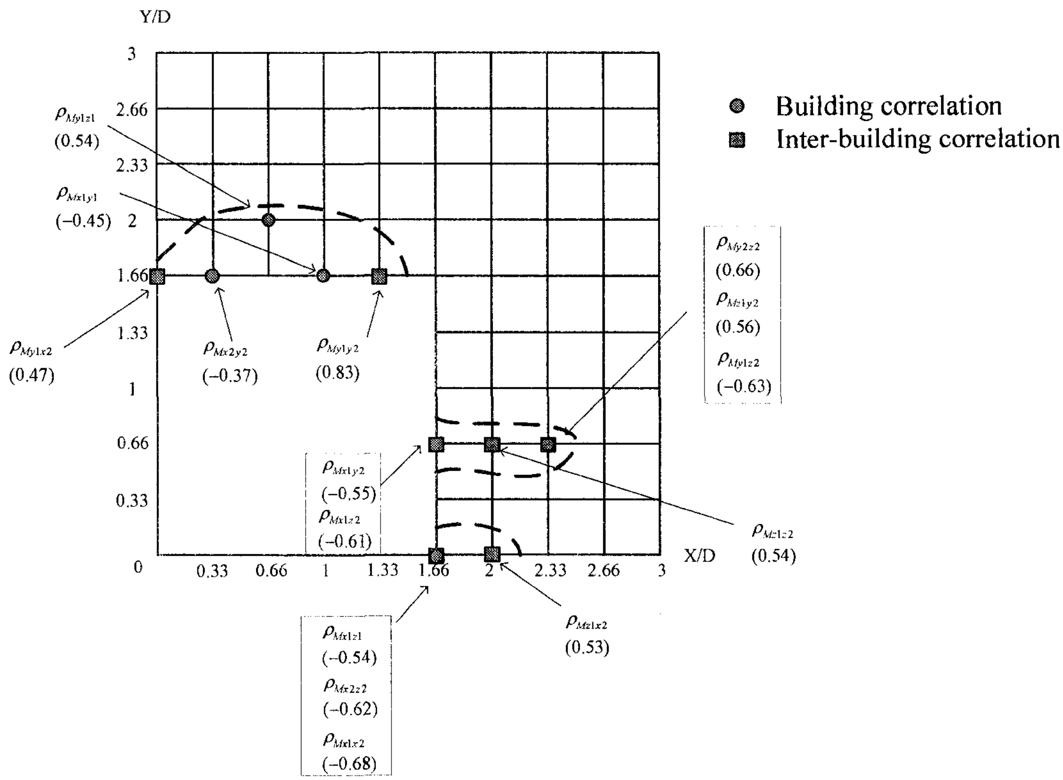

Fig. 3.6 Building locations associated with the highest wind loading correlations

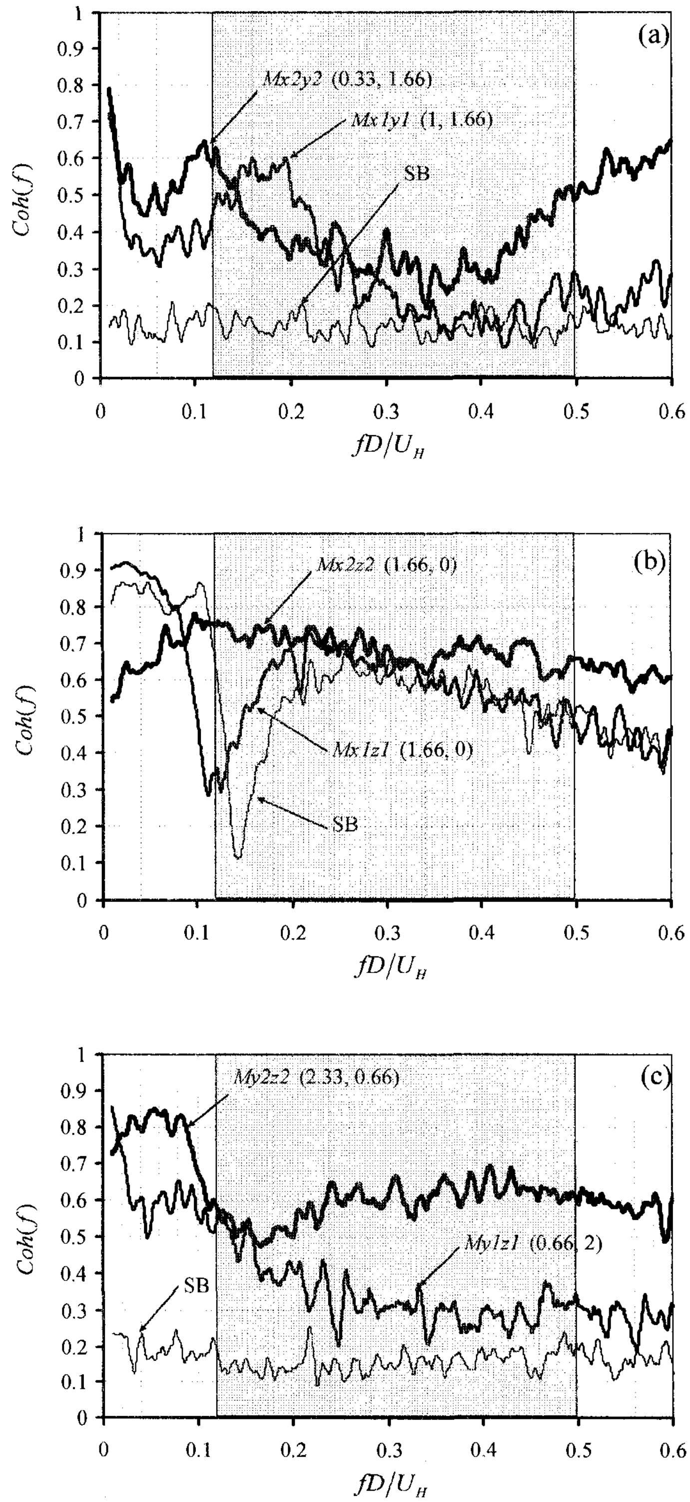

Fig. 3.7 Building coherences of loading components for critical building spacing

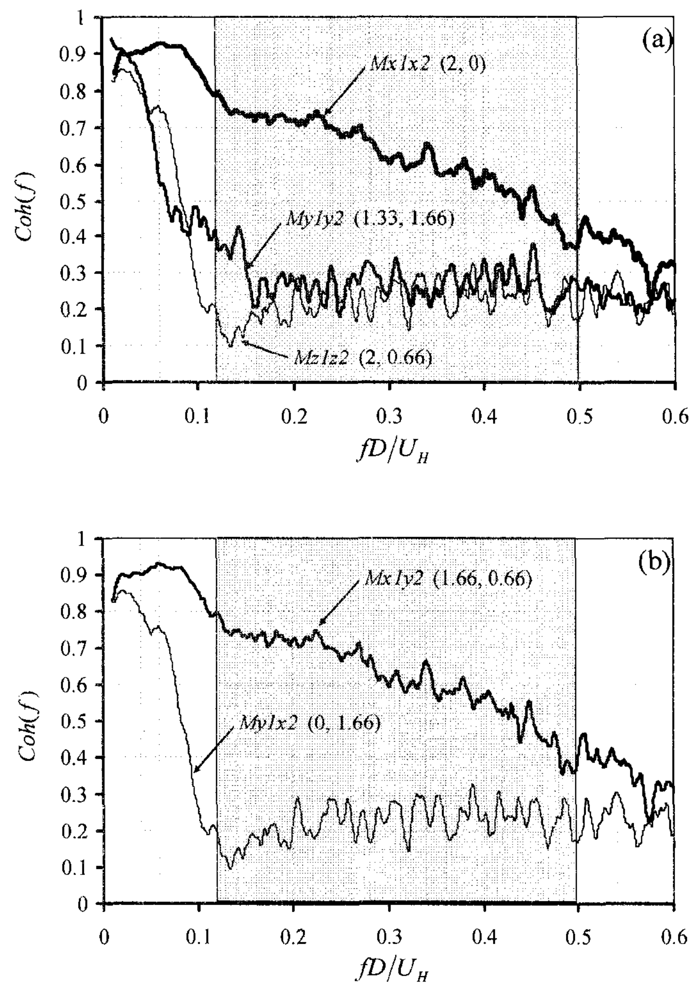

Fig. 3.8 Inter-building coherences of wind loading components for critical building spacing

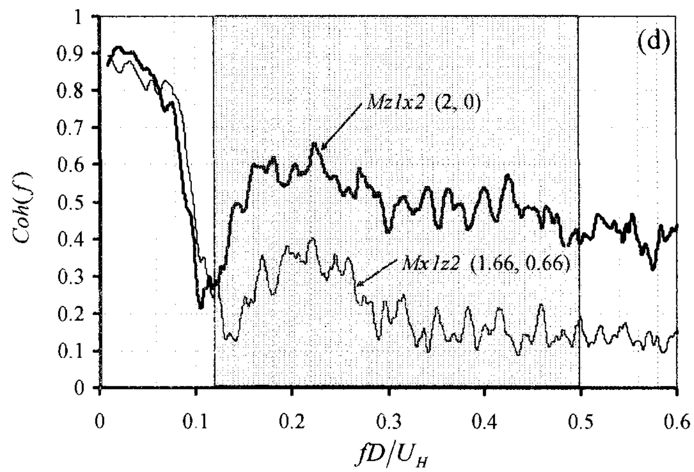

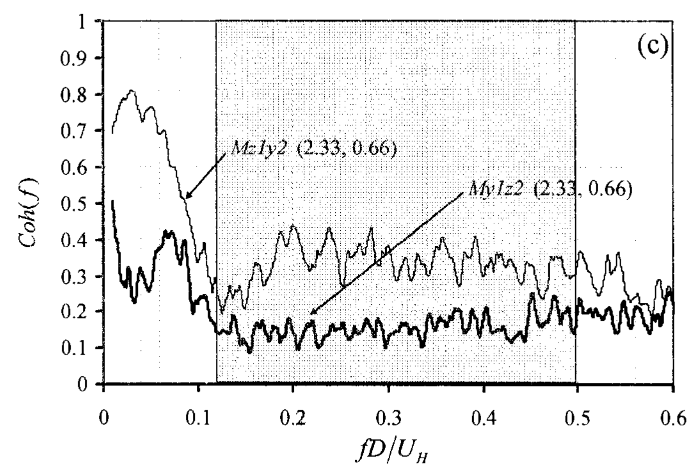

Fig. 3.8 (continued) Inter-building coherences of wind loading components for critical building spacing

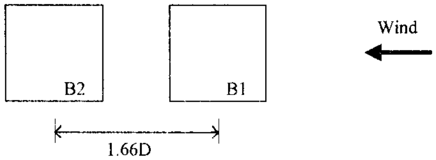

	*Mx*1	*My*1	*Mz*1	*Mx*2	*My*2	*Mz*2
*Mx*1	1	0.14	**0.58**	**0.71**	0.14	**0.49**
*My*1		1	0.14	0.15	**0.64**	0.15
*Mz*1			1	**0.58**	0.14	**0.52**
*Mx*2				1	0.14	**0.69**
*My*2		Symmetric			1	0.17
*Mz*2						1

(a)

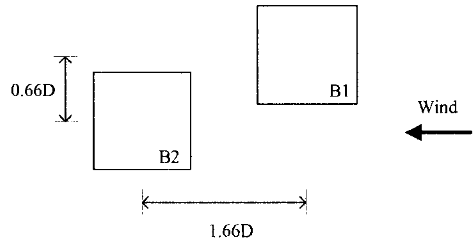

	*Mx*1	*My*1	*Mz*1	*Mx*2	*My*2	*Mz*2
*Mx*1	1	0.36	**0.47**	**0.45**	**0.61**	0.21
*My*1		1	0.3	0.21	0.26	0.23
*Mz*1			1	0.36	0.37	0.2
*Mx*2				1	**0.55**	**0.55**
*My*2		Symmetric			1	**0.57**
*Mz*2						1

(b)

Fig. 3.9 Configurations of the highest average coherences

3.8 Table

Table 3.1 Summary of loading correlations and coherences for critical building spacing

Aerodynamic coupling		Loading components	Location (building B1)	Correlation coefficient (magnitude)	Coherence (average)
Building coupling	B1	*My1x1*	(1, 1.66)	0.45	0.3
		Mx1z1	(1.66, 0)	0.62	0.58
		My1z1	(0.66, 2)	0.54	0.34
	B2	*Mx2y2*	(0.33, 1.66)	0.37	0.37
		Mx2z2	(1.66, 0)	0.54	0.69
		My2z2	(2.33, 0.66)	0.66	0.59
Inter-building coupling	Same	*Mx1x2*	(1.66, 0)	0.68	0.71
		My1y2	(1.33, 1.66)	0.83	0.28
		Mz1z2	(2, 0.66)	0.54	0.22
	A-C	*Mx1y2*	(1.66, 0.66)	0.55	0.61
		My1x2	(0, 1.66)	0.47	0.22
	A-T	*My1z2*	(2.33, 0.66)	0.63	0.16
		Mz1y2	(2.33, 0.66)	0.56	0.33
	C-T	*Mz1x2*	(2, 0)	0.53	0.51
		Mx1z2	(1.66, 0.66)	0.61	0.21

Note: A (alongwind), C (crosswind) and T (torsional)

CHAPTER 4

MODELING OF STRUCTURAL COUPLING FOR ASSESSMENT OF WIND EFFECTS ON TWIN TALL BUILDINGS WITH A SKYBRIDGE

Chapter 4 has been submitted for publication to Journal of Wind Engineering and Industrial Aerodynamics.

4.1 Introduction

Contemporary designs of tall buildings in close proximity incorporate various structural systems that provide inter-building linkages. Configurations employed to engineer such features include skybridges, skygardens and common podiums. Twin buildings connected by a skybridge or skybridges are examples of such building complexes. Prediction of the wind-induced response of interconnected buildings involves analyses incorporating structural coupling (Boggs and Hosoya, 2000; Xie and Irwin, 2001; Lim and Bienkiewicz, 2007). Since the skybridge tends to synchronize the motion of the buildings, the maximum building response is reduced in such a case. Thus structural coupling has a potential to lead to more efficient wind-resistant designs of tall buildings. In addition to the inter-building structural coupling, the complexity of each building may result in coupled motions even in absence of the skybridge. Regardless of its origins, the importance of structural coupling has been recognized as an important factor to be incorporated in the design of tall structures.

Extensive analyses of wind effects on single (isolated) tall buildings with coupled motions were described by various researchers (Holmes et al., 2003; Chen and Kareem, 2005; Ho and Jeong, 2008). These efforts provided a better understanding of wind-induced dynamic response of such buildings. However, only a limited number of studies dealing with coupled motions of twin buildings are available in the open literature (Boggs and Hosoya, 2000; Xie and Irwin, 2001; Lim and Bienkiewicz, 2007). Several outstanding issues related to wind-resistant design of such buildings were identified, e.g. questions regarding the natural frequencies and coupled modes of vibration of generic twin buildings, the effects of the inter-building structural coupling on these properties and the wind-induced response of the buildings.

This chapter addresses some of the aspects listed above of the dynamic analysis of twin tall buildings structurally connected using a skybridge. A generic twin-building configuration is considered. The structural system of the buildings and the skybridge is replaced by a six-degree-of-freedom lumped mass model at the skybridge level. The dynamic equations of motion of this model are derived and the natural frequencies and coupled modal shapes are obtained. The effects of the axial and bending coupling stiffness (due to the skybridge) on these properties are investigated. Approximate empirical formulas describing these effects are developed.

4.2 System reduction to skybridge level

Two identical tall buildings, B1 and B2, linked by a skybridge are considered. The isometric view and the plan view of the buildings (at the skybridge level) are schematically shown in Fig. 4.1. The centers of mass and stiffness of each building are assumed to be coincident with the building geometric centers. As a result, the dynamic or static coupling within each building is eliminated (Thomson and Dahleh, 1997).

An analytical model of the twin building configuration is obtained by reducing the system to a six-degree-of-freedom model lumped at the skybridge level. The mass and stiffness distributed along the building height are replaced by equivalent mass and stiffness applied at the skybridge elevation. The resulting system is then used to determine the natural frequencies and modes of vibration of the coupled buildings.

Provided that the uncoupled motions of vibration of each of the two buildings are represented by only the first three modes of vibration, the equations of motion of the undamped coupled building system are

$$m_s(z)\ddot{u}_s(z,t)+k_s(z)u_s(z,t)=p_s(z,t) \tag{4.1}$$

where $m_s(z)$, $k_s(z)$, $p_s(z,t)$, and $u_s(z,t)$ are the mass or polar mass moment of inertia, stiffness, external loading, and displacement in the principal structural s-direction (x, y, θ); z is the vertical ordinate above the ground level; t is the instant of time.

The displacement $u_s(z,t)$ is expressed using a single mode representation:

$$u_s(z,t) = \Phi_s(z) q_s(t) \tag{4.2}$$

where

$$\Phi_s(z) = \left(\frac{z}{H}\right)^{\beta_s} \tag{4.3}$$

is the mode shape; $q_s(t)$ is the generalized coordinate; H is the building height; and β_s is the exponent of the mode shape.

The building displacement at the skybridge level is written as follows

$$u_s(h,t) = \left(\frac{h}{H}\right)^{\beta_s} q_s(t) \tag{4.4}$$

where h is the skybridge elevation above the ground level. Thus the building displacement at the elevation z can be expressed as follows

$$u_s(z,t) = \Phi_s(z)\left(\frac{H}{h}\right)^{\beta_s} u_s(h,t) \tag{4.5}$$

Substitution of Eq. (4.5) in Eq. (4.1) leads to

$$\Phi_s(z)\left(\frac{H}{h}\right)^{\beta_s}\left[m_s(z)\ddot{u}_s(h,t)+k_s(z)u_s(h,t)\right]=p_s(z,t) \tag{4.6}$$

Pre-multiplying Eq. (4.6) by Eq. (4.3) and integration along the building height result in the following modal equations of motion:

$$m_s^*\left(\frac{H}{h}\right)^{\beta_s}\left[\ddot{u}_s(h,t)+\omega_s^2 u_s(h,t)\right]=P_s^*(t) \tag{4.7}$$

where

$$m_s^*=\int_0^H m_s(z)\Phi_s^2(z)dz=\frac{m_s H}{2\beta_s+1} \tag{4.8}$$

$$m_x=m_y=\rho_m D^2,\ \ m_\theta=\rho_m D^2 r_o^2 \tag{4.9}$$

$$P_s^*(t)=\int_0^H \Phi_s(z)p_s(z,t)dz \tag{4.10}$$

where m_s^* and $P_s^*(t)$ are the generalized mass (or polar mass moment of inertia) and loading; ω_s is the circular natural frequency; $m_s(z)=m_s$ is the constant mass (or polar mass moment of inertia) per unit height; ρ_m is the building mass density; D is the planar dimension of a building of square cross-section; and r_o is the radius of gyration about the mass center (O), see Fig. 4.1.

The generalized loading $P_s^*(t)$ in Eq. (4.7) can be expressed in terms of the base moments and torque:

$$P_s^* = \frac{\lambda_s}{H^{\gamma_s}} M_{\tilde{s}}(t) \tag{4.11}$$

where $M_{\tilde{s}}(t)$ denotes the base overturning moments and torque; $\tilde{s}$ indicates the base wind loading component induced by an external force acting along the s-axis, e.g. $M_{\tilde{x}}(t) = M_y(t)$, $M_{\tilde{y}}(t) = M_x(t)$ and $M_{\tilde{\theta}}(t) = M_\theta(t)$; λ_s is the empirical mode correction factor; and γ_s ($\gamma_x = \gamma_y = 1$, $\gamma_\theta = 0$) is the directional parameter.

The reduction of Eq. (4.1) to the skybridge level is made by transforming the base wind loading in Eq. (4.11) into equivalent forces (and torques) applied at the skybridge elevation. Substituting Eq. (4.11) in Eq. (4.7) and multiplying the resulting equation by $(H/h)^{\gamma_s}$ lead to the following equations of motion of the equivalent system reduced to the skybridge:

$$m_s^e \ddot{u}_s^e(t) + k_s^e u_s^e(t) = p_s^e(t) \tag{4.12}$$

where

$$m_s^e = m_s^* \left(\frac{H}{h}\right)^{\beta_s + \gamma_s} \tag{4.13}$$

$$k_s^e = m_s^e \omega_s^2 = m_s^* \left(\frac{H}{h}\right)^{\beta_s + \gamma_s} (2\pi f_s)^2 \tag{4.14}$$

$$p_s^e(t) = \frac{\lambda_s M_{\tilde{s}}(t)}{h^{\gamma_s}} \tag{4.15}$$

$$u_s^e(t) = u_s(h,t) = q_s(t)\left(\frac{h}{H}\right)^{\beta_s} \tag{4.16}$$

are, respectively, the equivalent mass or polar mass moment of inertia, stiffness, loading, and displacement.

4.3 Modeling of structural coupling of reduced twin building system

In contrast with the vibration of single tall buildings, twin buildings with structural coupling involve six (or more) coordinates to describe the coupled building motions. A simplified (six-degree-of-freedom) model to represent such coupling, for a twin building system reduced to the skybridge level, is proposed in Fig. 4.2. Two buildings, B1 and B2, of square plan, uniformly distributed mass and coinciding elastic and mass centers are assumed to have the same mass and polar mass moment of inertia. The elastic restoring forces associated with *x*-, *y*- and θ-motions of each building are represented by introduction of the (equivalent) stiffnesses, k_x^e, k_y^e and k_θ^e, respectively. The structural coupling between the buildings is modeled by axial k_{Ac} and bending k_{Bc} stiffnesses, see Fig. 4.2(a). For simplicity, these coupling stiffnesses are modeled using an equivalent fixed-fixed beam representing the skybridge, see Fig. 4.2(b). To account for the skybridge stiffening due to the size of the building cross-section, the beam end portions within the building perimeter – each of length b – are given an infinite bending stiffness ($EI = \infty$), as is indicated in Fig. 4.2(b). Adjustments in the beam dimensions (lengths l and b) and elastic properties (axial stiffness EA/l and bending stiffness EI/l^3) allow for control of structural coupling between the buildings. This feature is utilized in investigation of the effects of the inter-building structural coupling on the natural frequencies and modes of vibration of the buildings in twin building configuration.

4.4 Equations of motion of reduced system

4.4.1 x-motion

The force-displacement relationships for the equivalent fixed-fixed beam representing a skybridge are derived in Appendix 4.7. Following D'Alembert's principle, the equivalent forces of the reduced twin building system, acting in the x-direction, are depicted in Fig. 4.3(a). Accordingly, the equations of motion in the x-direction can be written as follows

$$m_x^e \ddot{u}_{x1}^e(t) + \left(k_x^e + \frac{k_{Ac}}{\varepsilon_1} \right) u_{x1}^e(t) - \frac{k_{Ac}}{\varepsilon_1} u_{x2}^e(t) = p_{x1}^e(t) \tag{4.17}$$

$$m_x^e \ddot{u}_{x2}^e(t) - \frac{k_{Ac}}{\varepsilon_1} u_{x1}^e(t) + \left(k_x^e + \frac{k_{Ac}}{\varepsilon_1} \right) u_{x2}^e(t) = p_{x2}^e(t) \tag{4.18}$$

where

$$\varepsilon_1 = 1 - 2\frac{b}{l}; \tag{4.19}$$

$k_{Ac} = EA/l$ is the axial coupling stiffness of the skybridge; E is the Young's modulus of elasticity; A is the effective cross-sectional area of the skybridge; and subscript Ac denotes the axial coupling.

4.4.2 y-θ motion

The equations of motion in the y- and θ-directions are coupled. The forces and torques involved are respectively shown in Figs. 4.3(b) and (c). The resulting equations of motion in the y-direction are

$$m_y^e \ddot{u}_{y1}^e(t) + \left(k_y^e + \frac{12k_{Bc}}{\varepsilon_1^3} \right) u_{y1}^e(t) - \frac{12k_{Bc}}{\varepsilon_1^3} u_{y2}^e(t) + 6\frac{k_{Bc}l}{\varepsilon_1^3} u_{\theta 1}^e(t) + 6\frac{k_{Bc}l}{\varepsilon_1^3} u_{\theta 2}^e(t) = p_{y1}^e(t) \qquad (4.20)$$

$$m_y^e \ddot{u}_{y2}^e(t) - 12\frac{k_{Bc}}{\varepsilon_1^3} u_{y1}^e(t) + \left(k_y^e + 12\frac{k_{Bc}}{\varepsilon_1^3} \right) u_{y2}^e(t) - 6\frac{k_{Bc}l}{\varepsilon_1^3} u_{\theta 1}^e(t) - 6\frac{k_{Bc}l}{\varepsilon_1^3} u_{\theta 2}^e(t) = p_{y2}^e(t) \qquad (4.21)$$

where $k_{Bc} = EI/l^3$ is the bending coupling stiffness of the skybridge; I is the effective moment of inertia of the skybridge; and subscript Bc denotes the bending structural coupling.

The equations of motion in the θ-direction, compare Fig. 4.3(c), are as follows

$$m_\theta^e \ddot{u}_{\theta 1}^e(t) + 6\frac{k_{Bc}l}{\varepsilon_1^3} u_{y1}^e(t) - 6\frac{k_{Bc}l}{\varepsilon_1^3} u_{y2}^e(t) + \left(k_\theta^e + 4\frac{k_{Bc}l^2}{\varepsilon_1^3}\varepsilon_2 \right) u_{\theta 1}^e(t) + 2\frac{k_{Bc}l^2}{\varepsilon_1^3}\varepsilon_3 u_{\theta 2}^e(t) = p_{\theta 1}^e(t)$$

(4.22)

$$m_\theta^e \ddot{u}_{\theta 2}^e(t) + 6\frac{k_{Bc}l}{\varepsilon_1^3}u_{y1}^e(t) - 6\frac{k_{Bc}l}{\varepsilon_1^3}u_{y2}^e(t) + 2\frac{k_{Bc}l^2}{\varepsilon_1^3}\varepsilon_3 u_{\theta 1}^e(t) + \left(k_\theta^e + 4\frac{k_{Bc}l^2}{\varepsilon_1^3}\varepsilon_2\right)u_{\theta 2}^e(t) = p_{\theta 2}^e(t)$$

(4.23)

where

$$\varepsilon_2 = \left\{1 - \frac{b}{l} + \left(\frac{b}{l}\right)^2\right\}, \quad \varepsilon_3 = \left\{1 + 2\left(\frac{b}{l}\right) - 2\left(\frac{b}{l}\right)^2\right\} \tag{4.24}$$

4.5 Free vibration analysis

4.5.1 x-motion

Examination of Eqs. (4.17) and (4.18) shows that the dynamic motions of the buildings in the x-direction are decoupled from those in the y- and θ-directions. As a result, the x-motions can be determined using a two-degree-of-freedom (2DOF) system. Using matrix notation, Eqs. (4.17) and (4.18) can be expressed as follows

$$\left[m^e\right]_x \left\{\ddot{u}^e\right\}_x + \left[k^e\right]_x \left\{u^e\right\}_x = \left\{p^e\right\}_x \tag{4.25}$$

where

$$\left[m^e\right]_x = \begin{bmatrix} m_x^e & 0 \\ 0 & m_x^e \end{bmatrix} \tag{4.26}$$

$$\left[k^e\right]_x = k_x^e \begin{bmatrix} 1+\dfrac{\psi_A}{\varepsilon_1} & -\dfrac{\psi_A}{\varepsilon_1} \\ -\dfrac{\psi_A}{\varepsilon_1} & 1+\dfrac{\psi_A}{\varepsilon_1} \end{bmatrix} \tag{4.27}$$

$$\psi_A = \frac{k_{Ac}}{k_x^e} = \text{axial coupling-to-building stiffness ratio (relative axial coupling)} \tag{4.28}$$

$$\left\{u^e\right\}_x^T = \left\{u_{x1}^e \quad u_{x2}^e\right\},\ \left\{p^e\right\}_x^T = \left\{p_{x1}^e \quad p_{x2}^e\right\}; \tag{4.29}$$

and superscript T denotes the transpose of a matrix.

A straightforward free vibration analysis of the above (2DOF) system leads to the following two natural frequencies and modes of vibration:

$$\Omega_{in-phase} = \frac{f_{xc,in-phase}}{f_x} = 1 \qquad \left\{\phi\right\}_{in-phase}^T = \left\{1 \quad 1\right\} \tag{4.30}$$

$$\Omega_{out-phase} = \frac{f_{xc,out-phase}}{f_x} = \sqrt{1+2\frac{\psi_A}{\varepsilon_1}} \qquad \left\{\phi\right\}_{out-phase}^T = \left\{1 \quad -1\right\} \tag{4.31}$$

where Ω is the coupled-to-uncoupled frequency ratio; f_{xc} is the coupled (twin building) frequency; $f_x = 1/(2\pi)\sqrt{k_x^e / m_x^e}$ is the uncoupled frequency – the natural frequency of an isolated (structurally uncoupled) building; and ϕ is the natural (coupled) mode of vibration.

4.5.2 y-θ motion

Eqs. (4.20) through (4.23) show that y- and θ-motions are coupled. As a result, a four-degree-of-freedom (4DOF) system needs to be considered in the analysis of the y-θ motions of the two buildings. Using matrix notation, the equations are written as follows

$$\left[m^e\right]_{y\theta}\left\{\ddot{u}^e\right\}_{y\theta}+\left[k^e\right]_{y\theta}\left\{u^e\right\}_{y\theta}=\left\{p^e\right\}_{y\theta} \tag{4.32}$$

where

$$\left[k^e\right]_{y\theta}=k_y^e\left[\begin{array}{cc|cc} 1+12\frac{\psi_B}{\varepsilon_1^3} & -12\frac{\psi_B}{\varepsilon_1^3} & 6\frac{\psi_B l}{\varepsilon_1^3} & 6\frac{\psi_B l}{\varepsilon_1^3} \\ -12\frac{\psi_B}{\varepsilon_1^3} & 1+12\frac{\psi_B}{\varepsilon_1^3} & -6\frac{\psi_B l}{\varepsilon_1^3} & -6\frac{\psi_B l}{\varepsilon_1^3} \\ \hline 6\frac{\psi_B l}{\varepsilon_1^3} & -6\frac{\psi_B l}{\varepsilon_1^3} & \frac{k_\theta^e}{k_y^e}+4\frac{\psi_B l^2}{\varepsilon_1^3}\varepsilon_2 & 2\frac{\psi_B l^2}{\varepsilon_1^3}\varepsilon_3 \\ 6\frac{\psi_B l}{\varepsilon_1^3} & -6\frac{\psi_B l}{\varepsilon_1^3} & 2\frac{\psi_B l^2}{\varepsilon_1^3}\varepsilon_3 & \frac{k_\theta^e}{k_y^e}+4\frac{\psi_B l^2}{\varepsilon_1^3}\varepsilon_2 \end{array}\right] \tag{4.33}$$

$$\left\{u^e\right\}_{y\theta}^T=\left\{u_{y1}^e \quad u_{y2}^e \quad u_{\theta1}^e \quad u_{\theta2}^e\right\},\quad \left\{p^e\right\}_{y\theta}^T=\left\{p_{y1}^e \quad p_{y2}^e \quad p_{\theta1}^e \quad p_{\theta2}^e\right\} \tag{4.34}$$

$$m_\theta^e=m_y^e\left(\frac{h}{H}\right)r_o^2 \tag{4.35}$$

$\psi_B=\dfrac{k_{Bc}}{k_y^e}$ = bending coupling-to-building stiffness ratio (relative bending coupling) (4.36)

By numerically solving the matrix eigenvalue problem associated with Eq. (4.32), four natural frequencies and four modal shapes are determined.

4.5.3 Uncoupled y-θ motion

If cross-coupling between the y- and θ-directions is insignificant, the motions in the y- and θ-directions can be analyzed independently. By assuming off-diagonal (2 x 2) sub-matrices in the stiffness matrix, Eq. (4.33) to be negligible, the equations of motion in the y- and θ-directions can be treated as two independent 2DOF systems. In such a case, the coupled natural frequencies and modal shapes (for the y- and θ-directions) can be determined analytically, in a manner similar to that employed for the x-direction, see Section 4.5.1.

The analytical solutions for the y-direction are given by

$$\Omega_{in-phase} = \frac{f_{yc,in-phase}}{f_y} = 1 \qquad \{\phi\}^T_{in-phase} = \{1 \quad 1\} \tag{4.37}$$

$$\Omega_{out-phase} = \frac{f_{yc,in-phase}}{f_y} = \sqrt{1 + 24\frac{\psi_B}{\varepsilon_1^3}} \qquad \{\phi\}^T_{out-phase} = \{1 \quad -1\} \tag{4.38}$$

The corresponding results for the θ-direction are

$$\Omega_{in-phase} = \frac{f_{\theta c,in-phase}}{f_\theta} = \sqrt{1 + 6\frac{\psi_B l^2}{\varepsilon_1^3}\left(\frac{k_y^e}{k_\theta^e}\right)} \qquad \{\phi\}^T_{in-phase} = \{1 \quad 1\} \tag{4.39}$$

$$\Omega_{out-phase} = \frac{f_{\theta c,out-phase}}{f_\theta} = \sqrt{1+2\frac{\psi_B l^2}{\varepsilon_1}\left(\frac{k_y^e}{k_\theta^e}\right)} \qquad \{\phi\}^T_{out-phase} = \{1 \quad -1\} \tag{4.40}$$

4.6 Application and discussion

4.6.1 Building properties

For illustration of the developed dynamic model, the prototype twin building configuration consisting of the following two identical buildings was considered: each building has a square cross-section of 38 m x 38 m (*D* x *D*), a height of 305 m (*H*), a spacing of 63 m (*l*) between the buildings, and a gross mass density of 200 kg/m^3 (ρ_m). In the parametric study, the rigid portion of the coupling beam (*b*) was varied in the range of 0 through 19 m. The natural frequencies of the uncoupled three modes assumed for each of the buildings not connected by the skybridge were: 0.16 Hz for the two translational (*x* and *y*) modes and 0.24 Hz for the torsional mode (θ). The mode shapes were approximated using a power law with the exponent $\beta_s = 1.3$ ($s = x, y, \theta$).

4.6.2 Modal natural frequencies

The natural frequencies and modal shapes of the coupled buildings were calculated for the range of the axial and bending coupling stiffnesses. The coupling stiffness was varied by adjusting the structural properties of the skybridge, namely the axial (*EA*) and flexural (*EI*) rigidity and the span (*l*), see Fig. 4.2(b). The frequencies for *x*-modes were calculated using Eqs. (4.30) and (4.31), while the coupled y-θ case was analyzed numerically, as indicated in Section 4.5.2. The natural frequencies obtained for six modes associated with a selected relative coupling stiffnesses – axial ψ_A and bending ψ_B – were arranged in an ascending order. The normalized frequencies Ω associated with x-modes, see Eqs. (4.30) and (4.31), are shown in Fig. 4.4(a), while those for the coupled y-θ modes are plotted in Figs. 4.4(b) through (d). As expected, the frequencies associated with the in-phase x- and y-modes – Mode 1 in Fig. 4.4(a) and Mode 2 in Fig 4.4(b) – were independent of the coupling stiffness. The remaining natural frequencies increased with an increase in the coupling stiffness. The out-phase x-mode frequency (Mode 4) increased with the relative axial coupling ψ_A and the skybridge restrain length ratio b/l, while the frequencies of the y-θ modes (Modes 3, 5 and 6) increased with an increase in the relative bending coupling ψ_B and b/l.

Fig. 4.5 shows the comparisons of the numerically calculated coupled and analytically obtained uncoupled (see Section 4.5.3) frequencies, for the y-θ modes. It is noteworthy that the analytical results (obtained for the uncoupled case) were in an approximate agreement with the numerical values obtained for the coupled case, except for Mode 3, $b/l = 0.3$.

Based on the above observations, the following empirical formula has been developed for the (numerically obtained) coupled relative natural frequencies.

$$\Omega_j = \sqrt{1 + C_j \psi_j} \qquad (j = 1 \text{ through } 6) \tag{4.41}$$

where

$$C_1 = C_2 = 0,\ C_3 = \frac{25}{\varepsilon_1^2},\ C_4 = \frac{2}{\varepsilon_1},\ C_5 = \frac{2l^2}{\varepsilon_1}\left(\frac{k_y^e}{k_\theta^e}\right),\ C_6 = \frac{6.4l^2}{\varepsilon_1^3}\left(\frac{k_y^e}{k_\theta^e}\right) \tag{4.42}$$

$$\psi_j = \psi_A \ \text{ for } j = 1, 4; \ \text{ otherwise } \psi_j = \psi_B \tag{4.43}$$

The effective coupling stiffness ψ_j depends on an engineered skybridge and a building-skybridge connection. Initial estimates of ψ_j can be used in Eq. (4.41) to calculate initial predictions of the relative coupled frequencies. Such estimates can be employed in preliminary assessments of wind resistance and in design of twin buildings.

4.6.3 Modal shapes

The modal shapes associated with coupled vibrations and frequencies discussed in Section 4.6.2 are shown in Fig. 4.6. Modes 1 and 4, see Fig. 4.6(a), were respectively the in-phase and out-phase x-modes, independent of the y- and θ-motions. These two modes would contribute to the building response in the x-direction.

As seen in Fig. 4.6(b), Mode 2 was the pure in-phase y-motion, independent of the x- and θ-modes. Mode 5 was the pure out-phase θ-mode, without any displacements in lateral y –direction. The coupled lateral-torsional building motions occurred in Modes 3 and 6. In those modes, the building motion in the primary direction was accompanied by oscillation in the secondary component. Mode 3 was the predominantly out-phase y-mode coupled with the in-phase θ-mode, while Mode 6 was the predominantly in-phase θ-mode accompanied by the out-phase y-mode. These observations imply that in modal superposition analysis, Mode 2, the dominant component of Mode 3 and the secondary component of Mode 6 would contribute to the building response in the y-direction. The torsional building response would be affected by Mode 5, the secondary component of Mode 3 and the primary of Mode 6.

The lateral-torsional contributions of the coupled Modes 3 and 6, shown in Fig. 4.6(b), are further examined in Fig. 4.7. Mode 3, see Fig. 4.7(a) was primarily translational, in the y-direction. The secondary (torsional) component of this mode was characterized by the effective radius ($r_N = u_y^e / u_\theta^e$) of rotation about point (N). It can be seen that as the relative bending coupling stiffness ψ_B approached zero, the magnitude of the normalized radius of rotation (r_N / D) became very large. This implies the pure translational mode in the y-direction, with negligible any torsional (rotational) contributions. As ψ_B was increased to very large value (not shown in Fig 4.7(a)), the relative radius asymptotically approached $l/2D = 0.83$, i.e. the two buildings connected by an infinitely rigid skybridge rotated about the skybridge mid-point. For a given coupling ψ_B the rotational modal contributions were smaller as b/l was reduced.

The above dependence of r_N / D can be approximately described using the following empirical equation involving $l/2D$, ψ_B and ε_1. It should be recalled that ε_1 is dependent on b/l, see Eq. (4.19).

$$\left(\frac{r_N}{D}\right)_{Mode\,3} = \frac{l}{2D} + \frac{\varepsilon_1^3}{200\psi_B} \tag{4.44}$$

A similar analysis was carried out for Mode 6, see Fig. 4.7(b). It can be seen that as ψ_B tended to zero, the relative radius of rotation r_N/D was approaching zero. This led to the pure rotational θ-mode, without any translational contribution. When ψ_B was increased, the relative radius of rotation increased and it reached an asymptotic value of 0.1. The rate of increase in r_N/D was also depended on ε_1. The following approximate empirical formula was developed

$$\left(\frac{r_N}{D}\right)_{Mode\,6} = \frac{\psi_B}{10\psi_B + 0.06\varepsilon_1^3} \tag{4.45}$$

The empirical expressions for the radiuses of rotation, Eq. (4.44) and Eq. (4.45), can be used to describe the coupled modes of vibration. For Mode 3, the coupled modal values are normalized using the (primary) transitional y-component

$$\{\phi\}_3^T = \{u_{y1}^e \quad u_{y2}^e \quad u_{\theta 1}^e \quad u_{\theta 2}^e\} = \left\{1 \quad -1 \quad -\frac{u_\theta^e}{u_y^e} \quad -\frac{u_\theta^e}{u_y^e}\right\} \tag{4.46}$$

and Eq. (4.44) is used to express the (secondary) rotational contributions

$$\frac{u_\theta^e}{u_y^e} = \left(\frac{1}{r_N}\right)_{\text{Mode 3}} = \frac{1}{\dfrac{l}{2} + \dfrac{D\varepsilon_1^2}{200\psi_B}} \tag{4.47}$$

In the case of Mode 6, the coupled mode is normalized by the (primary) rotational θ-component

$$\{\phi\}_6^T = \{u_{y1}^e \quad u_{y2}^e \quad u_{\theta1}^e \quad u_{\theta2}^e\} = \left\{\frac{u_y^e}{u_\theta^e} \quad -\frac{u_y^e}{u_\theta^e} \quad 1 \quad 1\right\} \tag{4.48}$$

and Eq. (4.46) is used to express the (secondary) translational contributions

$$\frac{u_y^e}{u_\theta^e} = (r_N)_{\text{Mode 6}} = \frac{\psi_B D}{10\psi_B + 0.06\varepsilon_1^2} \tag{4.49}$$

The obtained coupled modal quantities, the normalized frequencies and modes, are gathered in Table 1. They are proposed as a tool for preliminary determination of dynamic characteristics of twin buildings with structural coupling.

4.7 Concluding remarks

The main findings of this study are summarized as follows:

(1) The coupled motions of vibration of the twin buildings with a skybridge were described by a six-degree-of-freedom model.

(2) The building motions in the x-direction were independent of those in the lateral y- and torsional θ-directions. The building motions in the y- and θ-directions consisted of two coupled lateral-torsional (y-θ) and two uncoupled (pure y- and θ-) modes.

(3) The obtained coupled frequencies and modes were dependent on the inter-building structural coupling and on the effective skybridge length, except for the in-phase x- and y-modes. This dependence was approximated using the empirical formulas.

(4) The empirically determined formulas were proposed as a design tool for preliminary determination of natural frequencies and modes of twin buildings with structural coupling.

(5) Although the proposed model was found to be useful in the described research, further efforts are desired to develop refined modeling of structural coupling of the twin-building configurations, suitable for parametric studies of wind-induced building responses.

4.8 Appendix: Force-displacement relationship

The force in the x-direction on the building B1 can be associated with the axial coupling stiffness of the skybridge. If a positive x-displacement is imposed on the building B1, as shown in Fig. 4.A1, the equivalent axial forces are obtained

$$p_{x1}^{e} = \frac{AE}{l\left(1-2\frac{b}{l}\right)} u_{x1}^{e}, \quad p_{x2}^{e} = -\frac{AE}{l\left(1-2\frac{b}{l}\right)} u_{x1}^{e} \tag{4.A1}$$

If the building B2 experiences a positive x-displacement, the equivalent axial forces are

$$p_{x1}^{e} = -\frac{AE}{l\left(1-2\frac{b}{l}\right)} u_{x2}^{e}, \quad p_{x2}^{e} = \frac{AE}{l\left(1-2\frac{b}{l}\right)} u_{x2}^{e} \tag{4.A2}$$

Applying the conjugate-beam method, a positive y-displacement imposed to the building B1 introduces not only the lateral forces in the y-direction, but also the torques, as shown in Fig. 4.A2. The equivalent torques are given by

$$\sum M_1 = 0;$$

$$\begin{aligned} -u_{y1}^{\circ} &- \frac{p_{\theta 1}^{e}}{2EI}\left(1-\frac{b}{l}\right)(l-2b)\left(\frac{l+b}{3}\right) - \frac{p_{\theta 1}^{e}}{2EI}\left(\frac{b}{l}\right)(l-2b)\left(\frac{2l-b}{3}\right) \\ &+ \frac{p_{\theta 2}^{e}}{2EI}\left(\frac{b}{l}\right)(l-2b)\left(\frac{l+b}{3}\right) + \frac{p_{\theta 2}^{e}}{2EI}\left(1-\frac{b}{l}\right)(l-2b)\left(\frac{2l-b}{3}\right) = 0 \end{aligned} \tag{4.A3}$$

$$p_{\theta 1}^{e} = p_{\theta 2}^{e} \tag{4.A4}$$

$$p_{\theta 1}^{e} = \frac{6EI}{l^{2}\left(1-2\dfrac{b}{l}\right)^{3}} u_{y1}^{e}, \quad p_{\theta 2}^{e} = \frac{6EI}{l^{2}\left(1-2\dfrac{b}{l}\right)^{3}} u_{y1}^{e} \tag{4.A5}$$

If a positive y-displacement is imposed to the building B2, the equivalent torques are developed

$$p_{\theta 1}^{e} = -\frac{6EI}{l^{2}\left(1-2\dfrac{b}{l}\right)^{3}} u_{y2}^{e}, \quad p_{\theta 2}^{e} = -\frac{6EI}{l^{2}\left(1-2\dfrac{b}{l}\right)^{3}} u_{y2}^{e} \tag{4.A6}$$

For equilibrium, the equivalent torques are accompanied with the lateral forces in the y-direction. The required y-forces are expresses as

$$p_{y1}^{e} = \frac{12EI}{l^{3}\left(1-2\dfrac{b}{l}\right)^{3}} u_{y1}^{e}, \quad p_{y1}^{e} = -\frac{12EI}{l^{3}\left(1-2\dfrac{b}{l}\right)^{3}} u_{y1}^{e} \tag{4.A7}$$

$$p_{y1}^{e} = -\frac{12EI}{l^{3}\left(1-2\dfrac{b}{l}\right)^{3}} u_{y2}^{e}, \quad p_{y1}^{e} = \frac{12EI}{l^{3}\left(1-2\dfrac{b}{l}\right)^{3}} u_{y2}^{e} \tag{4.A8}$$

Applying a positive angular displacement to the building B1, see Fig. 4.A3, leads to the torsional forces on both buildings. The relationships between the torques and the angular displacement are expressed as

$$\sum M_1 = 0;$$

$$-\frac{p_{\theta 1}^e}{2EI}\left(1-\frac{b}{l}\right)(l-2b)\left(\frac{l+b}{3}\right)-\frac{p_{\theta 1}^e}{2EI}\left(\frac{b}{l}\right)(l-2b)\left(\frac{2l-b}{3}\right)$$
$$+\frac{p_{\theta 2}^e}{2EI}\left(\frac{b}{l}\right)(l-2b)\left(\frac{l+b}{3}\right)+\frac{p_{\theta 2}^e}{2EI}\left(1-\frac{b}{l}\right)(l-2b)\left(\frac{2l-b}{3}\right)=0 \tag{4.A9}$$

$$p_{\theta 1}^e = 2p_{\theta 2}^e \frac{\left\{1-\frac{b}{l}+\left(\frac{b}{l}\right)^2\right\}}{\left\{1+2\left(\frac{b}{l}\right)-2\left(\frac{b}{l}\right)^2\right\}} \tag{4.A10}$$

$$\sum M_2 = 0;$$

$$-u_{\theta 1}^e l+\frac{p_{\theta 1}^e}{2EI}\left(1-\frac{b}{l}\right)(l-2b)\left(\frac{2l-b}{3}\right)+\frac{p_{\theta 1}^e}{2EI}\left(\frac{b}{l}\right)(l-2b)\left(\frac{l+b}{3}\right)$$
$$-\frac{p_{\theta 2}^e}{2EI}\left(\frac{b}{l}\right)(l-2b)\left(\frac{2l-b}{3}\right)-\frac{p_{\theta 2}^e}{2EI}\left(1-\frac{b}{l}\right)(l-2b)\left(\frac{l+b}{3}\right)=0 \tag{4.A11}$$

$$p_{\theta 1}^e = \frac{4EI\left\{1-\frac{b}{l}+\left(\frac{b}{l}\right)^2\right\}}{l\left(1-2\frac{b}{l}\right)^3}u_{\theta 1}^e,\quad p_{\theta 2}^e = \frac{2EI\left\{1+2\left(\frac{b}{l}\right)-2\left(\frac{b}{l}\right)^2\right\}}{l\left(1-2\frac{b}{l}\right)^3}u_{\theta 1}^e \tag{4.A12}$$

Imposing a positive angular displacement on the building B2, the equivalent torques are obtained

$$p_{\theta 1}^e = \frac{2EI\left\{1+2\left(\frac{b}{l}\right)-2\left(\frac{b}{l}\right)^2\right\}}{l\left(1-2\frac{b}{l}\right)^3}u_{\theta 2}^e,\quad p_{\theta 2}^e = \frac{4EI\left\{1-\frac{b}{l}+\left(\frac{b}{l}\right)^2\right\}}{l\left(1-2\frac{b}{l}\right)^3}u_{\theta 2}^e \tag{4.A13}$$

For equilibrium, the lateral forces in the y-direction come along with the obtained torsional forces. The relationships between the lateral y-forces and the angular displacement are equal to

$$p_{y1}^{e} = \frac{6EI}{l^2\left(1-2\frac{b}{l}\right)^3} u_{\theta 1}^{e}, \quad p_{y2}^{e} = -\frac{6EI}{l^2\left(1-2\frac{b}{l}\right)^3} u_{\theta 1}^{e} \tag{4.A14}$$

$$p_{y1}^{e} = -\frac{6EI}{l^2\left(1-2\frac{b}{l}\right)^3} u_{\theta 2}^{e}, \quad p_{y2}^{e} = \frac{6EI}{l^2\left(1-2\frac{b}{l}\right)^3} u_{\theta 2}^{e} \tag{4.A15}$$

4.9 References

Boggs, D.W. and Hosoya, N. (2001), "Wind-tunnel techniques to address structures with multiple coupled interactions", In: Proceedings of Structures Congress 2001 – A Structural Engineering Odyssey, Washington, D.C., USA, pp. 8.

Chen, X. and Kareem, A. (2005), "Coupled dynamic analysis and equivalent static wind loads on buildings with three-dimensional modes", Journal of Structural Engineering, 131(7), 1071-1082.

Ho, T.C.E. and Jeong, U.Y. (2008), "Components of force balance data analysis", In: Proceedings of 4th International Conference on Advances in Wind and Structures, Jeju, Korea, 453-466.

Holmes, J.D., Rofail, and A., Aurelius, L. (2003), "High frequency base balance methodologies for tall buildings with torsional and coupled resonant modes", In: Proceedings of the 11th International Conference on Wind Engineering, Lubbock, TX, USA, pp. 8.

Lim, J. and Bienkiewicz, B. (2007), "Wind-induced response of structurally coupled twin tall buildings", Wind Structure, An International Journal, 10(4), 383-398.

Thomson, W.T. and Dahleh, M.D. (1997), Theory of Vibrations with Applications, 5th Edition, Prentice Hall, NJ, USA.

Xie, J. and Irwin, P.A. (2001), "Wind-induced response of a twin-tower structure", Wind Structure, An International Journal, 4(6), 495-504.

4.10 Figures

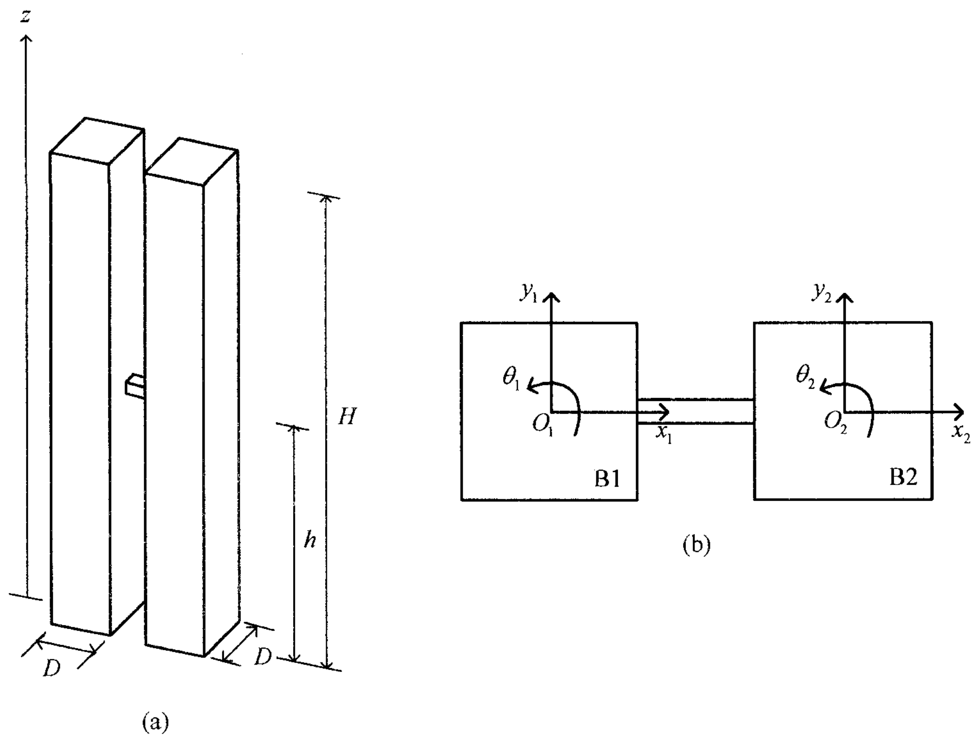

Fig. 4.1 Schematic representation of twin buildings connected by a skybridge: (a) isometric view and (b) plan view at skybridge elevation

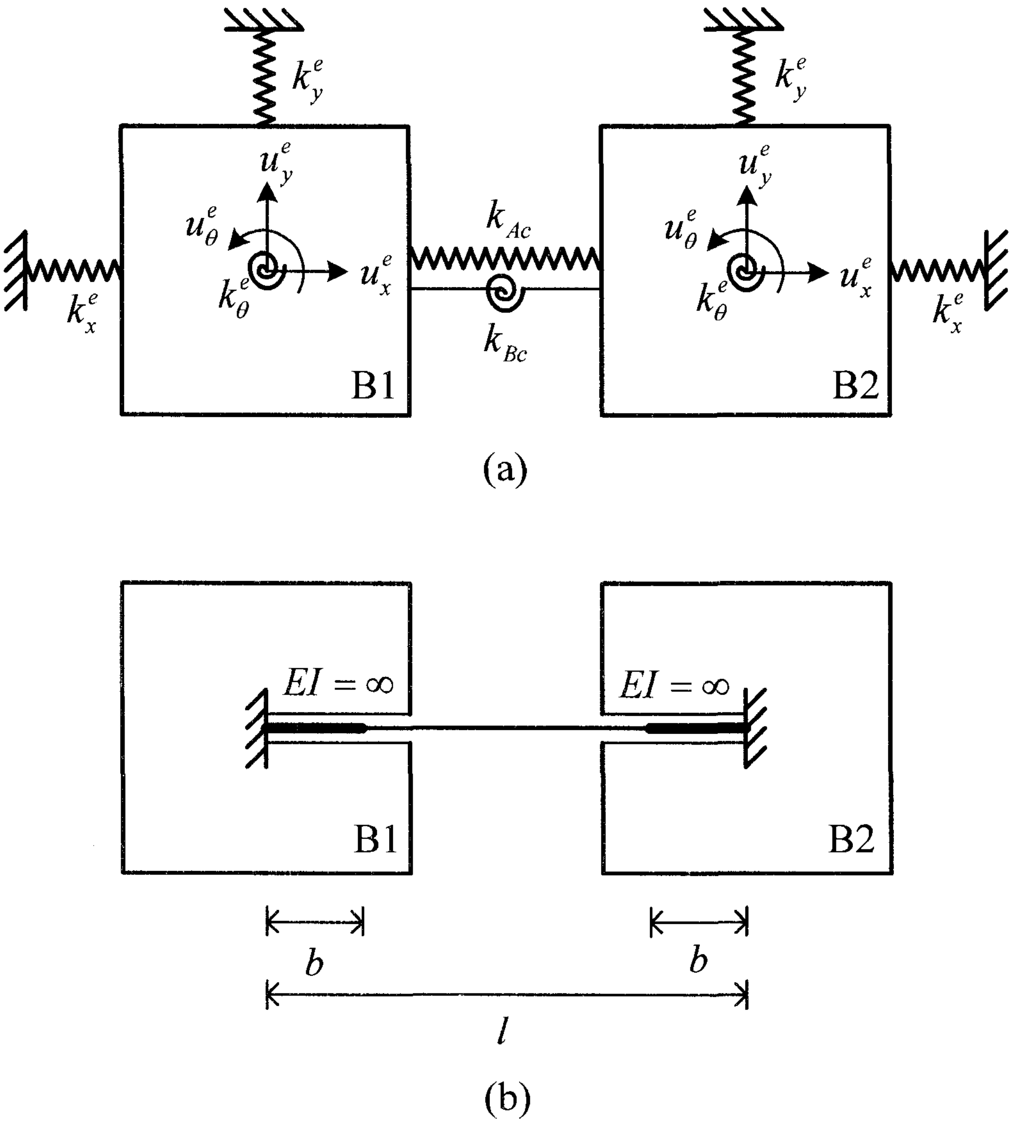

Fig. 4.2 Proposed model: (a) properties of six-degree-of-freedom model and (b) fixed-fixed beam representing the skybridge

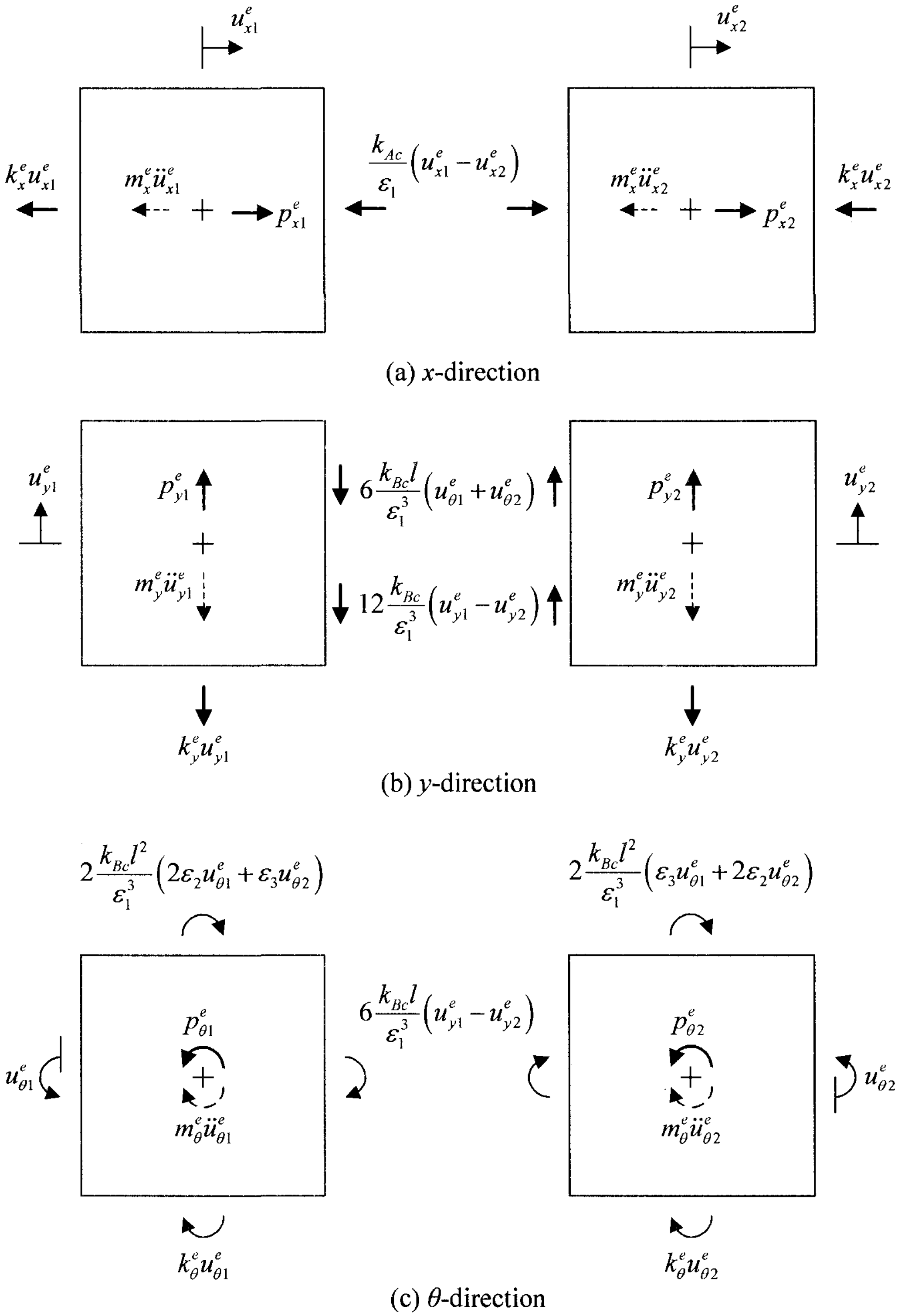

Fig. 4.3 Free-body diagrams of six-degree-of-freedom system of twin buildings

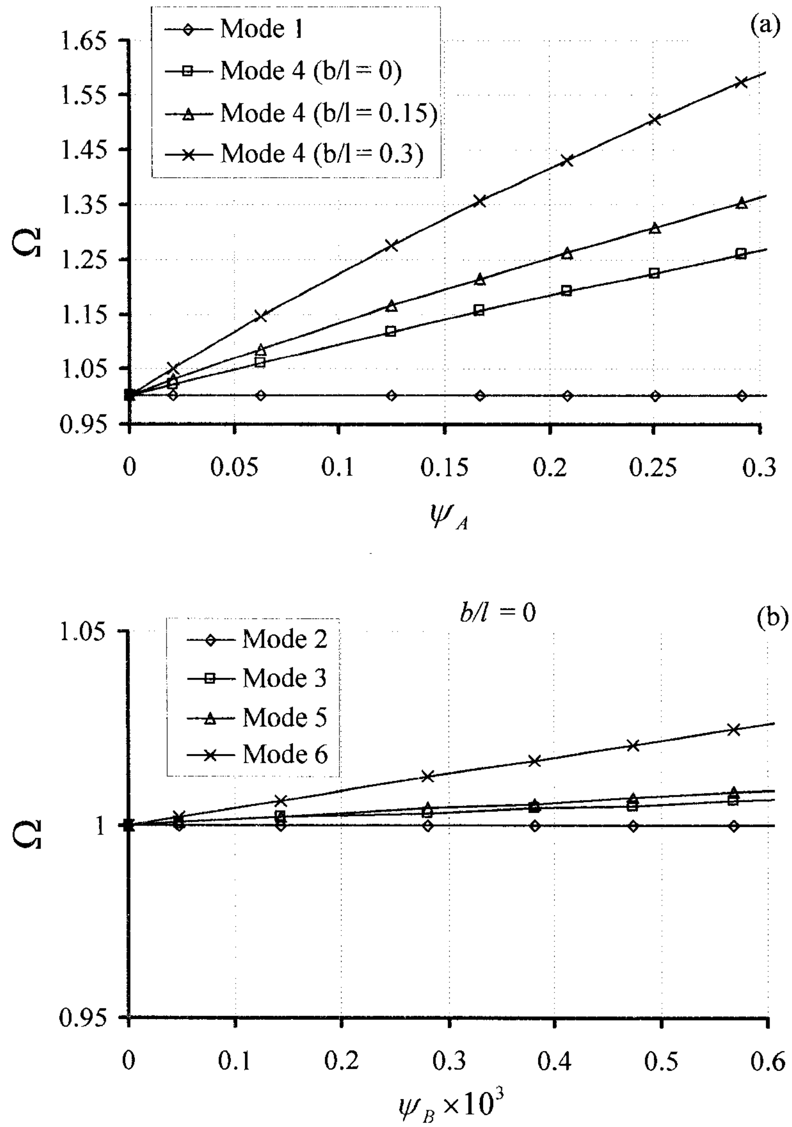

Fig. 4.4 Effects of coupling stiffness and skybridge restrain parameter on frequency ratios: (a) x-modes and (b-d) y-θ modes

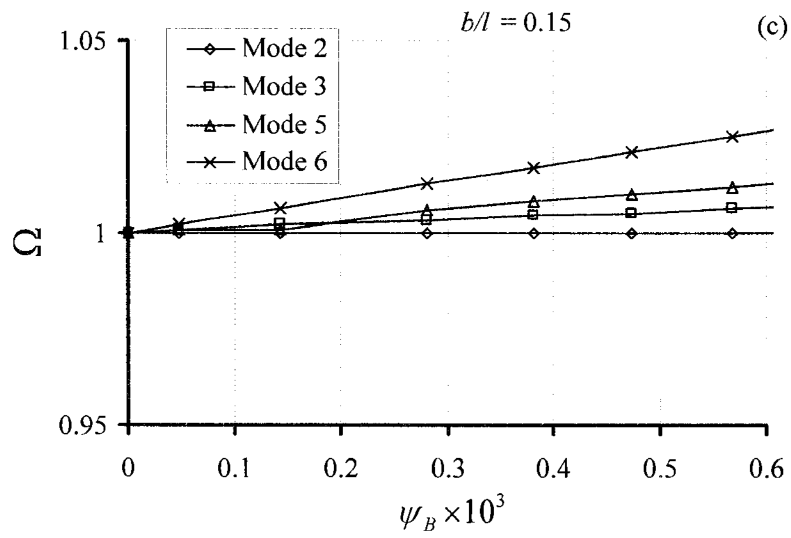

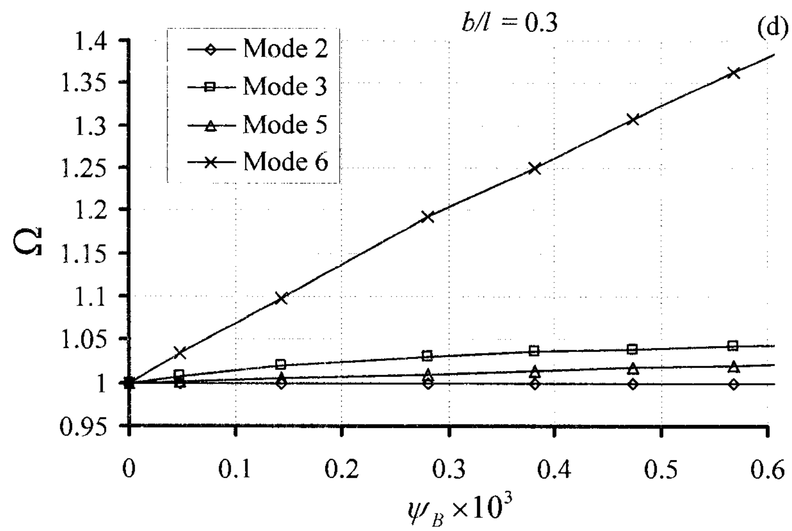

Fig. 4.4 (continued) Effects of coupling stiffness and skybridge restrain parameter on frequency ratios: (a) x-modes and (b-d) y-θ modes

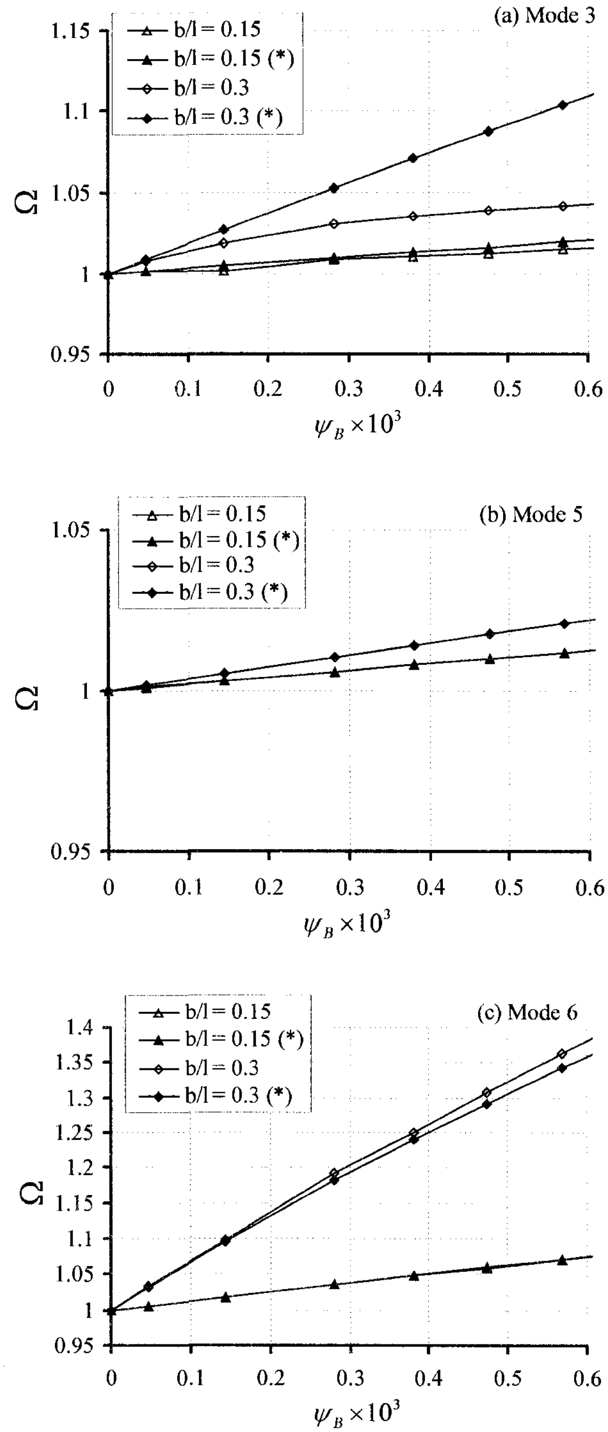

Fig. 4.5 Comparison of numerically and analytically calculated relative frequencies: (*) denotes analytical result

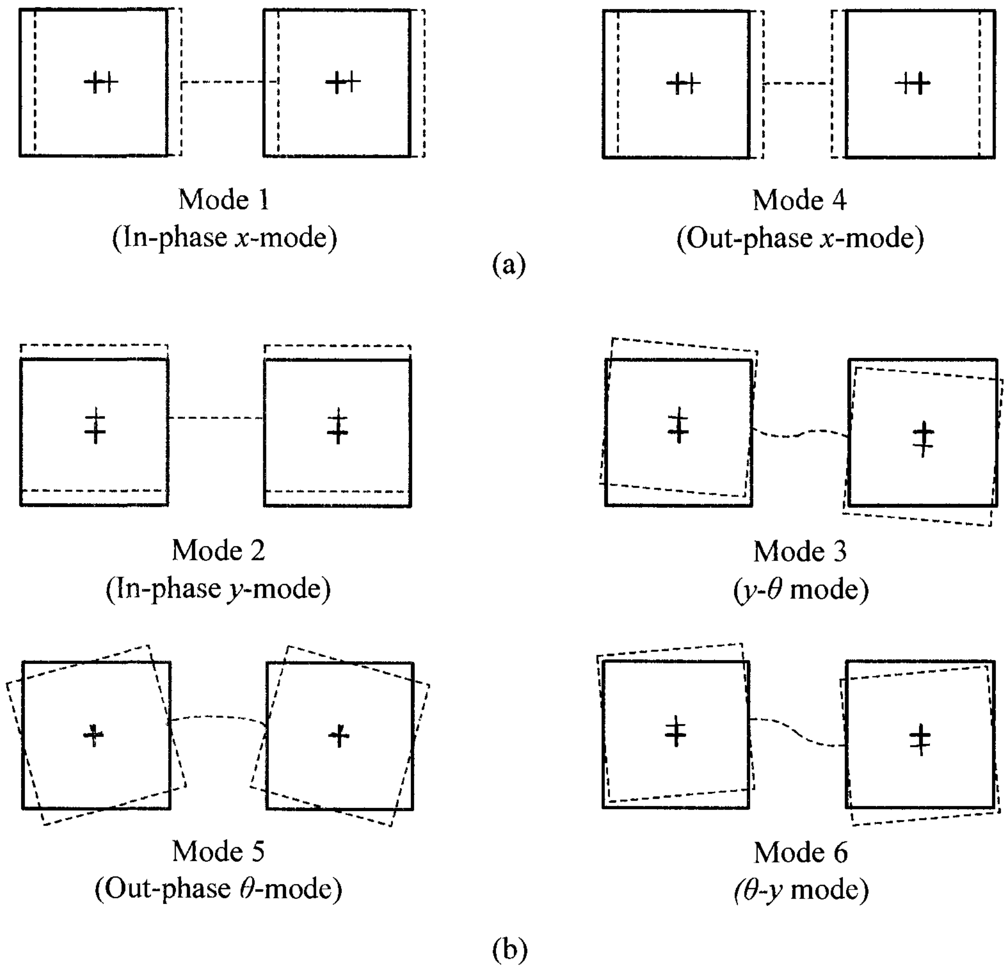

Fig. 4.6 Topology of modes of vibration of generic coupled twin tall buildings: (a) x-modes and (b) y-θ modes

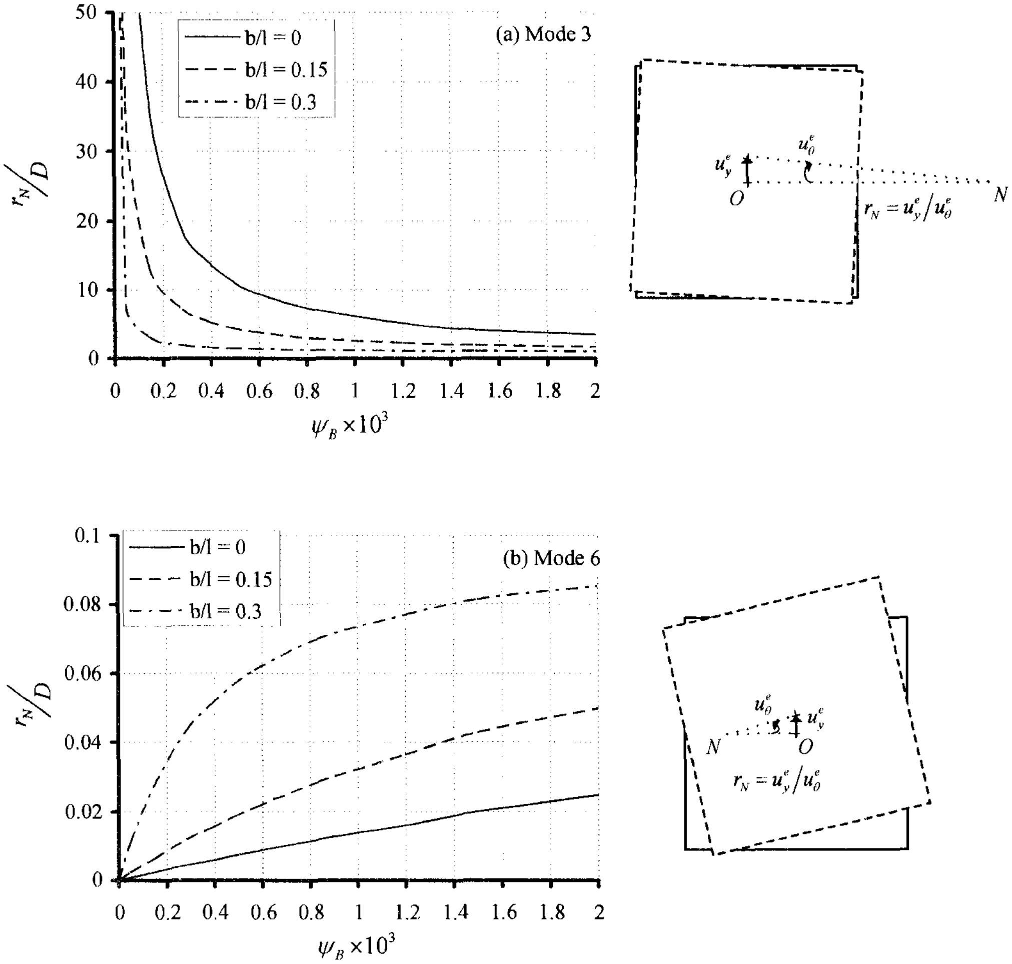

Fig. 4.7 Relative radius of rotation of coupled y-θ modes, for building B1

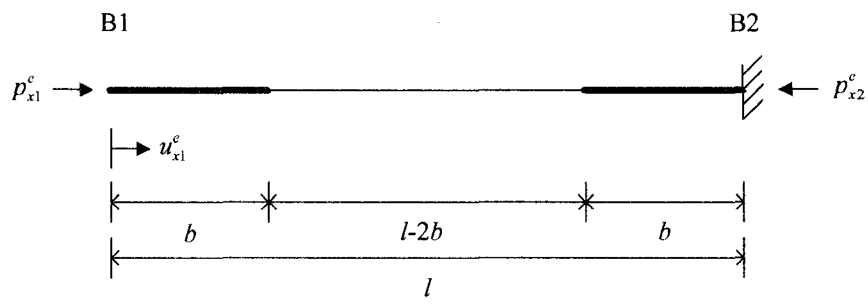

Fig. 4.A1 Effects of axial displacement of equivalent beam support

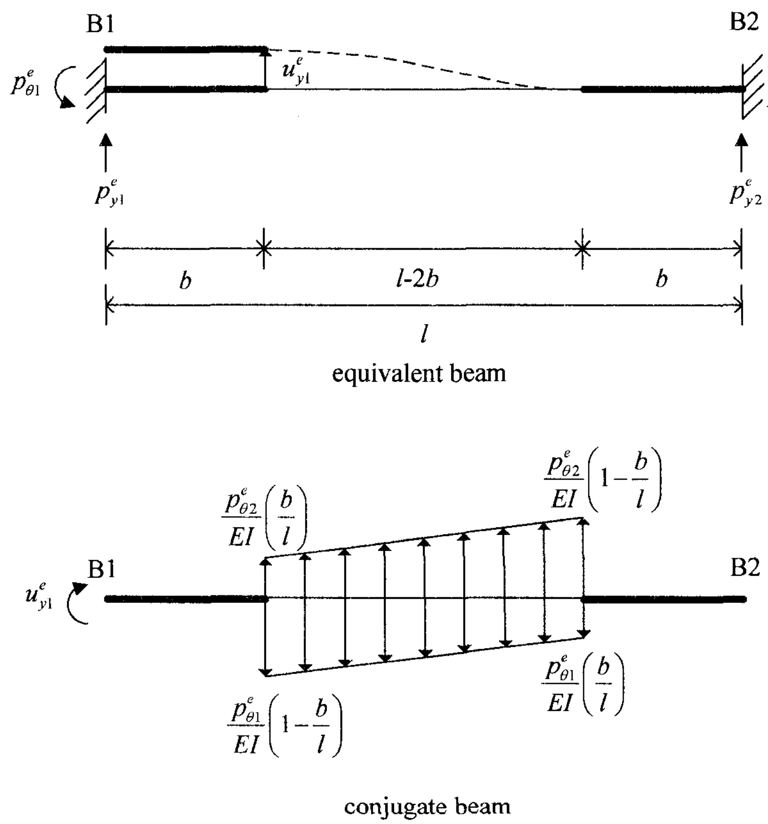

Fig. 4.A2 Effects of transverse displacement of equivalent beam support

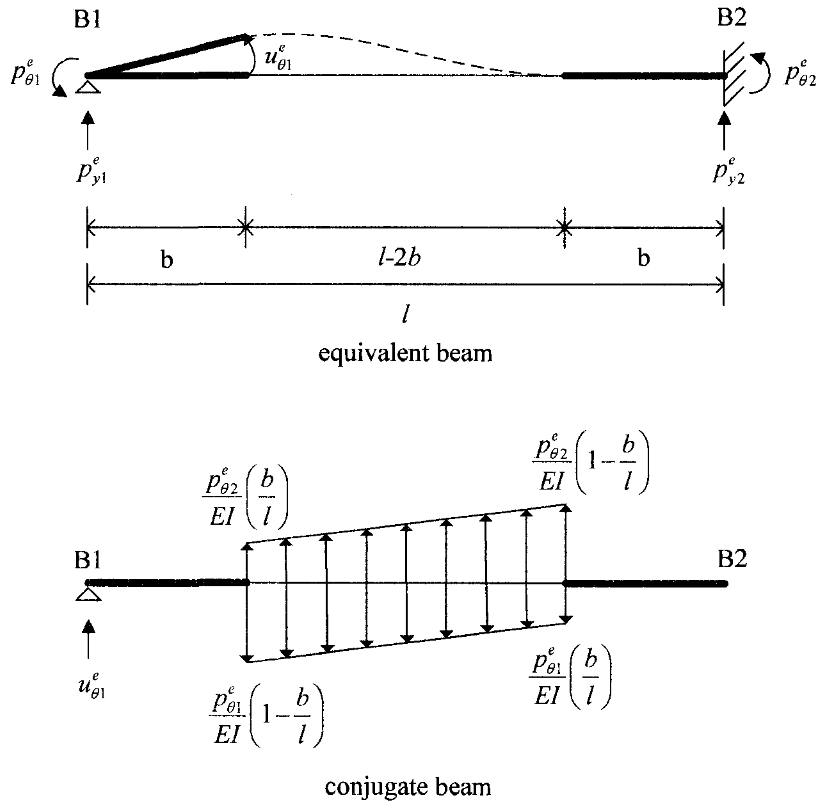

Fig. 4.A3 Effects of rotational displacement of equivalent beam support

4.11 Table

Table 4.1 Summary of proposed coupled modal quantities

Mode	Coupled modal quantities		
	Normalized frequency* Ω	Mode $\{\phi\}^T$	Modal shape
1	$\Omega_1 = 1$	$\{1 \quad 1\}$	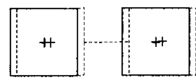 (in-phase x-mode)
2	$\Omega_2 = 1$	$\{1 \quad 1 \quad 0 \quad 0\}$	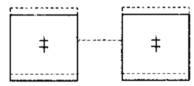 (in-phase y-mode)
3	$\Omega_3 = \sqrt{1 + \frac{25\psi_B}{\varepsilon_1^2}}$	$\left\{1 \quad -1 \quad -\frac{u_\theta^e}{u_y^e} \quad -\frac{u_\theta^e}{u_y^e}\right\}$ $\frac{u_\theta^e}{u_y^e} = \frac{1}{\frac{l}{2} + \frac{D\varepsilon_1^3}{200\psi_B}}$	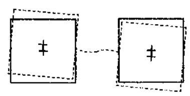 (coupled y-θ mode)
4	$\Omega_4 = \sqrt{1 + \frac{2\psi_A}{\varepsilon_1}}$	$\{1 \quad -1\}$	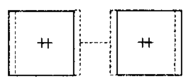 (out-phase x-mode)
5	$\Omega_5 = \sqrt{1 + \frac{2\psi_B l^2}{\varepsilon_1}\left(\frac{k_y^e}{k_\theta^e}\right)}$	$\{0 \quad 0 \quad 1 \quad -1\}$	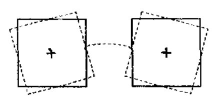 (out-phase θ-mode)
6	$\Omega_6 = \sqrt{1 + \frac{6.4\psi_B l^2}{\varepsilon_1^3}\left(\frac{k_y^e}{k_\theta^e}\right)}$	$\left\{\frac{u_y^e}{u_\theta^e} \quad -\frac{u_y^e}{u_\theta^e} \quad 1 \quad 1\right\}$ $\frac{u_y^e}{u_\theta^e} = \frac{\psi_B D}{10\psi_B + 0.06\varepsilon_1^3}$	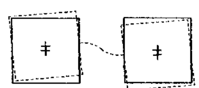 (coupled θ-y mode)

* Coupled-to-uncoupled frequency ratio

CHAPTER 5

EFFECTS OF STRUCTURAL AND AERODYNAMIC COUPLINGS ON THE DYNAMIC WIND RESPONSE OF TWIN BUILDINGS WITH A SKYBRIDGE

Chapter 5 will be submitted for publication to Journal of Wind Engineering and Industrial Aerodynamics.

5.1 Introduction

Two types of coupling may emerge in wind-resistant designs of twin buildings connected by a skybridge. One is aerodynamic coupling due to a high level of cross-correlation between the wind loading components exerted on the buildings (Lim and Bienkiewicz, 2008a). The other is structural coupling, introduced by the skybridge, synchronizing the motions of vibration of the buildings (Lim and Bienkiewicz, 2008b). Recently, these types of coupling have been of primary interest to engineers interested in accurately estimating the aerodynamic response of structurally connected tall buildings.

The above coupling issues have stimulated wind tunnel studies utilizing an expanded high-frequency force balance (HFFB) technique, originally developed and utilized in laboratory investigations of single tall buildings. To date, only a limited number of studies employing an enhanced HFFB approach have been published in the open literature (Xie and Irwin, 1998, 2001; Boggs and Hosoya, 2000; Lim and Bienkiewicz, 2007). Xie and Irwin (1998) developed a multi-HFFB system and proposed a generalized loading model formulated in the time domain. They combined the base wind loading, the non-linear mode shapes, building eccentricity and an assumed wind pressure scheme. The proposed framework was applied in the estimation of the dynamic wind response of a twin-tower (Xie and Irwin, 2001). Boggs and Hosoya (2000) studied a two-tower structure with coupled motions and they employed six (coupled) modes in the modal superposition analysis of the vibration of the buildings. Lim and Bienkiewicz (2007) developed a dual high-frequency force balance (DHFFB) system to measure the correlated wind loading which they subsequently used to predict the coupled building response. Of main interest in their study were the wind-induced rooftop accelerations of twin tall buildings with various aspect ratios.

The above efforts have shown useful applications of an enhanced HFFB system in experiments and analyses of building complexes with coupled motions. However, it has been recognized that in-depth studies are needed to better understand the aerodynamic response of twin building configurations. The issues of primary interest include:

- The effects of structural linkages between tall buildings;
- The role of correlated wind loading exerted on the two buildings;
- The accuracy of calculations of spectral modal loading and response; and

- The combination of coupled modal responses.

This chapter is concerned with issues associated with structural and aerodynamic couplings: (1) How such couplings are incorporated into the analytical treatment of the HFFB technique; and (2) What are the effects of these couplings on the rooftop acceleration of the buildings. A refined HFFB to account for such couplings is formulated based on a traditional HFFB treatment. Building accelerations calculated using the integration of modal response spectrum and the white-noise approximation of the spectral response integration are compared. The effects of the aerodynamic coupling are evaluated by including and excluding the cross-correlations of the wind loading components. Five levels of structural coupling are considered and their effects on the building aerodynamic accelerations are investigated for wind speeds associated with three representative return periods.

5.2 Formulation of coupled building response

5.2.1 Spectral integration method

The spectral integration method (hereafter, SI) has been gaining popularity in the HFFB technique, compared with the white-noise approximation (hereafter, WNA), in estimating the dynamic wind response of tall buildings (Islam et al., 1990; Ni et al., 2001; Fu et al., 2008; Ho and Jeong, 2008; Wu et al., 2008). A methodology to incorporate structural and aerodynamic couplings of twin buildings into the analytical treatment of the HFFB approach is first formulated based on the SI method.

The modal equation of twin tall building response to wind excitation can be expressed, using matrix representation, in the following form

$$\mathbf{m}^*\ddot{\mathbf{q}}(t)+\mathbf{c}^*\dot{\mathbf{q}}(t)+\mathbf{k}^*\mathbf{q}(t)=\mathbf{P}^*(t) \tag{5.1}$$

where

$$\mathbf{m}^* = \int_0^H \mathbf{\Phi}^T(z)\mathbf{m}(z)\mathbf{\Phi}(z)dz \tag{5.2}$$

$$\mathbf{c}^* = \int_0^H \mathbf{\Phi}^T(z)\mathbf{c}(z)\mathbf{\Phi}(z)dz \tag{5.3}$$

$$\mathbf{k}^* = \int_0^H \mathbf{\Phi}^T(z)\mathbf{k}(z)\mathbf{\Phi}(z)dz \tag{5.4}$$

$$\mathbf{P}^*(t) = \int_0^H \mathbf{\Phi}^T(z)\mathbf{p}(z,t)dz\,; \tag{5.5}$$

Since the modal components are orthogonal, $\mathbf{m}^*$, $\mathbf{c}^*$, and $\mathbf{k}^*$ are the j x j matrices of the modal mass, damping, and stiffness, having only diagonal elements, respectively. j denotes the mode number (j = 1 to 6); $\mathbf{P}^*(t)$ is the j x 1 vector of modal loading; $\mathbf{p}(z,t)$ is the s x 1 vector of the wind loading components; s denotes the principal structural direction ($s = x$, y, θ for each building); $\mathbf{q}(t)$ is the j x 1 vector of modal coordinates, at time t; $\mathbf{\Phi}(z)$ is the s x j modal matrix, consisting of the mode shape $\Phi_{jsn}(z)=\phi_{jsno}\left(z/H\right)^{\beta_s}$; subscripts n and o respectively denote the building number (n = 1, 2) and the modal amplitude at the building top; z is the vertical ordinate above the ground level; H is the height of the building; β is the power law exponent; and superscript T denotes the transpose of a matrix.

The vector of modal loading in Eq. (5.5) synthesizes the base wind loading exerted on each of the twin buildings, and takes the form

$$\mathbf{P}^{*}(t) = \boldsymbol{\eta}\mathbf{M}(t) \tag{5.6}$$

where $\boldsymbol{\eta}$ is the j x s matrix of mode corrections; and $\mathbf{M}(t)$ is the s x 1 vector of base wind loading measured (during wind tunnel testing) using the DHFFB (Lim and Bienkiewicz, 2007). For reference, matrices and vectors used in this chapter are presented in Appendix 5.5.

The spectral modal loading is obtained from Eq. (5.6)

$$\mathbf{S}_{P^{*}}(f) = \boldsymbol{\eta}\mathbf{S}_{M}(f)\boldsymbol{\eta}^{T} \tag{5.7}$$

where $\mathbf{S}_{P^{*}}(f)$ and $\mathbf{S}_{M}(f)$ are the j x j and s x s spectral matrices of modal loading and base wind loading, respectively; and f is the frequency.

The j x j spectral matrix of modal coordinates is given by

$$\mathbf{S}_{q}(f) = \overline{\mathbf{H}}(f)\mathbf{S}_{P^{*}}(f)\mathbf{H}^{T}(f) \tag{5.8}$$

where the j x j diagonal matrix of the complex frequency response function is of the form

$$\mathbf{H}(f) = diag\left\{H_{11}(f)\cdots H_{jj}(f)\right\} \tag{5.9}$$

$$H_{jj}(f) = \frac{1}{k_j^*\left\{1-\left(\frac{f}{f_j}\right)^2 + i2\xi_j\left(\frac{f}{f_j}\right)\right\}} \qquad (i=\sqrt{-1}); \tag{5.10}$$

$\bar{\mathbf{H}}(f)$ is the matrix conjugate of $\mathbf{H}(f)$; $diag\{\}$ denotes the diagonal matrix; $k_j^* = m_j^*\left(2\pi f_j\right)^2$ is the j-th modal stiffness; m_j^* is the modal mass, obtained from Eq. (5.2); f_j is the j-th modal frequency; and ξ_j is the j-th damping ratio.

The diagonal and off-diagonal elements of $\mathbf{S}_q(f)$ are, respectively, expressed as

$$S_{q_{jj}}(f) = \left|H_j(f)\right|^2 S_{P_{jj}^*}(f) \qquad (j=j) \tag{5.11}$$

$$\begin{aligned} S_{q_{jm}}(f) &= \bar{H}_j(f) S_{P_{jm}^*}(f) H_m(f) \\ &= \overline{\bar{H}_m(f) S_{P_{mj}^*}(f) H_j(f)} \qquad (j \neq m) \\ &= \bar{S}_{q_{mj}}(f) \end{aligned} \tag{5.12}$$

where subscript m denotes the mode number, different from j. The real part (Re) of $S_{q_{jm}}(f)$ in Eq. (5.12) is considered in the subsequent analysis

$$\mathrm{Re}[S_{q_{jm}}(f)] = \mathrm{Re}[H_{jm}(f)]\mathrm{Re}[S_{P_{jm}^*}(f)] - \mathrm{Im}[H_{jm}(f)]\mathrm{Im}[S_{P_{jm}^*}(f)] \tag{5.13}$$

where

$$\mathrm{Re}[H_{jm}(f)]=\frac{\left\{1-\left(\frac{f}{f_j}\right)^2\right\}\left\{1-\left(\frac{f}{f_m}\right)^2\right\}+\left\{2\xi_j\left(\frac{f}{f_j}\right)\right\}\left\{2\xi_m\left(\frac{f}{f_m}\right)\right\}}{k_j^*k_m^*\sqrt{\left\{1-\left(\frac{f}{f_j}\right)^2\right\}^2+\left\{2\xi_j\left(\frac{f}{f_j}\right)\right\}^2}\sqrt{\left\{1-\left(\frac{f}{f_m}\right)^2\right\}^2+\left\{2\xi_m\left(\frac{f}{f_m}\right)\right\}^2}} \tag{5.14}$$

$$\mathrm{Im}[H_{jm}(f)]=\frac{\left\{1-\left(\frac{f}{f_j}\right)^2\right\}\left\{2\xi_m\left(\frac{f}{f_m}\right)\right\}-\left\{1-\left(\frac{f}{f_m}\right)^2\right\}\left\{2\xi_j\left(\frac{f}{f_j}\right)\right\}}{k_j^*k_m^*\sqrt{\left\{1-\left(\frac{f}{f_j}\right)^2\right\}^2+\left\{2\xi_j\left(\frac{f}{f_j}\right)\right\}^2}\sqrt{\left\{1-\left(\frac{f}{f_m}\right)^2\right\}^2+\left\{2\xi_m\left(\frac{f}{f_m}\right)\right\}^2}} \tag{5.15}$$

Based on Eq. (5.8), the j x j spectral matrix of modal acceleration is expressed as

$$\mathbf{S}_{\ddot{q}}(f)=(2\pi f)^4\,\mathbf{S}_q(f) \tag{5.16}$$

Because of the multiplier of $(2\pi f)^4$ in Eq. (5.16), the spectral modal acceleration $\mathbf{S}_{\ddot{q}}(f)$ leads to a significant reduction in the background contributions, at low frequencies.

The modal spectra in Eqs. (5.8) and (5.16) are integrated over the entire frequency range. Consequently, the j x j covariance matrices of the modal displacement σ_q and acceleration $\sigma_{\ddot{q}}$ of the building are, respectively, obtained as follows

$$\boldsymbol{\sigma}_q^2=\int_0^\infty \mathbf{S}_q(f)df \tag{5.17}$$

$$\boldsymbol{\sigma}_{\ddot{q}}^2=\int_0^\infty \mathbf{S}_{\ddot{q}}(f)df \tag{5.18}$$

Although Eqs. (5.17) and (5.18) include the coherences of the modal loading, an additional procedure to combine the modal responses is required to account for the cross-correlations of the modal frequencies, in the determination of the dynamic wind response of the building. Applying the complete quadratic combination (CQC), Der Kiureghian (1981), the standard deviations (hereafter, SD) of the directional displacement and acceleration, at the top-floor corner of the n-th building, are written as

$$\sigma_{u_{sn}} = \sqrt{\sum_{j=1}^{6}\sum_{m=1}^{6} \phi_{jsno}\sigma_{q_{jsn}}\phi_{msno}\sigma_{q_{msn}}\rho_{jm}} \tag{5.19}$$

$$\sigma_{a_{sn}} = \sqrt{\sum_{j=1}^{6}\sum_{m=1}^{6} \phi_{jsno}\sigma_{\ddot{q}_{jsn}}\phi_{msno}\sigma_{\ddot{q}_{msn}}\rho_{jm}} \tag{5.20}$$

where the cross-modal coefficient between the j-th and m-th modes is expressed as

$$\rho_{jm} = \frac{8\sqrt{\zeta_j\zeta_m}(\zeta_j + r_{jm}\zeta_m)r_{jm}^{1.5}}{(1-r_{jm}^2)^2 + 4\zeta_j\zeta_m r_{jm}(1+r_{jm})^2 + 4(\zeta_j^2+\zeta_m^2)r_{jm}^2} \qquad \left(r_{jm} = f_j / f_m\right) \tag{5.21}$$

The resultant acceleration at the roof-top corner of the building, reflecting the cross-correlation between the loading components, is expressed in the following form

$$\sigma_a = \sqrt{\sigma_{a_x}^2 + \sigma_{a_y}^2 + \sigma_{a_\theta}^2 - 2\sigma_{a_x}\sigma_{a_\theta}\rho_{My\theta}\sin\varphi + 2\sigma_{a_y}\sigma_{a_\theta}\rho_{Mx\theta}\cos\varphi} \tag{5.22}$$

where φ is the angle between the windward roof-corner and the x-axis of the building.

5.2.2 Approximation method

Provided that most of $\mathbf{S}_q(f)$ and $\mathbf{S}_{\ddot{q}}(f)$ exist in the vicinity of the natural frequency of the building, i.e. narrow-band excitation, the solutions of Eqs. (5.17) and (5.18) can be approximated using the WNA method. In such a case the coupled modal response is resolved into the background and resonant components.

The j x j covariance matrix of modal loading is expressed as

$$\boldsymbol{\sigma}_{P^*}^2 = \boldsymbol{\eta}\boldsymbol{\sigma}_M^2\boldsymbol{\eta}^T \tag{5.23}$$

where the s x s covariance matrix of base wind loading is given by

$$\boldsymbol{\sigma}_M^2 = diag\left\{\boldsymbol{\sigma}_M\right\}^T \boldsymbol{\rho}_M diag\left\{\boldsymbol{\sigma}_M\right\}; \tag{5.24}$$

and $\boldsymbol{\sigma}_M$ and $\boldsymbol{\rho}_M$ are the s x s SD and cross-covariance matrices of the base wind loading, respectively.

The j x j covariance vectors of the background displacement and acceleration are expressed as

$$\boldsymbol{\sigma}_{u_b}^2 = diag\left\{\boldsymbol{\Phi}\mathbf{k}^{*-1}\boldsymbol{\sigma}_{P^*}^2\mathbf{k}^{*-T}\boldsymbol{\Phi}^T\right\} \tag{5.25}$$

$$\boldsymbol{\sigma}^2_{a_b} = diag\left\{\boldsymbol{\Phi}\mathbf{m}^{*-1}\boldsymbol{\sigma}^2_{P^*}\mathbf{m}^{*-T}\boldsymbol{\Phi}^T\right\} \tag{5.26}$$

where subscript b denotes the background component.

For the resonant response, based on Eq. (5.8), the s x 1 covariance matrix of modal displacements is determined as

$$\boldsymbol{\sigma}^2_{q_r} = \int_{f_j-\Delta f}^{f_j+\Delta f} \mathbf{S}_q(f)df \tag{5.27}$$

where the diagonal and off-diagonal elements are obtained as follows

$$\sigma_{q_{rjj}} \simeq \frac{1}{k_j^*}\sqrt{\frac{\pi f_j S_{P_{jj}^*}(f_j)}{4\zeta_j}} \qquad (j = j) \tag{5.28}$$

$$\sigma_{q_{rjm}} \simeq \sigma_{q_{rj}}\sigma_{q_{rm}}\Upsilon_{S_{P_j^*}S_{P_m^*}} \qquad (j \neq m) \tag{5.29}$$

$$\Upsilon_{S_{P_j^*}S_{P_m^*}} = \frac{\mathrm{Re}\left[S_{P_{jm}^*}(f)\right]}{\sqrt{S_{P_{jj}^*}(f)S_{P_{mm}^*}(f)}} \qquad \left(f = f_j \; or \; f_m\right); \tag{5.30}$$

subscript r denotes the resonant component; $S_{P_{jj}^*}(f_j)$ is the spectral modal loading; and $\Upsilon_{S_{P_j^*}S_{P_m^*}}$ is the coherence between the cross-power spectra of modal loading.

The SDs of the directional displacement and acceleration at the top-floor corner of the n-th building, are determined using Eqs. (5.19) and (5.20). In the CQC method, ρ_{jm}

accounts for the cross-modal frequencies, while $\Upsilon_{S_{p_j^*}S_{p_m^*}}$ is taken into account because $\sigma_{q_{rjm}}$ cannot be directly determined, Chen and Kareem (2005).

5.3 Application and discussion

5.3.1 Twin building configuration

A twin building configuration comprising of two identical buildings was assumed. Each building had a square plan of 38 m x 38 m (*D* x *D*), a height of 305 m (*H*) and a gross mass density of 200 kg/m^3 (ρ_m). A skybridge connecting the buildings was located at mid-height of the buildings. In the study, the distance (*l*) between the building centers, the depth (*d*) and the rigid beam portion (*b*) of the skybridge were respectively set to: 25 m, 6 m and 19 m. The structural damping ratio of the buildings was assumed to be 1.5%. The mode shapes of the two buildings were approximated, for all principal structural directions, using a power law with the exponent (β) set to 1.3.

A model of the above twin building was tested in a boundary layer wind tunnel at the Wind Engineering and Fluids Laboratory at Colorado State University (Lim and Bienkiewicz, 2007). Fig. 5.1 shows the reference coordinate systems of each building and the definition of wind direction. The wind loading obtained during the testing for wind direction of 0° were used to calculate the building response discussed herein. The rooftop building accelerations for 5-year mean return periods were computed and compared with the results for 1- and 10-year mean return periods. The corresponding design (mean) wind speeds at the rooftop of the building were 20.6 m/s (1 year), 25.1 m/s

(5 years) and 27.1 m/s (10 years), respectively. These speeds were obtained using the Type I extreme value distribution fitted for mean wind speeds recorded in a city. For reference, the spectra of the base wind loading exerted on the twin building configuration, acquired from the DHFFB measurements, are presented in Fig. 5.2.

5.3.2 Structural coupling

Five representative levels of structural coupling were considered and the natural frequencies and modal shapes were determined (for each level) using empirical formulas proposed by Lim and Bienkiewicz (2008b). The calculated frequencies and modes are listed in Tables 5.1 and 5.2, respectively. For convenience, the relative axial and bending coupling stiffnesses used in the empirical formulas are defined as

$$\psi_A = \frac{EA}{lk_x^e}, \quad \psi_B = \frac{EI}{l^3 k_y^e} \tag{5.31}$$

where E is the modulus of elasticity; I is the skybridge effective cross-sectional area moment of inertia; l is the distance between the building centers; A is the skybridge effective cross-sectional area; and k_x^e and k_y^e are the equivalent building stiffnesses. For the idealized rectangular cross-section of the skybridge, see Eq. (5.A8) in Appendix 5.5, the relationship between ψ_A and ψ_B is

$$\psi_B = \psi_A \left(\frac{0.5d}{l} \right)^2 \tag{5.32}$$

Hereafter, the effects of the structural coupling are expressed in terms of ψ_B.

5.3.3 Loading correlations

Using the DHFFB, the correlations among the components of wind loading on twin buildings can be readily obtained. The loading correlations play an important role in the dynamic wind analysis of tall buildings (Thoroddsen et al., 1988; Ni et al., 2001; Holmes et al., 2003; Lim and Bienkiewicz, 2008a). The cross-correlation coefficients of the loading components, calculated for the measured wind loading measurements, are presented in Table 5.3. As can be seen, the alongwind components (*My1* and *My2*) on the two buildings were moderately correlated, but they were not correlated with the crosswind (*Mx*) and torsional (*Mz*) components. The high magnitude (0.67) of cross-correlation between the crosswind components (*Mx1* and *Mx2*) was observed. The torsional components (*Mz1* and *Mz2*) on the twin buildings showed a low level of the cross-correlation. However, they were strongly correlated with the crosswind components. A high level of the loading correlations indicate substantial aerodynamic coupling, involving loading components on the same building and the two twin buildings. As discussed by Lim and Bienkiewicz (2008a), for a given geometry of each building, the aerodynamic coupling is dependent on the wind direction and spacing between the buildings.

5.3.4 Aerodynamic coupling cases

The aerodynamic coupling can be classified into the following three cases, see Fig. 5.3:

- Case I (fully coupled) – all loading correlations are accounted for;
- Case II (not coupled) – all loading cross-correlations are ignored; and
- Case III (partially coupled) – cross-correlations involving the loading components of two buildings are ignored.

To identify the effects of aerodynamic coupling on the wind-induced building accelerations, the responses of the twin buildings were calculated for the above three cases. It should be noted that the cross-correlations of Case I require the use of DHFFB in measurement of the base wind loading, while the correlations of Cases II and III do not require the use of DHFFB, as they can be determined from wind loading measurements resulting from the use of a (single) HFFB.

5.3.5 Effects of spectral calculation of building accelerations

The SI and WNA methods discussed in Sections 5.2.1 and 5.2.2 were applied in the spectral calculation of the building modal responses. The effects of these two methods on the roof-corner accelerations of the building were investigated for both the aerodynamically uncoupled and coupled cases. It should be noted that, for the SI method, the building acceleration was directly calculated by integrating the spectral modal acceleration without separating the background and resonant contributions. In calculations involving the WNA method, the background response contributions were found to be small and they were ignored in the comparisons of the SI and WNA methods.

Table 5.4 presents a comparison of the top floor corner accelerations of the buildings B1 (downwind) and B2 (upwind), for the aerodynamically uncoupled case. As can be seen, the relative differences between the results obtained using the SI and WNA methods ranged from 3% to 7% for the accelerations in the alongwind and crosswind directions. They were significantly small (less than 1%) for the torsional component. The differences for the resultant (total) accelerations were 4% for building B2 and lower than 1% for building B1.

Detailed results for the aerodynamically coupled case are presented in Figs. 5.4 through 5.7. It can be seen that for the alongwind acceleration, shown in Fig. 5.4, the differences between the compared results were significantly lower than 1% and 2%, respectively for the buildings B1 and B2. A similar comparison for the crosswind acceleration is shown in Fig. 5.5. It can be seen that the difference between the results obtained using the two methods did not exceed 7% for the building B1 and 9% for the building B2. The differences in the torsional accelerations, see Fig. 5.6, were similar for the two buildings and they did not exceed 4% and 12%, respectively for the low and high level of structural coupling.

The resultant acceleration exhibited the differences of up to 6% and 5% for the buildings B1 and B2, respectively, as shown in Fig. 5.7. In the case of the building B1 in Fig. 5.7(a), the estimates of the accelerations computed using the WNA method were overall lower than those obtained using the SI method and they increased with an increase in the structural coupling level. On the other hand, the building B2 exhibited discrepancies which at the high structural coupling were low – less than 2%, see Fig. 5.7(b).

The above results show that overall the differences between the building accelerations calculated using the SI and WNA methods were considerably larger for the aerodynamically coupled case than those obtained for the uncoupled case. Thus, the SI method appears to be more suitable (than the WNA method) for the calculation of accelerations (of the structurally coupled buildings) with the aerodynamic coupling included in analysis. In this context, the SI method has been employed in the parametric studies of the effects of the aerodynamic and structural couplings, presented next.

5.3.6 Effects of aerodynamic coupling

High levels of cross-correlations of the loading components occurred for the twin building configuration in close proximity, as mentioned in Section 5.3.3. To assess the impact of such aerodynamic coupling on the building responses, the building roof-corner accelerations were calculated for three aerodynamic coupling cases – Cases I, II and III – defined in Section 5.3.4. It should be noted that inclusion of the aerodynamic coupling in calculations (in the spectral domain) entails use of the cross-spectra of the base wind loading.

Comparative results are presented in Figs. 5.8 through 5.11. Due to the structural coupling limited to x-components only, the accelerations calculated for Cases II and III were identical. Therefore only Cases I and II are compared in Fig. 5.8. The displayed data showed that neglecting of the aerodynamic coupling (Case II) led to the alongwind accelerations that were lower by up to 6% than those obtained when the full aerodynamic coupling, Case I, was accounted for. This discrepancy increased with an increase in the structural coupling level.

As seen in Fig. 5.9, the crosswind accelerations obtained for Cases II and III were in a close agreement – the discrepancy was lower than 1.4%. When the full aerodynamic coupling was included, Case I, the accelerations of the building B1 increased by up to 6%, while those for the building B2 were reduced by up to 9%.

For the torsional component in Fig. 5.10 the difference between Case II and III was insignificant as well. In presence of the complete aerodynamic coupling, Case I, the accelerations were reduced – a reduction of up to 11% – and this reduction increased with an increase in the structural coupling.

As shown in Fig. 5.11, the resultant accelerations obtained for Cases II and III were similar, however smaller than those obtained for Case I. Inclusion of the full aerodynamic coupling resulted in an increase of up to 3% in the resultant acceleration for the building B1 and a decrease of up to 6% for the building B2. For both the buildings, the largest discrepancy between the coupled and uncoupled cases occurred for an intermediate level of structural coupling.

The above findings indicate that the inter-building coupling of the aerodynamic loading significantly affects the building rooftop accelerations and it should be included in predictions of the building responses. Capturing of the coupling of the aerodynamic loading on the two buildings (of the twin-building configuration) requires the use of DHFFB.

In view of the importance of the full aerodynamic coupling, the parametric study presented in the remainder of this chapter is limited to Case I.

5.3.7 Effects of structural coupling

Figs. 5.12, 5.13 and 5.14 present the effects of structural coupling on the building roof-corner accelerations, for the mean return periods of 5, 11 and 1 years. The calculated building accelerations were compared with those obtained for the (structurally) uncoupled buildings. Fig. 5.12 synthesizes the results presented for Case I (and the mean return period of 5 years) displayed in Figs. 5.8 through 5.11. As can be seen from Fig. 5.12, when structural coupling was introduced, all the accelerations of the downstream building B1 and the crosswind acceleration of the upstream building B2 were significantly reduced. At the same time, the alongwind, torsional and resultant accelerations of the upstream building B2 were increased. The resultant acceleration reduction (for the downstream building B1) and increase (for the upstream building B2) were up to 15%.

The results for the return period of 10 years are presented in Fig. 5.13. It can be seen that the effects of the structural coupling were similar to those observed for the 5-year return period shown in Fig. 5.12.

Fig. 5.14 shows the building accelerations computed for a representative short mean return period (of 1 year). In comparison with the results obtained for longer periods (5 and 10 years, Figs. 5.12 and 5.13), the acceleration reduction and increase were larger. In addition, in contrast with the previous two cases, the crosswind component of the upstream building B2 increased when structural coupling was introduced. The acceleration reduction and increase reached up to 22%. Thus they were significantly larger than those observed for the remaining (longer) return periods (5 and 10 years).

The resultant accelerations from Figs. 5.12 through 5.14 were normalized using the accelerations computed for the structurally uncoupled buildings. The obtained acceleration ratios are shown in Fig. 5.15. This format captures the overall impact of the structural coupling on the response of buildings in the twin-building configuration considered in this study. Hence, the uncoupled analysis may lead to significant over- and underestimations of the roof-corner acceleration of structurally coupled twin buildings.

5.4 Concluding remarks

The main findings of this study can be summarized as follows:

(1) For the uncoupled case, the relative differences between the directional and resultant accelerations obtained using the SI and WNA methods were lower than 7% and 4%, respectively.

(2) The disparities between the directional and resultant accelerations predicted using the SI and WNA methods reached by up to 12% and 6%, respectively. These differences for the coupled case were higher than those for the uncoupled case.

(3) Integrating of the spectral modal acceleration can serve to accurately estimate the building acceleration, compared with the approximation method.

(4) The discrepancies between the aerodynamically coupled and uncoupled cases appeared by up to 11% for the directional accelerations and up to 6% for the resultant acceleration.

(5) The significant impact of the aerodynamic coupling can be fully accounted for using the DHFFB system. In order to avoid biased predictions of the building acceleration, the aerodynamic coupling should be included in experiment and analysis.

(6) Inclusion of the structural coupling made great reductions of up to 21% for the directional accelerations and up to 22% for the resultant acceleration, compared with the maximum acceleration of the structurally uncoupled buildings. This feature was attributed to a transfer of the building response between the two buildings.

(7) Coupling dependency of the building acceleration on mean wind speeds strongly appeared for a 1-year return period, compared with the mean return periods of 5 and 10 years. Considering of structural coupling may yield a beneficial impact on estimation of the building acceleration.

(8) A limited twin building configuration – components in the x-direction were decoupled with those in the y- and θ-directions – was considered in this study. However, in practice, more complicated structural coupling could be involved. Therefore, the use of a more refined structural model is desirable for further investigations.

5.5 Appendix

For the twin building configuration considered, the matrix of mode correction and the vector of base wind loading in Eq. (5.6) are rearranged as follows

$$\boldsymbol{\eta} = \begin{bmatrix} \eta_{1x1} & \eta_{4x1} & 0 & 0 & 0 & 0 \\ \eta_{1x2} & \eta_{4x2} & 0 & 0 & 0 & 0 \\ 0 & 0 & \eta_{2y1} & \eta_{3y1} & 0 & \eta_{6y1} \\ 0 & 0 & \eta_{2y2} & \eta_{3y2} & 0 & \eta_{6y2} \\ 0 & 0 & 0 & \eta_{3\theta1} & \eta_{5\theta1} & \eta_{6\theta1} \\ 0 & 0 & 0 & \eta_{3\theta2} & \eta_{5\theta2} & \eta_{6\theta2} \end{bmatrix} \tag{5.A1}$$

$$\mathbf{M}(t) = \left\{ M_{y1} \quad M_{y2} \quad M_{x1} \quad M_{x2} \quad M_{\theta1} \quad M_{\theta2} \right\}^T \tag{5.A.2}$$

The matrix of the spectral base wind loading in Eq. (5.7), based on Eq. (5.A.2), is expressed as

$$\mathbf{S}_M(f) = \begin{bmatrix} S_{My1y1} & S_{My1y2} & 0 & 0 & 0 & 0 \\ S_{My2y1} & S_{My2y2} & 0 & 0 & 0 & 0 \\ 0 & 0 & S_{Mx1x1} & S_{Mx1x2} & 0 & S_{Mx1\theta2} \\ 0 & 0 & S_{Mx2x1} & S_{Mx2x2} & 0 & S_{Mx2\theta2} \\ 0 & 0 & 0 & S_{M\theta1x2} & S_{M\theta1\theta1} & S_{M\theta1\theta2} \\ 0 & 0 & 0 & S_{M\theta2x2} & S_{M\theta2\theta1} & S_{M\theta2\theta2} \end{bmatrix} \tag{5.A.3}$$

The matrix of the spectral modal loading in Eq. (5.7) is written as

$$\mathbf{S}_{p^*}(f)=\begin{bmatrix} S_{p^*_{11}}(f) & S_{p^*_{14}}(f) & 0 & 0 & 0 & 0 \\ S_{p^*_{41}}(f) & S_{p^*_{44}}(f) & 0 & 0 & 0 & 0 \\ 0 & 0 & S_{p^*_{22}}(f) & S_{p^*_{23}}(f) & S_{p^*_{25}}(f) & S_{p^*_{26}}(f) \\ 0 & 0 & S_{p^*_{32}}(f) & S_{p^*_{33}}(f) & S_{p^*_{35}}(f) & S_{p^*_{36}}(f) \\ 0 & 0 & S_{p^*_{52}}(f) & S_{p^*_{53}}(f) & S_{p^*_{55}}(f) & S_{p^*_{56}}(f) \\ 0 & 0 & S_{p^*_{62}}(f) & S_{p^*_{63}}(f) & S_{p^*_{65}}(f) & S_{p^*_{66}}(f) \end{bmatrix} \tag{5.A.4}$$

The complex frequency response function in Eq. (5.8) is expressed as

$$\mathbf{H}(f)=\begin{bmatrix} H_1(f) & & & & & \\ & H_4(f) & & & & \\ & & H_2(f) & & & \\ & & & H_3(f) & & \\ & & & & H_5(f) & \\ & & & & & H_6(f) \end{bmatrix} \tag{5.A.5}$$

The real part of $S_{q_{jm}}(f)$ in Eqs. (5.12) and (5.13) is derived as

$$
\begin{aligned}
\mathrm{Re}[S_{q_{jm}}(f)] &= \mathrm{Re}[\bar{H}_j(f) S_{P^*_{jm}}(f) H_m(f)] \\
&= \mathrm{Re}[\left(\mathrm{Re}[H_j(f)] - i\,\mathrm{Im}[H_j(f)]\right)\left(\mathrm{Re}[H_m(f)] + i\,\mathrm{Im}[H_m(f)]\right)\left(\mathrm{Re}[S_{P^*_{jm}}(f)] + i\,\mathrm{Im}[S_{P^*_{jm}}(f)]\right)] \\
&= \frac{\left\{1-\left(\frac{f}{f_j}\right)^2\right\}\left\{1-\left(\frac{f}{f_m}\right)^2\right\}+\left\{2\xi_j\left(\frac{f}{f_j}\right)\right\}\left\{2\xi_m\left(\frac{f}{f_m}\right)\right\}}{m_j^*\omega_j^2 m_m^*\omega_m^2\sqrt{\left\{1-\left(\frac{f}{f_j}\right)^2\right\}^2+\left\{2\xi_j\left(\frac{f}{f_j}\right)\right\}^2}\sqrt{\left\{1-\left(\frac{f}{f_m}\right)^2\right\}^2+\left\{2\xi_m\left(\frac{f}{f_m}\right)\right\}^2}}\mathrm{Re}[S_{P^*_{jm}}(f)] \\
&- \frac{\left\{1-\left(\frac{f}{f_j}\right)^2\right\}\left\{2\xi_m\left(\frac{f}{f_m}\right)\right\}-\left\{1-\left(\frac{f}{f_m}\right)^2\right\}\left\{2\xi_j\left(\frac{f}{f_j}\right)\right\}}{m_j^*\omega_j^2 m_m^*\omega_m^2\sqrt{\left\{1-\left(\frac{f}{f_j}\right)^2\right\}^2+\left\{2\xi_j\left(\frac{f}{f_j}\right)\right\}^2}\sqrt{\left\{1-\left(\frac{f}{f_m}\right)^2\right\}^2+\left\{2\xi_m\left(\frac{f}{f_m}\right)\right\}^2}}\mathrm{Im}[S_{P^*_{jm}}(f)]
\end{aligned}
\tag{5.A.6}
$$

The modal matrix used in Eqs. (5.25) and (5.26) is of the form

$$
\mathbf{\Phi} = \begin{bmatrix}
\Phi_{1x1} & \Phi_{4x1} & 0 & 0 & 0 & 0 \\
\Phi_{1x2} & \Phi_{4x2} & 0 & 0 & 0 & 0 \\
0 & 0 & \Phi_{2y1} & \Phi_{3y1} & 0 & \Phi_{6y1} \\
0 & 0 & \Phi_{2y2} & \Phi_{3y2} & 0 & \Phi_{6y2} \\
0 & 0 & 0 & \Phi_{3\theta1} & \Phi_{5\theta1} & \Phi_{6\theta1} \\
0 & 0 & 0 & \Phi_{3\theta2} & \Phi_{5\theta2} & \Phi_{6\theta2}
\end{bmatrix}
\tag{5.A.7}
$$

Assuming a rectangular cross-section of skybridge as shown in Fig. 5.B1 and the same building stiffness ($k_x^e = k_y^e$) in the x- and y-directions, the relationship between ψ_A and ψ_B can be derived as

$$
\psi_B = \frac{EI}{l^3 k_y^e} = \frac{EA}{l k_x^e}\left(\frac{0.5d}{l}\right)^2 = \psi_A\left(\frac{0.5d}{l}\right)^2
\tag{5.A8}
$$

5.6 References

Boggs, D.W. and Hosoya, N. (2001), "Wind-tunnel techniques to address structures with multiple coupled interactions", In: Proceedings of Structures Congress – A Structural Engineering Odyssey, Washington, D.C., USA, pp. 8.

Chen, X. and Kareem, A. (2005), "Coupled dynamic analysis and equivalent static wind loads on buildings with three-dimensional modes", Journal of Structural Engineering, 131(7), 1071-1082.

Der Kiureghian, A. (1981), "A response spectrum method for random vibration analysis of MDF systems", Earthquake Engineering and Structural Dynamics, 9, 419-435.

Fu, J., Xie, Z., and Li, Q.S. (2008), "Equivalent static wind loads on long-span roof structures", Journal of Structural Engineering, 134(7), 1115-1128.

Ho, T.C.E. and Jeong, U.Y. (2008), "Components of force balance data analysis", In: Proceedings of 4th International Conference on Advances in Wind and Structures, Jeju, Korea, 453-466.

Holmes, J.D., Rofail, A., and Aurelius, L. (2003), "High frequency base balance methodologies for tall buildings with torsional and coupled resonant modes", In: Proceedings of the 11th International Conference on Wind Engineering, Lubbock, TX, USA, pp. 8.

Islam, M.S., Ellingwood, B., and Corotis, R.B. (1990), "Wind-induced response of structurally asymmetric high-rise buildings", Journal of Structural Engineering, 118, 207-222.

Lim, J. and Bienkiewicz, B. (2007), "Wind-induced response of structurally coupled twin tall buildings", Wind Structure, An International Journal, 10(4), 383-398.

Lim, J. and Bienkiewicz, B. (2008a), "Cross-correlation and coherence of wind loading on tall twin buildings in close proximity", Submitted for publication in Wind Structure, An International Journal.

Lim, J. and Bienkiewicz, B. (2008b). "Modeling of structural coupling for assessment of wind effects on twin buildings with a skybridge", Submitted for publication in Journal of Wind Engineering and Industrial Aerodynamics.

Ni, Z.H., He, C.K., Xie, Z.N., Shi, B.Q., and Chen, D.J. (2001), "Experimental test on bridge jointed twin-towered buildings to stochastic wind loads", Wind Structure, An International Journal, 4(1), 63-72.

Thoroddsen, S.T., Peterka, J.A., and Cermak, J.E. (1988), "Correlation of the components of wind-loading on tall buildings", Journal of Wind Engineering and Industrial Aerodynamics, 28(1-3), 351-360.

Xie, J. and Irwin, P.A. (1998), "Application of the force balance technique to a building complex", Journal of Wind Engineering and Industrial Aerodynamics, 77-78, 579-590.

Xie, J. and Irwin, P.A. (2001), "Wind-induced response of a twin-tower structure", Wind Structure, An International Journal, 4(6), 495-504.

Wu, J.R, Li, Q.S, and Tuan, A.Y. (2008), "Wind-induced lateral-torsional coupled responses of tall buildings", Wind Structure, An International Journal, 11(2), 153-178.

5.7 Figures

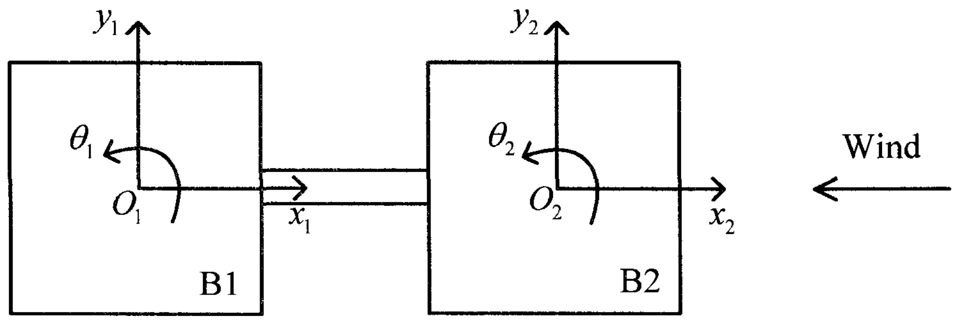

Fig. 5.1 Reference coordinate systems and wind direction

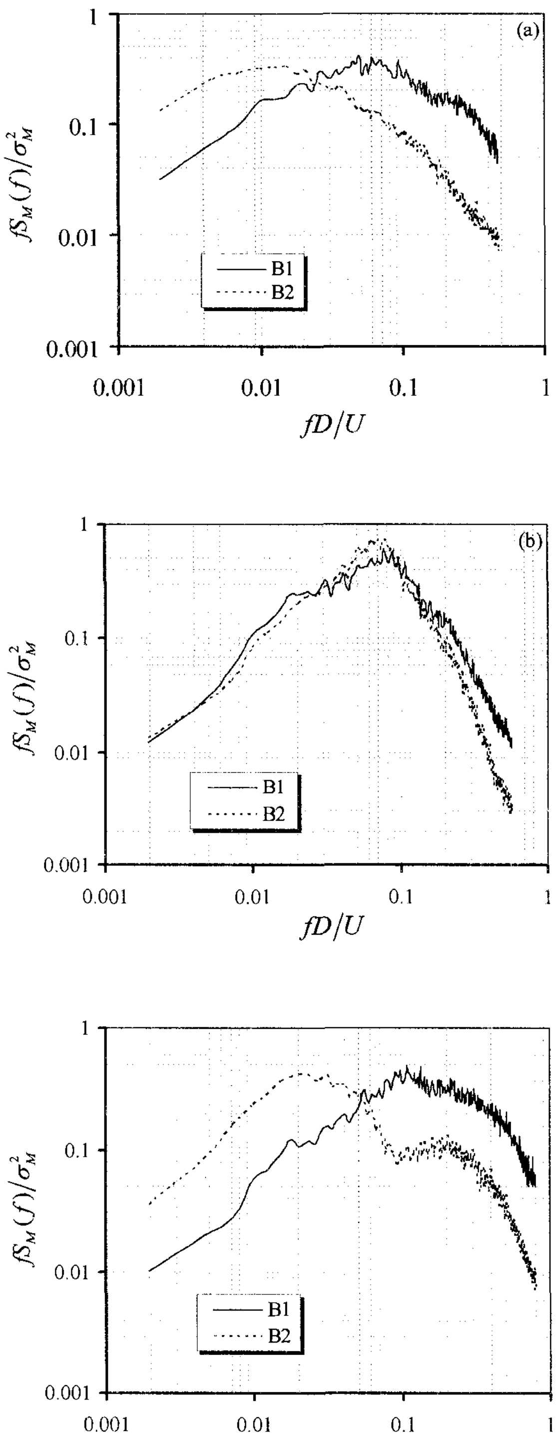

Fig. 5.2 Loading spectra in: (a) alongwind, (b) crosswind and (c) torsional directions

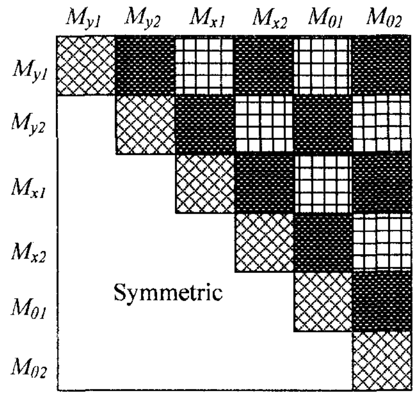

(a) Case I

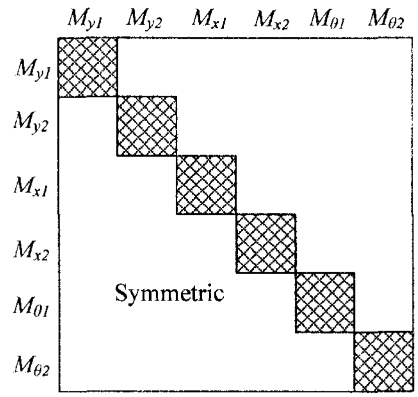

(b) Case II

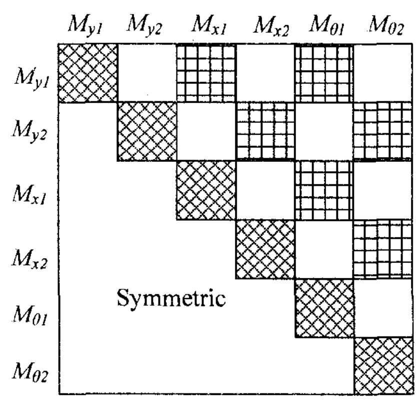

(c) Case III

Fig. 5.3 Aerodynamic coupling cases for twin building configuration (⊠: diagonal component, ⊞: building correlation and ■: inter-building correlation)

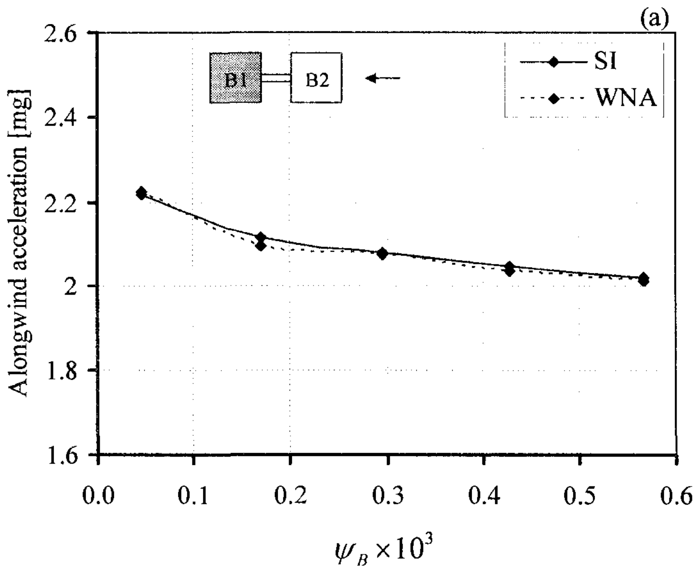

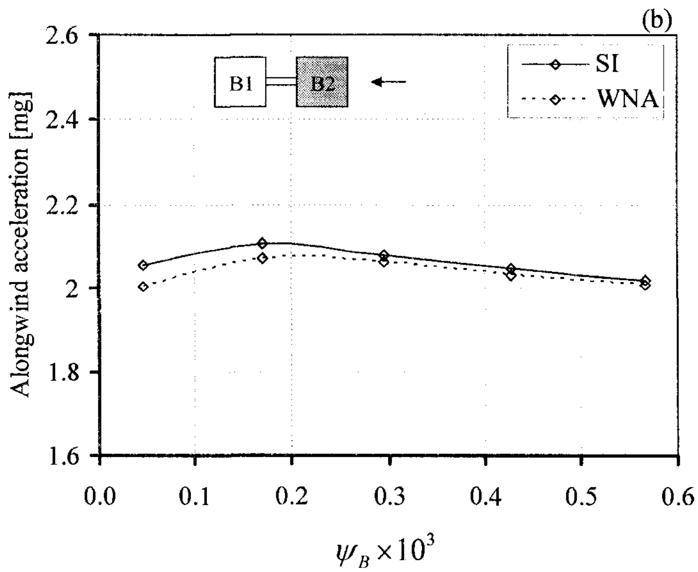

Fig. 5.4 Comparisons of SI and WNA in alongwind acceleration at roof-corner of each building: (a) B1 and (b) B2

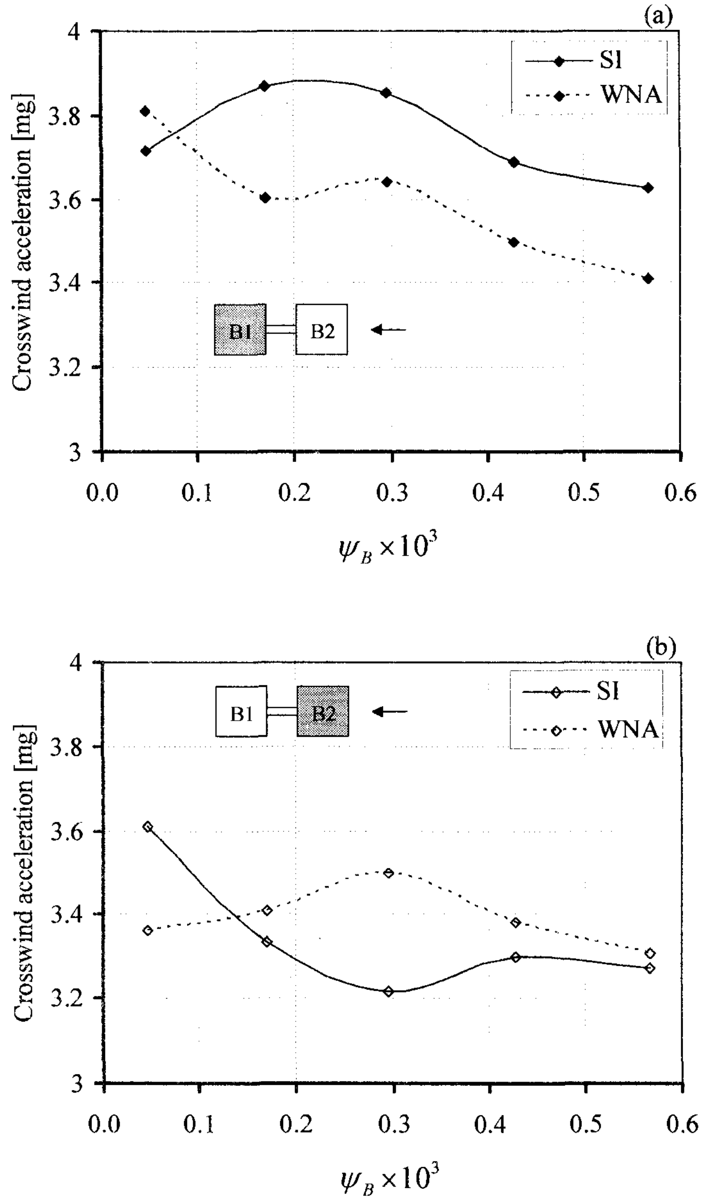

Fig. 5.5 Comparisons of SI and WNA in crosswind acceleration at roof-corner of each building: (a) B1 and (b) B2

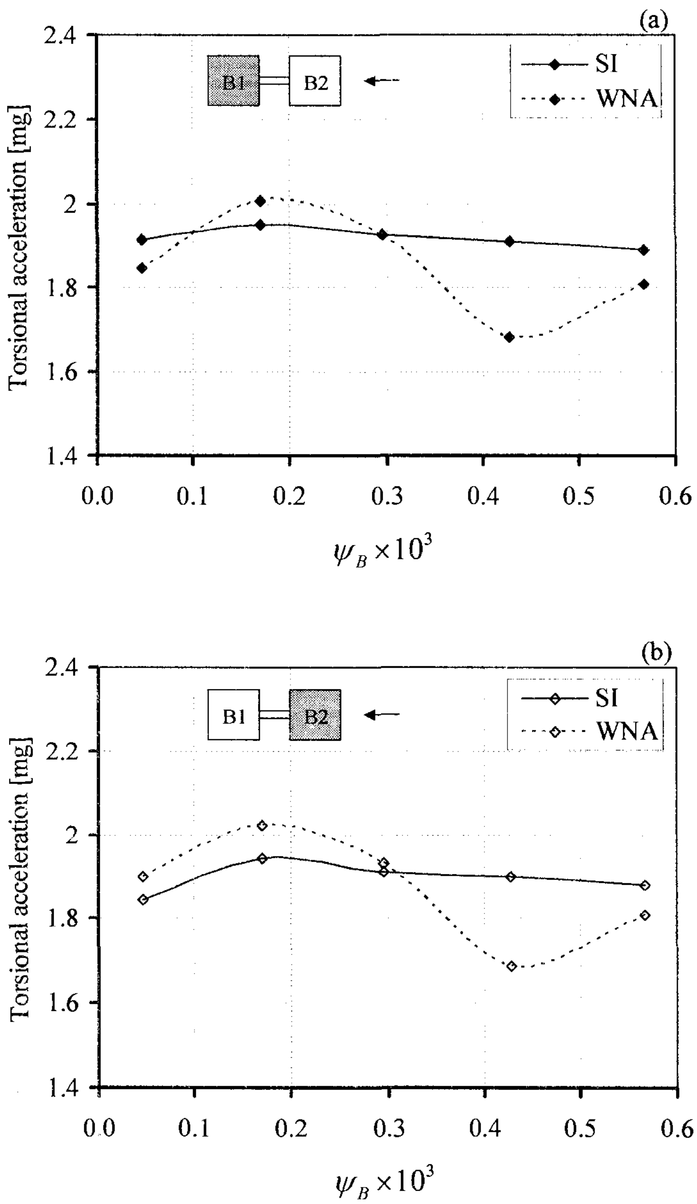

Fig. 5.6 Comparisons of SI and WNA in torsional acceleration at roof-corner of each building: (a) B1 and (b) B2

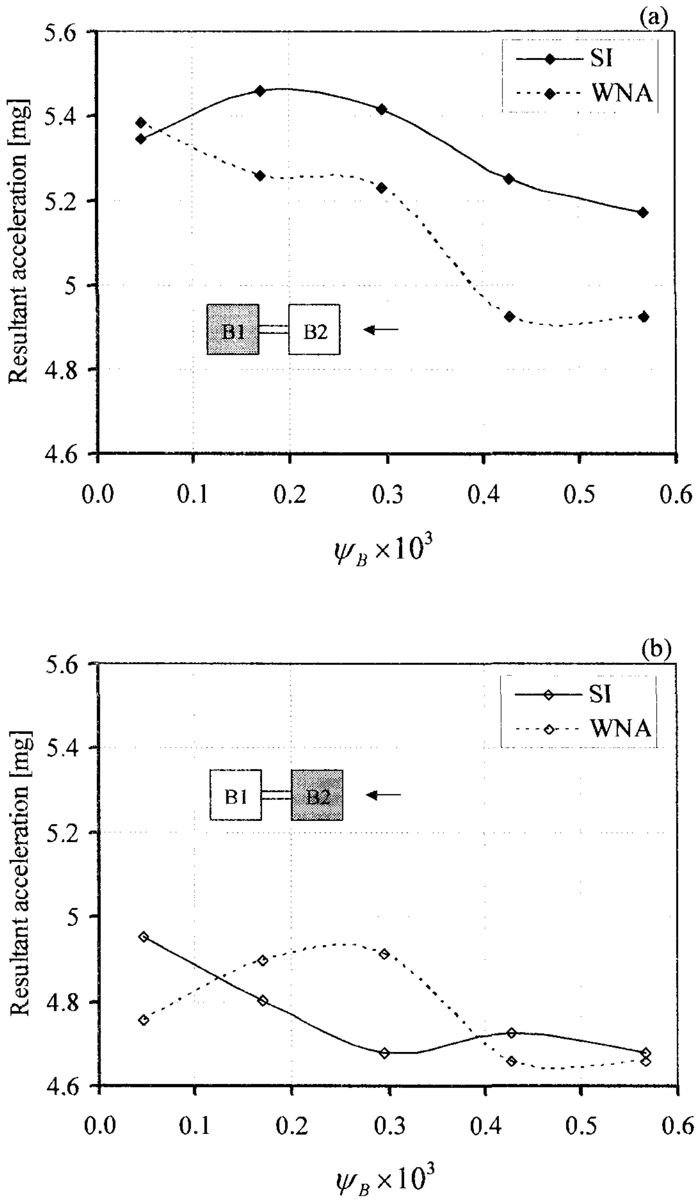

Fig. 5.7 Comparisons of SI and WNA in resultant acceleration at roof-corner of each building: (a) B1 and (b) B2

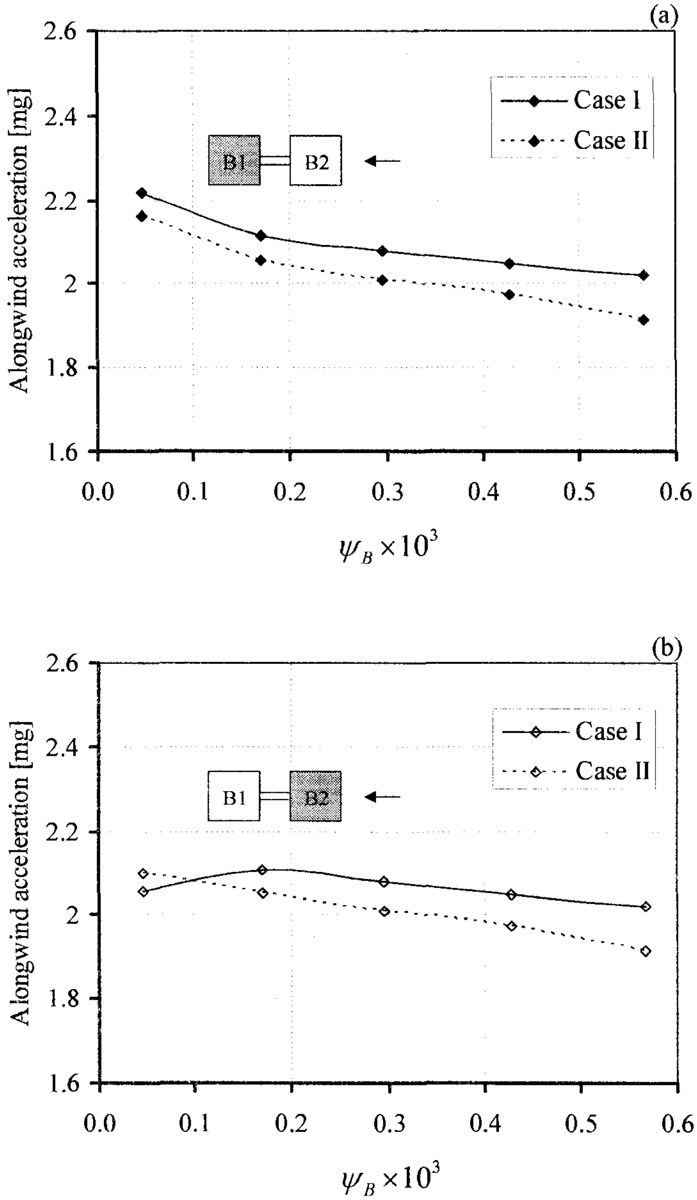

Fig. 5.8 Effects of aerodynamic coupling on alongwind acceleration at roof-corner of each building: (a) B1 and (b) B2

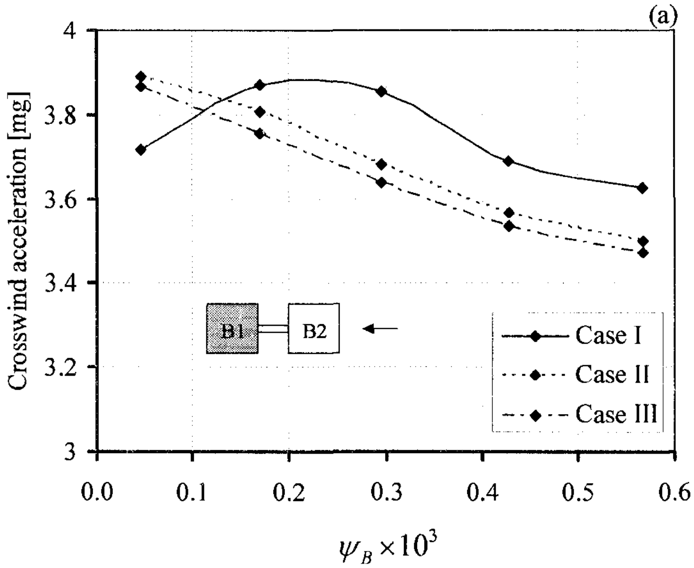

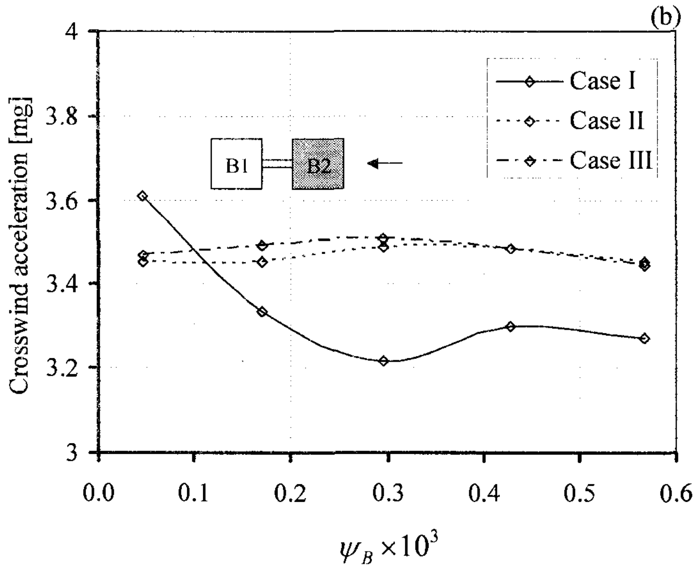

Fig. 5.9 Effects of aerodynamic coupling on crosswind acceleration at roof-corner of each building: (a) B1 and (b) B2

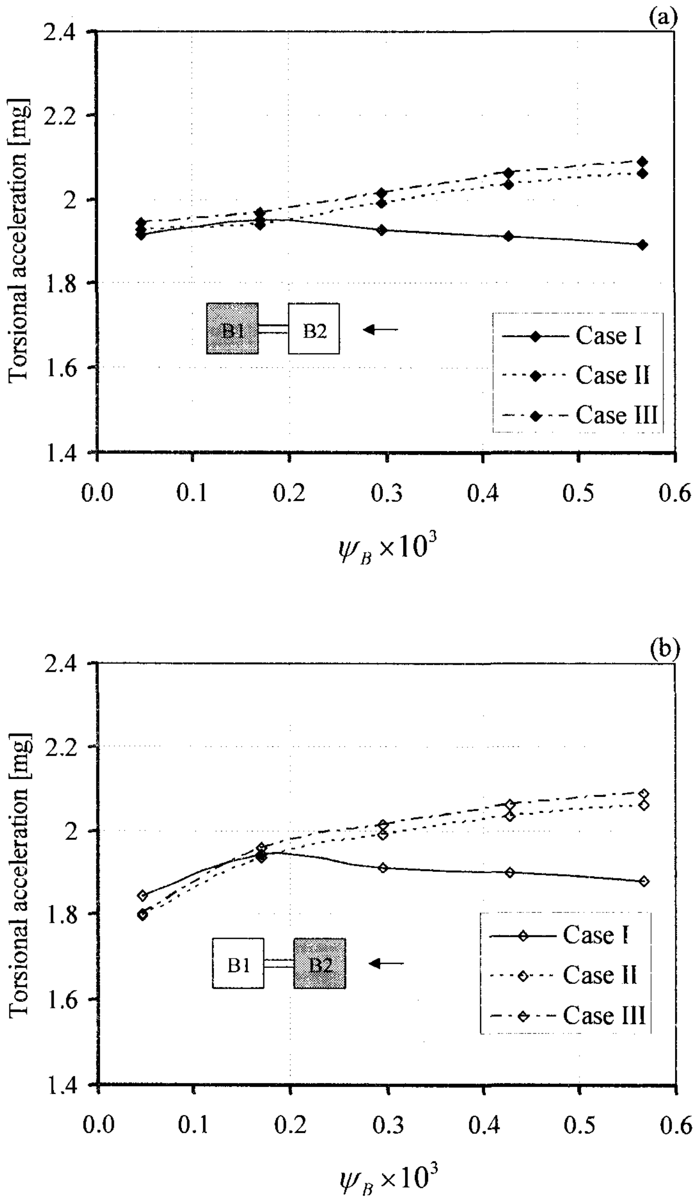

Fig. 5.10 Effects of aerodynamic coupling on torsional acceleration at roof-corner of each building: (a) B1 and (b) B2

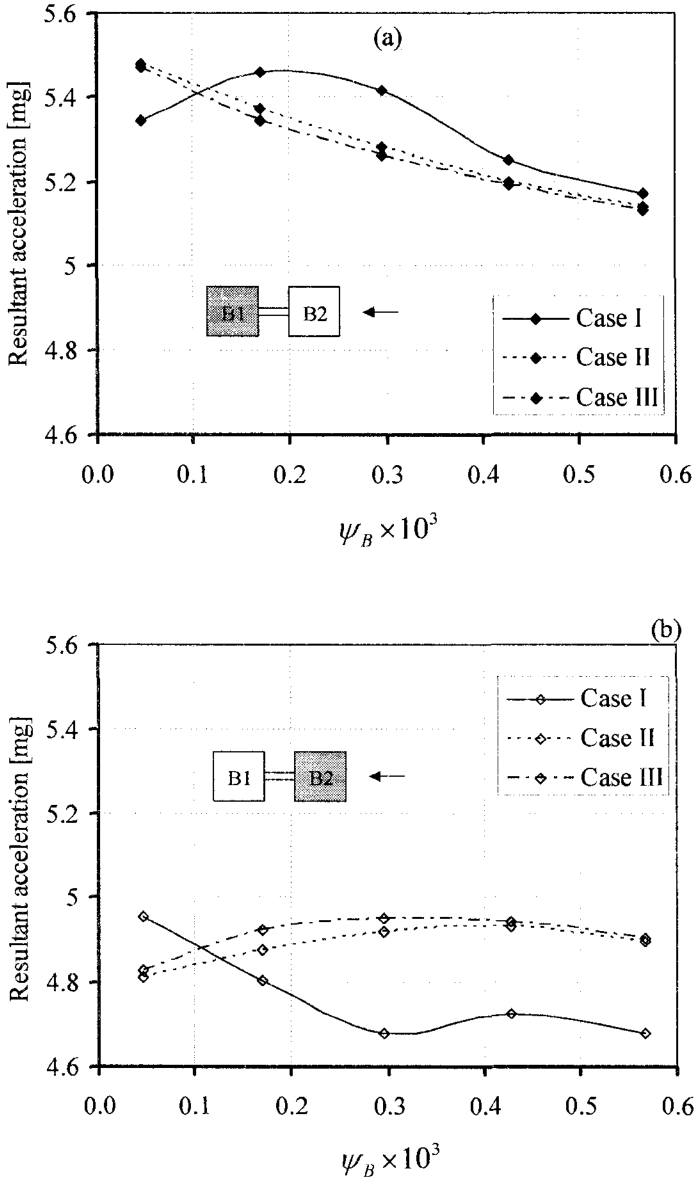

Fig. 5.11 Effects of aerodynamic coupling on resultant acceleration at roof-corner of each building: (a) B1 and (b) B2

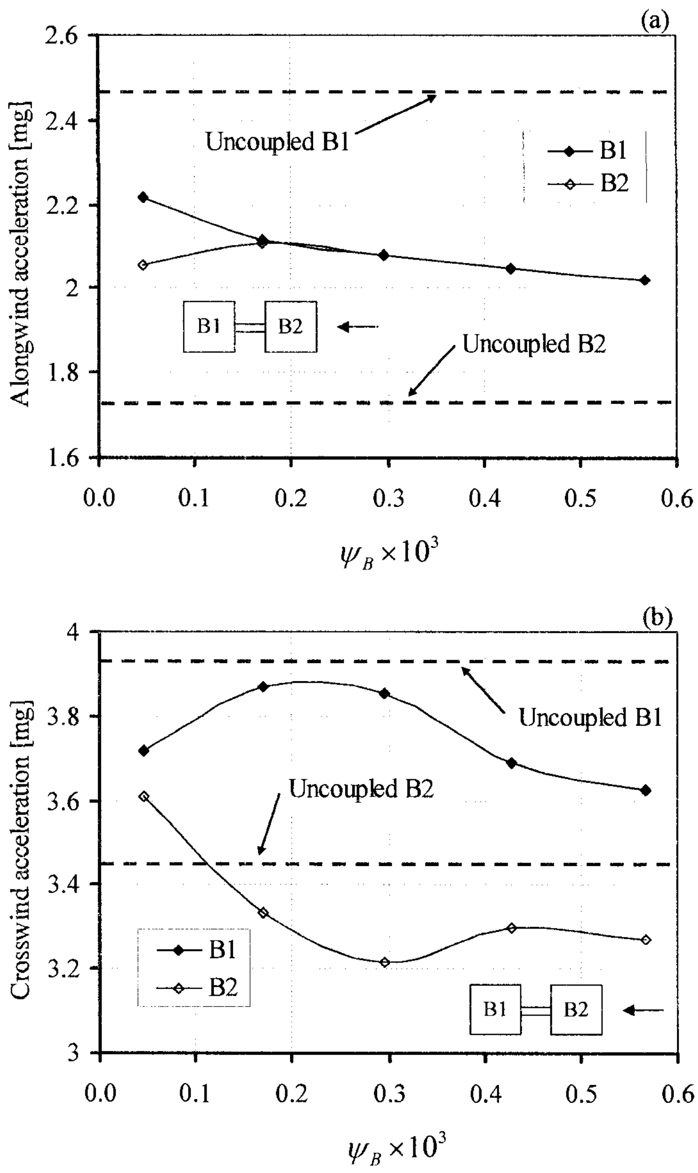

Fig. 5.12 Effects of structural coupling on (a) alongwind, (b) crosswind, (c) torsional and (d) resultant accelerations at roof-corner of each building (5 years)

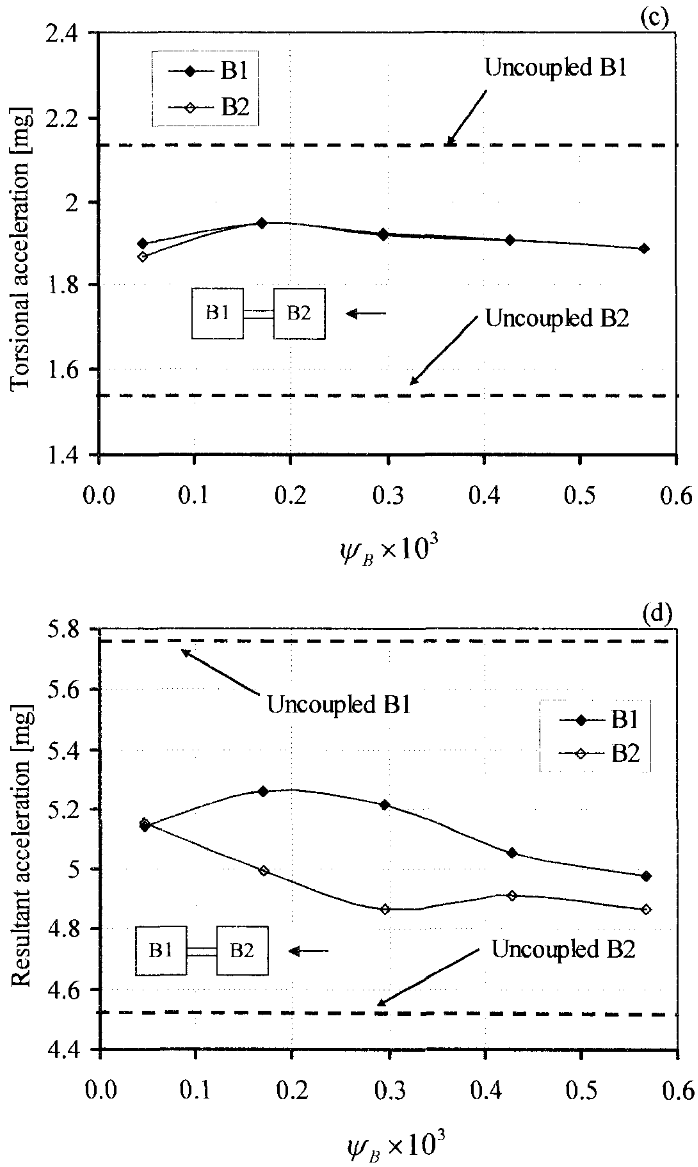

Fig. 5.12 (continued) Effects of structural coupling on (a) alongwind, (b) crosswind, (c) torsional and (d) resultant accelerations at roof-corner of each building (5 years)

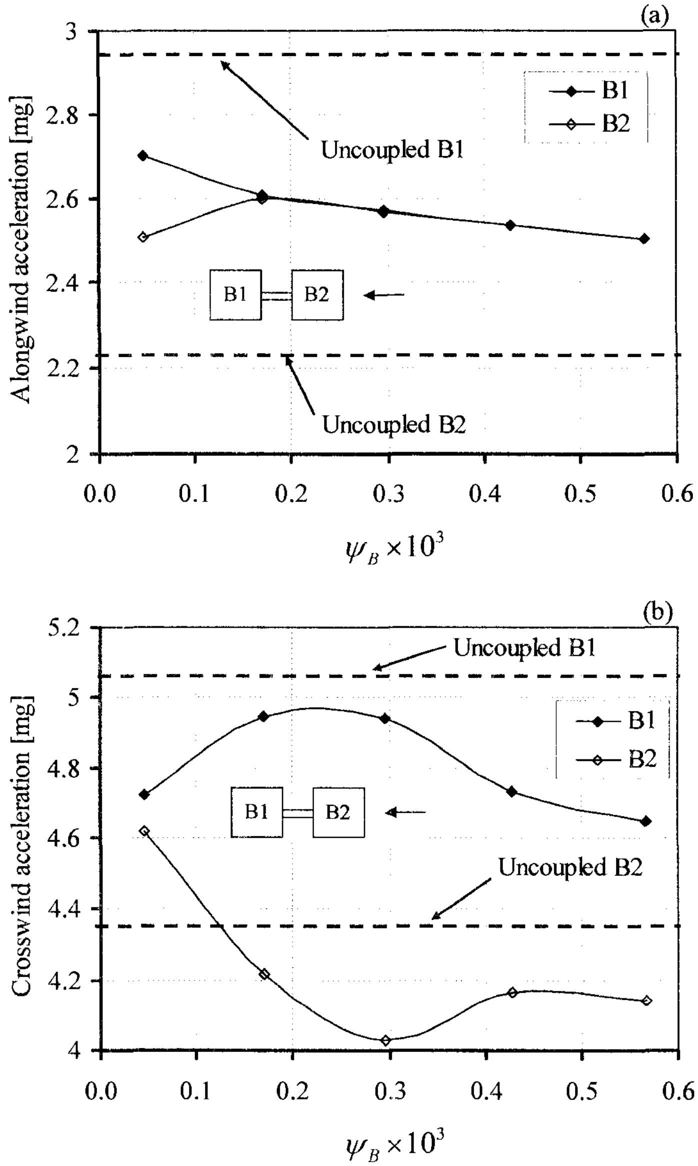

Fig. 5.13 Effects of structural coupling on (a) alongwind, (b) crosswind, (c) torsional and (d) resultant accelerations at roof-corner of each building (10-years)

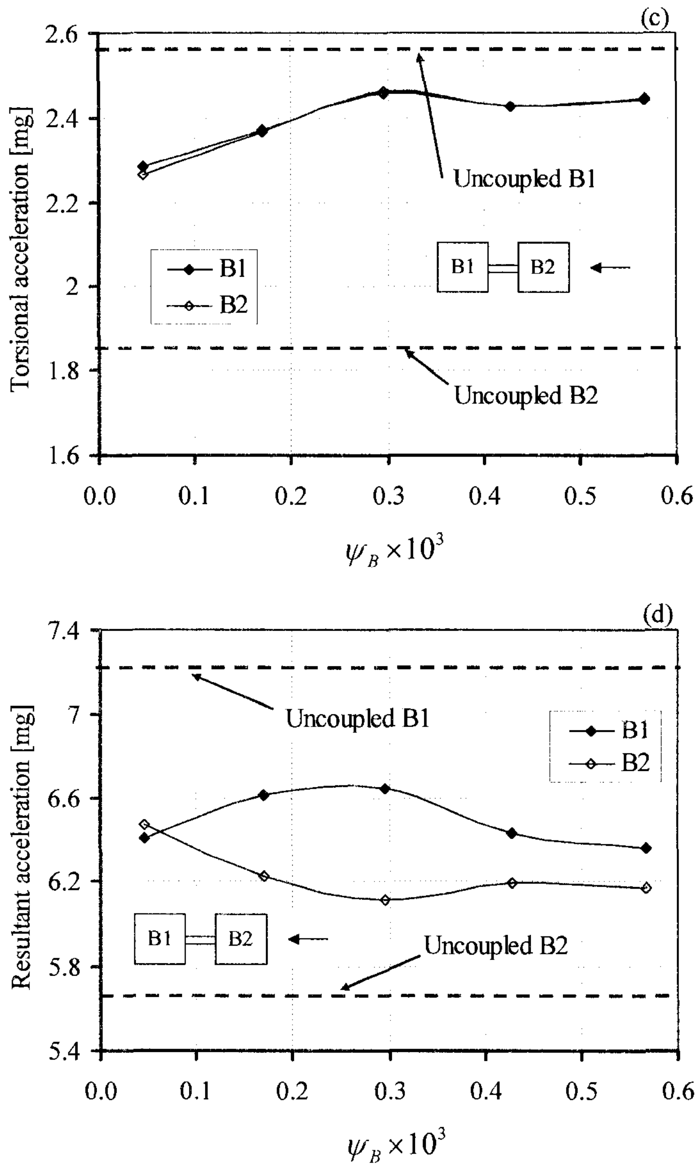

Fig. 5.13 (continued) Effects of structural coupling on (a) alongwind, (b) crosswind, (c) torsional and (d) resultant accelerations at roof-corner of each building (10 years)

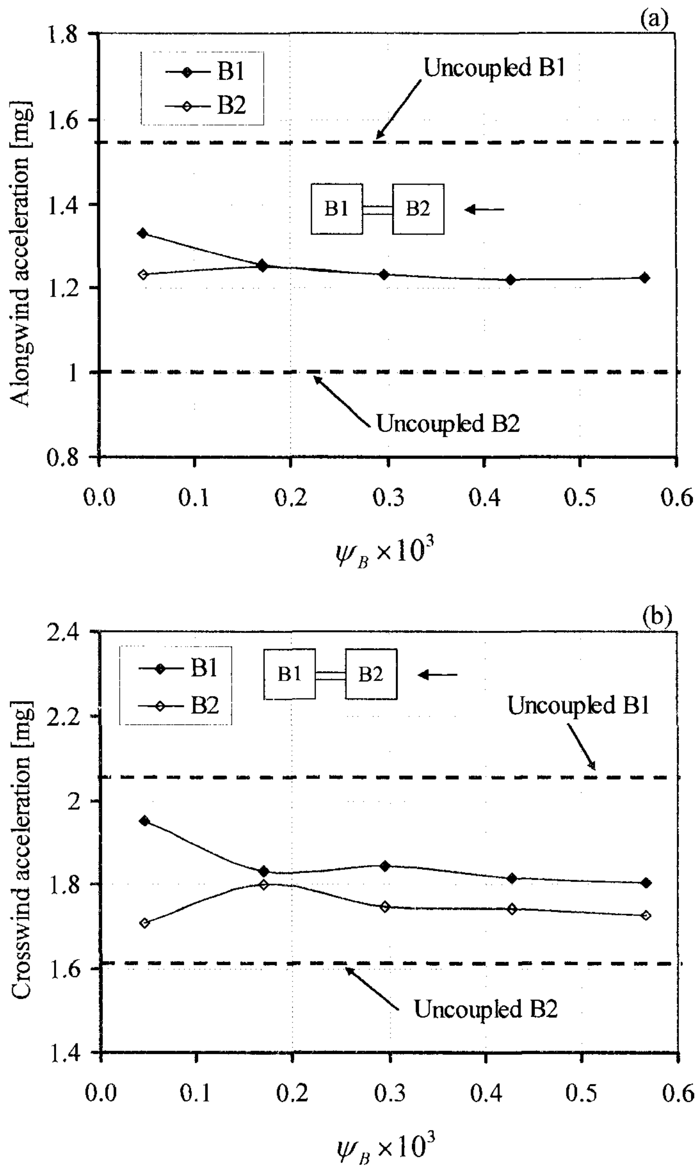

Fig. 5.14 Effects of structural coupling on (a) alongwind, (b) crosswind, (c) torsional and (d) resultant accelerations at roof-corner of each building (1 year)

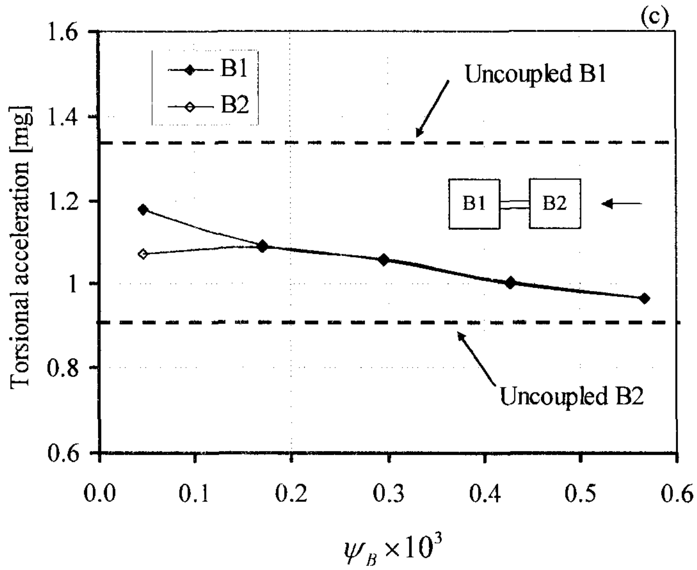

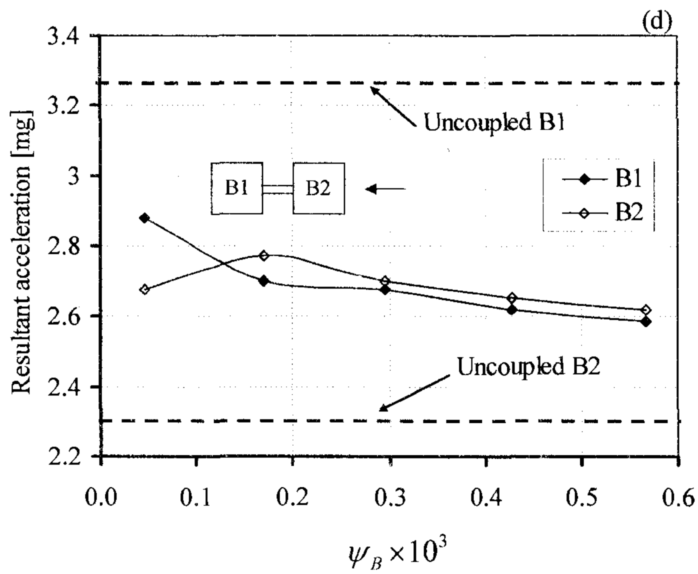

Fig. 5.14 (continued) Effects of structural coupling on (a) alongwind, (b) crosswind, (c) torsional and (d) resultant accelerations at roof-corner of each building (1 year)

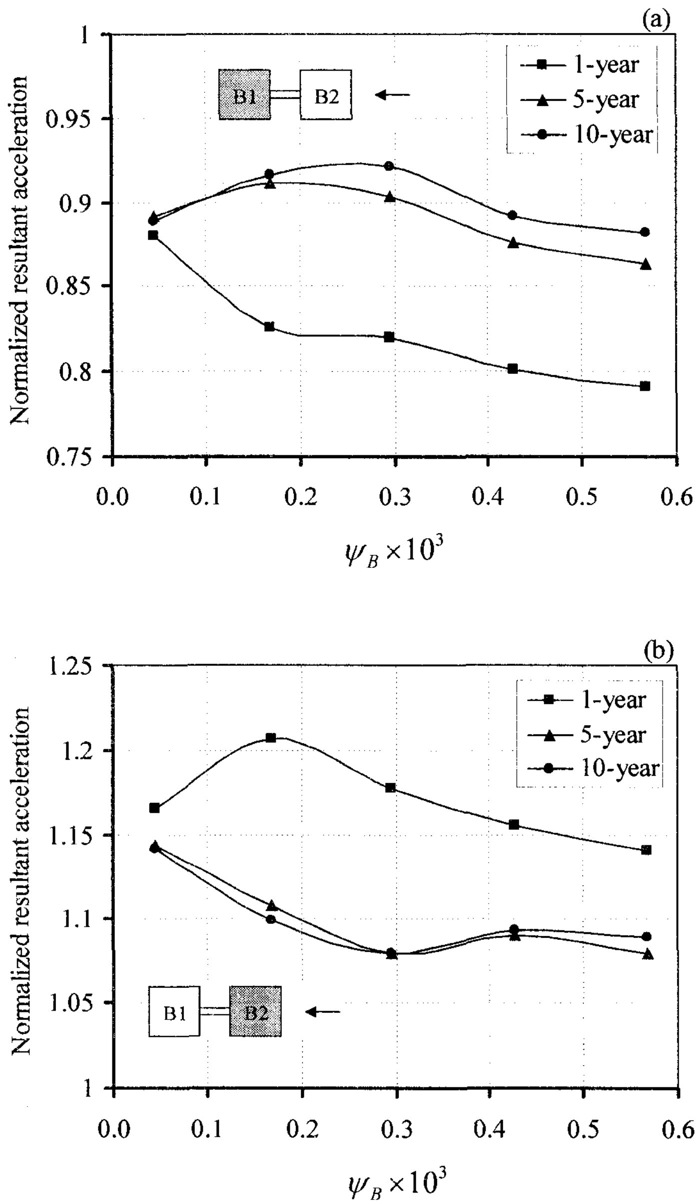

Fig. 5.15 Effects of wind mean return period on resultant acceleration for buildings B1 and B2

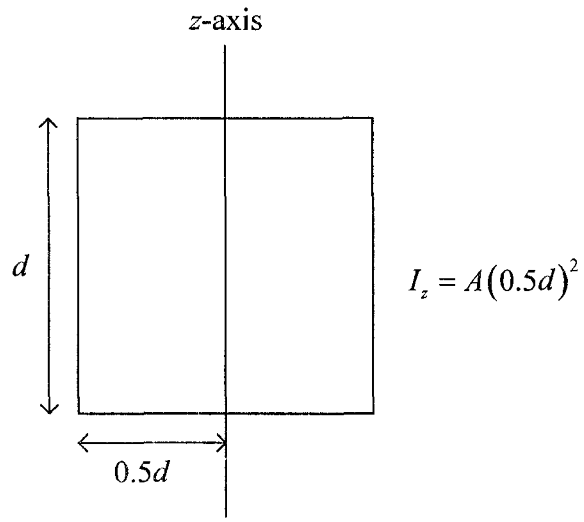

Fig. 5.A1 Idealized cross section of skybridge

5.8 Tables

Table 5.1 Modal frequencies (Hz) of prototype twin building configuration

ψ_A	$\psi_B \times 10^3$	Mode					
		Mode 1	Mode 4	Mode 2	Mode 3	Mode 5	Mode 6
0.021	0.048	0.160	0.168	0.160	0.161	0.24	0.248
0.075	0.170	0.160	0.188	0.160	0.162	0.241	0.269
0.130	0.295	0.160	0.206	0.160	0.164	0.243	0.288
0.189	0.429	0.160	0.223	0.160	0.166	0.244	0.308
0.250	0.567	0.160	0.241	0.160	0.168	0.245	0.327

Table 5.2 Representative modes of prototype twin building configuration ($\psi_B \times 10^3 =$ 0.295)

Component	Direction	Mode					
		Mode 1	Mode 4	Mode 2	Mode 3	Mode 5	Mode 6
Alongwind	*x1*	1	1				
	x2	1	-1				
Crosswind	*y1*			1	1		1.653
	y2			1	-1		-1.653
Torsional	$\theta 1$				-0.014	1	1
	$\theta 2$				-0.014	-1	1

Table 5.3 Cross-correlation coefficients (ρ_M) of loading components

	Component					
	Alongwind		Crosswind		Torsional	
Base wind loading	M_{y1}	M_{y2}	M_{x1}	M_{x2}	$M_{\theta 1}$	$M_{\theta 2}$
M_{y1}	1	-0.36	-0.06	0.09	-0.03	-0.1
M_{y2}		1	-0.06	0.04	0.05	-0.04
M_{x1}			1	-0.67	-0.63	-0.49
M_{x2}				1	0.39	-0.43
$M_{\theta 1}$		Symmetric			1	-0.25
$M_{\theta 2}$						1

Table 5.4 Comparison of building acceleration response for uncoupled case

		Building			
		B1		B2	
Component	Method	SD [mg]	Error [%]	SD [mg]	Error [%]
Alongwind	SI	2.47	-7	1.72	-3
	WNA	2.64		1.77	
Crosswind	SI	3.92	3	3.45	-5
	WNA	3.81		3.62	
Torsional	SI	2.13	-1	1.53	1
	WNA	2.16		1.51	
Resultant	SI	5.77	0	4.5	-4
	WNA	5.77		4.7	

Note: $\text{Error} = \left(\frac{\text{SI-WNA}}{\text{SI}}\right)\times 100$

CHAPTER 6

CONCLUSIONS AND RECOMMENDATIONS

6.1 Conclusions

This dissertation started with a preliminary study of twin tall buildings with a skybridge. In the initial study, a typical spacing between the buildings and one representative level of the structural coupling including assumed frequencies and idealized modal shapes were used. The conclusions of the preliminary study were:

- In absence of the structural coupling, the downstream building may experience unfavorable building acceleration due to aerodynamic interference effects, as previously pointed out by other researches.
- Structural coupling altered the wind-induced response of such tall buildings and tended to transfer the peak accelerations between the two buildings.
- Two issues were considered: the impacts of the correlated loading components and structural linkage on the wind-induced building response. Follow-up studies to accommodate these issues were performed to provide a better understanding of the wind-induced response of the twin building.

A systematic study of the aerodynamic coupling resulting from the cross-correlations of the loading components revealed the following findings:

- It was confirmed that, for single tall buildings, the alongwind loading was weakly correlated with the crosswind and torsional loadings, while the crosswind loading was highly correlated with the torsional loading. For twin building configurations in close proximity, in contrast with single tall buildings, the alongwind loading was strongly correlated with the crosswind and torsional loadings on each building. In addition, the cross-correlation between the crosswind and torsional loadings was significant by up to 0.66.
- The inter-building correlations between the two buildings were significant, reaching up to 0.83 and 0.63 for similar and different loading components, respectively. This feature was not addressed by other researchers, because they employed a single HFFB system and ignored the importance of the inter-building correlations. Therefore, the use of DHFFB system is appropriate for capturing the inter-building correlations as well as the building correlations.

Based on the above studies, one twin building configuration – two buildings aligned with the wind – was subsequently used for an analytical model describing the motions of vibration of the buildings. This modeling of the structural coupling revealed the following features:

- The motions of vibration of twin buildings with a skybridge were represented by a six-degree-of-freedom model. In the modeled system, the x-component of the buildings was separately analyzed, independent of the y- and θ-components. In practical design, given a more complicated building system – i.e. all components are structurally coupled – can be involved. Thus further investigations for such systems should be carried out.

- Six natural frequencies and modes – two for the x-component and four for the y- and θ-components – were calculated through free vibration analysis. The computed modal quantities were closely approximated by the proposed empirical formulas. Simple formulas were used as a useful tool for preliminary calculation of the natural frequencies and modes in the follow-up study.
- Dynamic behavior of a twin building configuration can be governed by an engineered connection such as a skybridge. Other types of inter-building connection will increase the difficulty of constructing an analytical model. A sophisticated building model should be developed, and comparative studies with a commercial tool are also necessary.

Based on the systematic mapping of the building and inter-building correlations and the analytical model, the effects of the aerodynamic and structural couplings on the roof-top accelerations of the buildings were assessed. This investigation unveiled the following facts:

- The integration method of the spectral modal response performed better for accurate predictions of the structurally coupled building response, compared with the approximation method. The relative differences between the estimates obtained for each method reached up to 12% and 6% for the directional and resultant accelerations, respectively. In future studies, the accuracy of the spectral integration method can be validated by using the multi-channel pressure integration method.

- Neglecting the aerodynamic coupling due to the cross-correlations of the loading components may lead to biased predictions of the building acceleration. The discrepancies were significant by up to 11% for the directional accelerations and up to 6% for the resultant acceleration. For the twin building configuration considered, most of the contributions of the aerodynamic coupling resulted from the inter-building correlations.
- The presence of structural coupling led to a significant reduction (up to 22%) in the maximum acceleration obtained for the structurally uncoupled buildings, while an increase occurred in the lower acceleration. In comparison with 5- and 10-year return periods, significant effects of structural coupling appeared for a 1-year return period. Overall, the impacts of the structural coupling were greater with an increase in the coupling level. Therefore, since the structural coupling may yield substantial impacts on estimations of the building acceleration, its inclusion in wind-resistant designs of structurally coupled twin buildings or other slender structures is desirable.

6.2 Recommendations for follow-up studies

In view of the significant impacts of the aerodynamic and structural couplings on the dynamic wind response of twin tall buildings, further investigations focused on these effects are desired to provide an improved quantification of these effects and their broader impacts on wind resistant designs of such building complexes.

Experimental data acquired during future studies utilizing advanced sensors, such as triple and quadruple-HFFB, multi-channel pressure integration, or hybrid measurement systems, will be very useful in confirmation of the results of this dissertation. Due to the importance of the aerodynamic coupling, extensive exploration and mapping of the loading correlations of tall twin buildings with various aspect ratios are desired.

Since the discussed analytical model was focused on only generic twin tall buildings with a skybridge, an enhanced structural modeling to improve its accuracy for calculating coupled modal quantities is needed. Furthermore, such extensive data and enhanced structural models will serve to explore physical aspects of aerodynamic and structural couplings.

Ultimately, these follow-up studies will contribute to cost efficient designs and construction practices for tall buildings and other slender structures in close proximity.

Appendix

REFERENCES RELATED TO WIND TUNNEL STUIDES OF TALL BUILDINGS

1. Armitt, J. and Counihan, J. (1968), "Simulation of atmospheric boundary layer in wind tunnel", Atmospheric Environment, 2(1), 49-71.
2. Bailey, P.A. and Kwok, K.C.S. (1985), "Interference excitation of twin tall buildings", Journal of Wind Engineering and Industrial Aerodynamics, 21(3), 323-338.
3. Balendra, T. (1983), "A simplified model for lateral load analysis of asymmetrical buildings", Engineering Structures, 5(3), 154-162.
4. Blessmann, J. (1985), "Buffeting effects on neighbouring tall buildings", Journal of Wind Engineering and Industrial Aerodynamics, 18(1), 105-110.
5. Boggs, D.W. (1992), "Validation of the aerodynamic model method", Journal of Wind Engineering and Industrial Aerodynamics, 42(1-3), 1011-1022.
6. Boggs, D.W. and Hosoya, N. (2001), "Wind-tunnel techniques to address structures with multiple coupled interactions", In: Structures 2001 – A Structural Engineering Odyssey, Washington, DC, USA, pp. 8.

7. Boggs, D.W. and Peterka, J.A. (1987), "Application of aerodynamic model tests to wind loading of tall buildings", In: Dynamics of Structures, Proceedings of the Sessions at Structures Congress '87, Orlando, FL, USA, 671-686.

8. Boggs, D.W. and Peterka, J.A. (1989), "Aerodynamic model tests of tall buildings", Journal of Engineering Mechanics, 115(3), 618-635.

9. Brownjohn, J.M.W., Pan, T.C. and Deng, X.Y. (2000), "Correlating dynamic characteristics from field measurements and numerical analysis of a high rise building", Earthquake Engineering and Structural Dynamics, 29, 523-543.

10. Cermak, J.E., Cochran, L.S. and Leffler, R.D. (1995), "Wind-tunnel modeling of the atmospheric surface layer", Journal of Wind Engineering and Industrial Aerodynamics, 54-55, 505-513.

11. Chan, C.-M. and Chui, J.K.L. (2006), "Wind-induced response and serviceability design optimization of tall steel buildings", Engineering Structures, 28(4), 503-513.

12. Chen, X. and Kareem, A. (2004), "Equivalent static wind loads on buildings: New Model", Journal of Structural Engineering, 130(10), 1425-1435.

13. Chen, X. and Kareem, A. (2005), "Validity of wind load distribution based on high frequency force balance measurements", Journal of Structural Engineering, 131(6), 984-987.

14. Chen, X and Kareem, A. (2005) "Dynamic wind effects on buildings with 3D coupled modes: application of high frequency force balance measurements", Journal of Engineering Mechanics, 131(11), 115-1125.

15. Chen, X. and Kareem, A. (2005), "Coupled dynamic analysis and equivalent static wind loads on buildings with three-dimensional modes", Journal of Structural Engineering, 131(7), 1071-1082.

16. Cheong, H.F., Balendra, Y., Chew, T., Lee, T.S. and Lee, S.L. (1992), "An experimental technique for distribution of dynamic wind loads on tall buildings", Journal of Wind Engineering and Industrial Aerodynamics, 40(3), 249-261.

17. Choi, C.K. and Kwon, D.K. (1998), "Wind tunnel blockage effects on aerodynamic behavior of bluff body", Wind & Structures, An International Journal, 1(4), 351-364.

18. Cook, N.J. (1978), "Determination of the model scale factor in wind-tunnel simulations of the adiabatic atmospheric boundary layer", Journal of Wind Engineering and Industrial Aerodynamics, 2(4), 311-321.

19. Counihan, J. (1973), "Simulation of an adiabatic urban boundary layer in a wind tunnel", Atmospheric Environment, 7(7), 673-689.

20. Davenport, A.G. (1961), "The application of statistical concepts to wind loading of structures", In: Proceedings of Institution of Civil Engineers, 449-472.

21. Der Kiureghian, A. (1980), "Structural response to stationary excitation", Journal of Engineering Mechanics, 106(6), 1195-1213.

22. English, E.C. (1993), "Shielding factors for paired rectangular prisms: an analysis of along-wind mean response data from several sources", In: Proceedings of the 7th US National Conference on Wind Engineering, Los Angles, CA, 193-201.

23. Ferraro, V., Irwin, P.A. and Stone, G.K. (1990), "Wind induced building accelerations", Journal of Wind Engineering and Industrial Aerodynamics, 36(2), 757-767.

24. Flay, R.G.J. and Vickery, B.J. (1997), "Comparison of response predictions for a rough cone from pressure and balance measurements", Journal of Wind Engineering and Industrial Aerodynamics, 69-71, 473-484.

25. Foutch, D.A. and Safak, E. (1981), "Torsional vibration of wind-excited symmetrical structures", Journal of Wind Engineering and Industrial Aerodynamics, 7(2), 191-201.

26. Gu, M. and Peng, F. (2002), "An experimental study of active control of wind-induced vibration of super-tall buildings", Journal of Wind Engineering and Industrial Aerodynamics, 90(12-15), 1919-1931.

27. Gu, M. and Quan, Y., (2004) "Across-wind loads of typical tall buildings", Journal of Wind Engineering and Industrial Aerodynamics, 92(13), 1147-1165.

28. Hansen, S.O. and Dyrbye, C. (1988), "Along-wind response of line-like structures", Journal of Wind Engineering and Industrial Aerodynamics, 30(1-3), 27-34.

29. Hayashida, H., Mataki, Y. and Iwasa, Y. (1992), "Aerodynamic damping effects of tall building for a vortex induced vibration", Journal of Wind Engineering and Industrial Aerodynamics, 43(3), 1973-1983.

30. Ho, T.C.E. and Jeong, U.Y. (2008), "Components of force balance data analysis", In: Proceedings of 4th International Conference on Advances in Wind and Structures, Jeju, Korea, 453-466.

31. Ho, T.C.E., Lythe, G.R. and Isyumov, N. (1999) "Structural loads from the integration of simultaneously measured pressures", In: Proceedings of the Tenth International Conference on Wind Engineering, Copenhagen, Denmark, 1505-1510.

32. Holmes, J.D. (1987), "Mode shape corrections for dynamic response to wind", Engineering Structures, 9(3), 210-212.

33. Holmes, J.D. (2002), "Effective static load distributions in wind engineering", Journal of Wind Engineering and Industrial Aerodynamics, 90(1-2), 135-150.

34. Holmes, J.D., Rofail, A. and Aurelius, L. (2003), "High frequency base balance methodologies for tall buildings with torsional and coupled resonant modes", In: Proceedings of the 11^{th} International Conference on Wind Engineering, Lubbock, TX, USA, pp. 8.

35. Huang, P. and Gu, M. (2005),"Experimental study on wind-induced dynamic interference effects between two tall buildings", Wind and Structures, An International Journal, 8(3), 147-161.

36. Irwin, P.A. (1981), "The design of spires for wind simulation", Journal of Wind Engineering and Industrial Aerodynamics, 7(3), 361-366.

37. Irwin, P.A. (1988), "Pressure model techniques for cladding tools", Journal of Wind Engineering and Industrial Aerodynamics, 29-2(1-3), 69-78.

38. Islam, M.S., Ellingwood, B. and Corotis, R.B. (1990), "Transfer function modeling of dynamic wind loads on buildings", Journal of Engineering Mechanics 116, 1473-1488.

39. Islam, M.S., Ellingwood, B. and Corotis, R.B. (1990), "Dynamic response of tall buildings to stochastic wind load", Journal of Structural Engineering, 116, 2982-3002.

40. Islam, M.S., Ellingwood, B. and Corotis, R.B. (1990), "Wind-induced response of structurally asymmetric high-rise buildings", Journal of Structural Engineering, 118, 207-222.

41. Isyumov, N. and Case, P.C. (2000), "Wind-induced torsional loads and responses of buildings", In: Structures 2000: Advanced Technology in Structural Engineering, Philadelphia, PA, USA, pp. 8.

42. Isyumov, N., Steckley, A., Amin, N. and Fatehi, H. (1990), "Effects of the orientation of the principal axis of stiffness on the dynamic response of a slender square building", Journal of Wind Engineering and Industrial Aerodynamics, 36(2), 769-778.

43. Kareem, A. (1981), "Wind induced torsional loads on structures", Engineering Structures, 3(2), 85-86.

44. Kareem, A. (1985), "Lateral-torsional motion of tall buildings to wind loads", Journal of Structural Engineering, 111(11), 2479-2496.

45. Kareem, A. (1987), "The effect of aerodynamic interference on the dynamic response of prismatic structures", Journal of Wind Engineering and Industrial Aerodynamics, 25(3), 265-372.

46. Kareem, A. (1992), "Dynamic response of high-rise buildings", Journal of Wind Engineering and Industrial Aerodynamics, 42(1-3), 1101-1112.

47. Katagiri, J., Okhuma, T. and Marukawa, H. (2002), "Analytical method for coupled across-wind and torsional wind responses with motion-induced wind forces", Journal of Wind Engineering and Industrial Aerodynamics, 90(12-15), 1795-1805.

48. Katsumura, A., Katagiri, J., Marukawa, H. and Fujii, K. (2001), "Effects of side ratio on characteristics of across-wind and torsional responses of high-rise buildings", Journal of Wind Engineering and Industrial Aerodynamics, 89(14), 1433-1444.

49. Kawai, H. (1993), "Bending and torsional vibration of tall buildings in strong wind", Journal of Wind Engineering and Industrial Aerodynamics, 50(1-2), 281-288.

50. Khanduri, A.C., Stathopoulos, T. and Bedard, C. (2000), "Generalization of wind-induced interference effects for two buildings", Wind and Structures, an International Journal, 3(4), 255-266.

51. Kijewski, T.L. and Kareem, A. (1998), "Dynamic wind effects: a comparative study of provisions in codes and standards with wind tunnel data", Wind & Structures, An International Journal, 1(1), 77-109.

52. Liang, S., Liu, S., Zhang, L., Gu, M. and Li, Q.S. (2004), "Torsional dynamic wind loads on rectangular tall buildings", Engineering Structures, 26(1), 129-137.

53. Liang, S., Li, Q.S., Zou, L., Wu, J.R. (2005),"Simplified formulas for evaluation of across-wind dynamic responses of rectangular tall buildings", Wind and Structures, An International Journal, 8(3), 197-212.

54. Liang, Bo, Tamura, Y. and Suganuma, S. (1997), "Simulation of wind-induced lateral-torsional motion of tall buildings", Computers and Structures, 63(3), 601-606.

55. Lim, J. and Bienkiewicz, B. (2007), "Wind-induced response of structurally coupled twin tall buildings", Wind Structure, An International Journal, 10(4), 383-398.

56. Lin, N., Letchford, C., Tamura, Y., Liang, B. and Nakamura, O. (2005), "Characteristics of wind forces acting on tall buildings", Journal of Wind Engineering and Industrial Aerodynamics, 93(3), 217-242.

57. Lythe, G.R. and Surry, D. (1990), "Wind-induced torsional loads on tall buildings", Journal of Wind Engineering and Industrial Aerodynamics, 36(1-3), 225-234.

58. Menun, C., and Der Kiureghian, A. (1998), "A replacement for the 30%, 40% and SRSS rules for multicomponent seismic analysis", Earthquake Spectra, 14(1), 153-156.

59. Ni, Z.H., He, C.K., Xie, Z.N., Shi, B.Q. and Chen, D.J. (2001), "Experimental test on bridge jointed twin-towered buildings to stochastic wind loads", Wind & Structures, An International Journal, 4(1), 63-72.

60. Ng, S.C. and Kuang, J.S. (2000), "Triply Coupled Vibration of Asymmetric Wall-Frame Structures", Journal of Structural Engineering, 126(8), 982-987.

61. Paterson, D.A. and Papenfuss, A.T. (1993), "Computation of wind flows around two tall buildings", Journal of Wind Engineering and Industrial Aerodynamics, 50, 69-74.

62. Perera, M.D.A.E.S. (1978), "A wind-tunnel study of the interaction between along-wind and cross-wind vibrations of tall, slender structures", Journal of Industrial Aerodynamics, 3(4), 315-341.

63. Quan, Y., Gu, M. and Tamura, Y. (2005), "Experimental evaluation of aerodynamic damping of square super high-rise buildings", Wind and Structures, An International Journal, 8(5), 309-324.

64. Reinhorn, A., Rutenberg, A. and Glueck, J. (1977), "Dynamic torsional coupling in asymmetric building structures", Building and Environment, 12(4), 251-261.

65. Ricciardelli, F. and Vickery, B.J. (1998), "The aerodynamic characteristics of twin column, high rise bridge towers", Wind & Structures, An International Journal, 1(3), 225-241.

66. Saunders, J.W. and Melbourne, W.H. (1979), "Buffeting effects of upstream buildings", In: Proceedings of the 5th International Conference on Wind Engineering, Fort Collins, CO, USA, 593-606.

67. Smeby, W., and Der Kiureghian, A. (1985), "Modal combination rules for multicomponent earthquake excitation", Earthquake Engineering & Structural Dynamics, 13(1), 1-14.

68. Snaebjeornsson, J. and Reed, D.A. (1991), "Wind-induced accelerations of a building. A case study", Engineering Structures, 13(3), 268-280.

69. Steckley, A., Accardo, M., Gamble, S.L, and Irwin, P.A. (1992), "The use of integrated pressures to determine over-all-wind-induced response", Journal of Wind Engineering and Industrial Aerodynamics, 42(1-3), 1023-1034.

70. Suarez, L.E. and Singh, M.P. (1987), “Modal coupling procedure for structural dynamics”, In: Dynamics of Structures, Proceedings of the Sessions at Structures Congress ’87, Orlando, FL, USA, 1-14.

71. Sun, T.F. and Gu, Z.F. (1995), "Interference between wind loading on group of structures", Journal of Wind Engineering and Industrial Aerodynamics, 54-55, 213-225.

72. Takeuchi, T. and Matsumoto, M. (1992), “Aerodynamic response characteristics of rectangular cylinders in tandem arrangement”, Journal of Wind Engineering and Industrial Aerodynamics, 41(1-3), 565-575.

73. Tamura, Y., Kikuchi, H. and Hibi, K. (2003), “Quasi-static wind load combinations for low- and middle-rise buildings”, Journal of Wind Engineering and Industrial Aerodynamics, 91(12-15), 1613-1625.

74. Tang, U.F. and Kwok, K.C.S. (2004), “Interference excitation mechanisms on a 3DOF aeroelastic CAARC building model”, Journal of Wind Engineering and Industrial Aerodynamics, 92(14-15), 1299-1314.

75. Tallin, A., Ellingwood, B. (1985), “Wind-induced motion of tall buildings”, Engineering Structures, 7(4), 245-252.

76. Tallin, A. and Ellingwood, B. (1985), “Wind induced lateral-torsional motion of buildings”, Journal of Structural Engineering, 111(10), 2197-2213.

77. Tallin, A. and Ellingwood, B. (1985), “Analysis of torsional moments on tall buildings”, Journal of Wind Engineering and Industrial Aerodynamics, 18(2), 191-195.

78. Tallin, A. and Ellingwood, B. (1985), "Serviceability limit states: Wind induced vibrations", Journal of Structural Engineering, 110(10), 2424-2437.

79. Taniike, Y. (1991), "Turbulence effect on mutual interference of tall buildings", Journal of Engineering Mechanics, 117(3), 443-456.

80. Taniike, Y. and Inaoka, H. (1988), "Aeroelastic behavior of tall buildings in wakes", Journal of Wind Engineering and Industrial Aerodynamics, 28(1-3), 317-327.

81. Thepmongkorn, S. and Kwok, K.C.S. (1998), "Wind-induced coupled translational-torsional motion of tall buildings", Wind and Structures, An International Journal, 1(1), 43-57.

82. Thornton, C.H., Hungspruke, U., Joseph, L.M. (1997), "Design of the worlds tallest buildings – PETRONAS Twin Towers at Kuala Lumpur City Centre", Structural Design of Tall Buildings, 6(4), 245-262.

83. Thoroddsen, S.T., Cermak, J.E. and Peterka, J.A. (1985), "Mean and dynamic wind loading caused by an upwind structure", In: Proceedings of the US National Conference on Wind Engineering, Lubbock, TX, USA, 4A 73-80.

84. Thoroddsen, S.T., Cermak, J.E. and Peterka, J.A. (1987), "Uncertainties in wind loads caused by adjacent buildings", In: Dynamics of Structures, Proceedings of the Sessions at Structures Congress '87, Orlando, FL, USA, 540-555.

85. Thoroddsen, S.T., Peterka, J.A. and Cermak, J.E. (1988), "Correlation of the components of wind-loading on tall buildings", Journal of Wind Engineering and Industrial Aerodynamics, 28(1-3), 351-360.

86. To, A.P. and Lam, K.M. (2003), "Wind-induced interference effects on a group of buildings", In: Proceedings of the 11th International Conference on Wind Engineering, Lubbock, TX, USA, pp. 6.

87. Tschanz, T. and Davenport, A.G. (1983), "The base balance technique for the determination of dynamic wind loads", Journal of Wind Engineering and Industrial Aerodynamics, 13(1-3), 429-439.

88. Vickery, B.J., Isyumov, N. and Davenport, A.G. (1983), "The role of damping, mass and stiffness in the reduction of wind effects on structures", Journal of Wind Engineering and Industrial Aerodynamics, 11(1-3), 285-294.

89. Vickery, B.J. and Kao, K.H. (1972), "Drag or along-wind response of slender structures", Journal of the Structural Division, 98(ST1), 21-36.

90. Vickery, P.J., Steckley, A., Isyumov, N. and Vickery, B.J. (1985), "The effect of modal shape on wind-induced response of tall buildings", In: Proceedings of the 5th US National Conference on Wind Engineering, Lubbock, TX, USA, 1B 41-48.

91. Wilson, E.L. and Button, M.R. (1982) "Three-dimensional dynamic analysis for multi-component earthquake spectra", Earthquake Engineering & Structural Dynamics, 10(3), 471-479.

92. Wilson, E.L., Der Kiureghian, A. Bayo, E.P. (1981), "A replacement for the SRSS method in seismic analysis", Earthquake Engineering & Structural Dynamics, 9(2), 187-192.

93. Wilson, E.L. and Habibullah, A. (1995) "A clarification of the orthogonal effects in a three-dimensional seismic analysis", Engineering Spectra, 11(4), 659-666.

94. Wu, J.R, Li, Q.S, and Tuan, A.Y. (2008), "Wind-induced lateral-torsional coupled responses of tall buildings", Wind and Structures, An International, 11(2), 153-178.

95. Xie, Z.N. and Gu, M. (2004), "Mean interference effects among tall buildings", Engineering Structures, 26(9), 1173-1183.

96. Xie, Z.N. and Gu, M. (2005), "A correlation-based analysis on wind-induced interference effects between two tall buildings", Wind and Structures, An International Journal, 8(3), 163-178.

97. Xie, Z.N. and Gu, M. (2007), "Simplified formulas for evaluation of wind-induced interference effects among three tall buildings", Journal of Wind Engineering and Industrial Aerodynamics, 95(1), 31-52.

98. Xie, J. and Irwin, P.A. (1998), "Application of the force balance technique to a building complex", Journal of Wind Engineering and Industrial Aerodynamics, 77-78, 579-590.

99. Xie, J. and Irwin, P.A. (2001), "Wind-induced response of a twin-tower structure", Wind and Structures, An International Journal, 4(6), 495-504.

100. Xie, J., Irwin, P.A. and Accardo, M. (1999), "Wind load combinations for structural design of tall buildings", In: Wind engineering into the 21st century; proceedings of the tenth annual Conference on Wind Engineering, Copenhagen, DNK, 163-168.

101. Xu, Y.L. and Kwok, K.C.S. (1993), "Mode shape corrections for wind tunnel tests of tall buildings", Engineering Structures, 15(5), 387-392.

102. Yahyai, M., Kumar, K., Krishna, P. and Pande, P.K. (1992), "Aerodynamic interference in tall rectangular buildings", Journal of Wind Engineering and Industrial Aerodynamics, 41(1-3), 859-866.

103. Yip, D.Y.N. and Flay, R.G.J. (1995), "A new force balance data analysis method for wind response predictions of tall buildings", Journal of Wind Engineering and Industrial Aerodynamics, 54-55, 457-471.

104. Zhang, W.J., Xu, Y.L. and Kwok, K.C.S. (1995), "Interference effects on aeroelastic torsional response of structurally asymmetric tall buildings", Journal of Wind Engineering and Industrial Aerodynamics, 57(1), 41-61.

105. Zhou, Y., Kareem, A. and Gu, M. (2002), "Mode shape corrections for wind loading effects", Journal of Engineering Mechanics, 128(1), 15-23.

106. Zhou, Y. and Kareem, A. (2002), "Definition of wind profiles in ASCE 7", Journal of Structural Engineering, 128(8), 1082-1086.

107. Zhou, Y., Kijewski, T.L. and Kareem, A. (2003), "Aerodynamic loads on tall buildings: Interactive database", Journal of Structural Engineering, 129(3), 394-404.